Title: Development of a Novel Method for Determination of Residual Stresses in a Friction Stir Weld

Type of Report: Summary of Research

Principal Investigator: Anthony P. Reynolds

Period Covered: 08/01/1999 through 07/31/2001

University of South Carolina
Office of Sponsored Programs and Research
901 Sumter Street, Fifth Floor
Columbia, SC 29308-0001

Grant #: NAG-1-2237

Abstract

Material constitutive properties, which describe the mechanical behavior of a material under loading, are vital to the design and implementation of engineering materials. For homogeneous materials, the standard process for determining these properties is the tensile test, which is used to measure the material stress-strain response. However, a majority of the applications for engineering materials involve the use of heterogeneous materials and structures (i.e. alloys, welded components) that exhibit heterogeneity on a global or local level. Regardless of the scale of heterogeneity, the overall response of the material or structure is dependent on the response of each of the constituents. Therefore, in order to produce materials and structures that perform in the best possible manner, the properties of the constituents that make up the heterogeneous material must be thoroughly examined.

When materials exhibit heterogeneity on a local level, such as in alloys or particle/matrix composites, they are often treated as statistically homogeneous and the resulting "effective" properties may be determined through homogenization techniques. In the case of globally heterogeneous materials, such as weldments, the standard tensile test provides the global response but no information on what is occurring locally within the different constituents. This information is necessary to improve the material processing as well as the end product.

The present work is concerned with the determination of local material constitutive properties of structures that are heterogeneous on a global scale using a technique employing standard tensile testing procedures and digital image correlation (DIC). In particular, the study is focused on friction stir welds (FSW) in aluminum alloy

2024 and the determination of the material properties associated with the heterogeneous structure. The experimentally determined local constitutive data is verified by 2-D and 3-D finite element simulations of the global and local mechanical response of the friction stir weld.

Table of Contents

List of Figures

List of Tables

Chapter 1 Introduction

1.1 Problem Description

Heterogeneity exists in many natural and artificial materials that play an important role in our society. Materials such as metals, alloys, polymers, fiber composites and structures such as weldments are used for a wide variety of applications and all exhibit heterogeneity on either a local or global level. Regardless of the application or scale of heterogeneity, all materials and structures must be studied and tested to determine the suitability for the target application. A key element in determining whether or not a material is suitable for a desired purpose is the material constitutive behavior. The constitutive behavior describes the response of the material under loading and provides the necessary information for design and implementation of engineering materials and structures.

The methods used to examine material constitutive behavior depend largely on the heterogeneous nature of the material or structure and all of these methods have associated advantages and disadvantages. The goal of the present work is to provide the foundation, development and application of an experimental technique, based on Digital Image Correlation, which may be used to examine the local material constitutive behavior of materials that exhibit heterogeneity on a global scale. In particular, the study is focused on the heterogeneous structure produced by the innovative, solid-state process of friction stir welding (FSW).

The problem description is posed in the following manner. Develop a technique that may be used to qualitatively and quantitatively describe the local material constitutive behavior of a heterogeneous material from a single tensile test and demonstrate the validity of the technique, as well as all of the necessary assumptions, using numerical modeling techniques.

1.2 Scope of Research

The scope of this investigation is separated into two categories, experimental and numerical. Although the technique itself is experimental in nature, development of the numerical model is directly related to the experimental results and so the two are not altogether separable. As a result, the experimental information gathered and discussed serves the dual purposes of demonstrating the capabilities of the proposed technique and providing the necessary information for construction of the finite element model.

Experimentally, the scope of this investigation includes demonstration of the full field measurement capabilities of the digital image correlation technique in examining the local material response of friction stir welded specimens under tensile loading conditions; quantitative description of the global weld responses in tension; quantitative description of the material distribution within the welds; and quantitative description of the local constitutive behavior of the various weld regions. These topics are each studied for three different weld conditions (hot, nominal, cold) using full size tensile specimens machined from welded plates. Additionally, thin specimens, cut from full size specimens of the nominal weld, are tested to demonstrate the iso-stress assumption associated with the proposed technique.

The scope of the numerical portion of this study includes validation of the experimentally determined local material properties, through direct comparison of the local and global mechanical responses of the different welds; justification for the iso-stress assumption; qualitative limit analysis through two-dimensional plane strain, two-dimensional plane stress and three-dimensional modeling; and demonstration of the benefit and application of the numerical model. The majority of the model development focuses on the nominal weld specimen. Two-dimensional plane strain and plane stress models of the full size specimen are constructed and analyzed to demonstrate the accuracy of the experimentally determined local material properties and provide evidence for the plane stress limiting condition. 3-D models of varying widths are then constructed and analyzed to verify these findings. On the basis of the 2-D and 3-D models, both the hot and cold welds are modeled using the 2-D plane stress model. The benefit of the detailed model is shown by comparing the results with a model incorporating an "average" material description of the heterogeneous weld. Finally, the model is applied to the investigation of the effect of weld defects on the mechanical response of the nominal weld and the mechanical response of the nominal weld under three-point bending.

Chapter 2 Background

2.1 Heterogeneous Materials

In an effort to explore heterogeneity, a distinction must be made between heterogeneous material and heterogeneous body. Heterogeneous materials may occur naturally as in polycrystalline metals or be artificially created in a variety of ways: the addition of particles or fibers in the case of particle/matrix and fiber/matrix composites, or through microstructural modifications in the case of alloying and heat treatment. Mechanical alloying, thermal heat treatments and the addition of particles and fibers are all processes that result in uniform material heterogeneity and they are almost exclusively designed to improve mechanical properties. According to Hashin [1], these materials may be regarded as statistically homogeneous in the sense that it is possible to define a representative volume element (RVE) that describes the heterogeneous nature of the material and is the same at any location within the material. The resulting mechanical properties are basically "effective" properties that describe the material as a whole. The analytical determination of the effective properties of particle/matrix composites dates back to the late 19^{th} and early 20^{th} centuries and includes works by J.C Maxwell, Lord Rayleigh and Albert Einstein [1].

Inhomogeneity, in the form of an ellipsoidal inclusion in a homogeneous matrix, was examined in the seminal work by Eshelby [2]. In this work he describes the theoretical foundations for determining the elastic field resulting from the presence of the

inclusion in an infinite, homogeneous medium using the concept of transformation strain. The more general problem of estimating macroscopic properties of two-phase materials with arbitrary concentrations and arbitrary inclusion shapes, covering elastic and elastoplastic behavior, was presented by Hill [3, 4] and Mori and Tanaka [5]. These works provide the origin for many subsequent techniques based on homogenization and micro-mechanics approaches, in addition to the well known rule of mixtures in the analysis of composites, that have been developed and applied to a variety of heterogeneous materials.

Van der Sluis et al. [6] use a homogenization procedure to examine the behavior of heterogeneous elastoviscoplastic materials with arbitrary microstructures. The effects of regular and irregular microstructure as well as boundary conditions on the mechanical behavior of the RVE were examined and the results compared with finite element calculations on a completely discretised heterogeneous structure to show the validity of the homogenization method. Garboczi and Day [7] utilize effective medium theory, a homogenization approach, in computing the effective linear elastic properties of two-phase composites. A finite element based algorithm was developed for use with 2-D or 3-D digital images, acquired using light or electron microscopy for example, or simulated from microstructural models, representing the material microstructure. Reynolds and Baxter [8] examine the hardening behavior of a dispersion strengthened aluminum alloy, under monotonic and fully reversed loading, using a micro-mechanics model known as the generalized method of cells. Alloy microstructure is represented by a repeating unit cell, which is divided into homogeneous subcells containing one of the heterogeneous material components. The relationship between global and subcell strains is established

and then subcell stresses are calculated from prescribed component constitutive laws. This average constitutive relationship defines the mechanical response of the heterogeneous material. Kanda et al. [9] model the tensile response of pseudo-strain-hardening fiber-reinforced cement composites via a micro-mechanics based theoretical approach. The analytical formulas provided by the model depend on the micro-mechanical properties of the fiber, matrix and fiber/matrix interface and are utilized to predict the stress-strain response, crack spacing and flaw size distribution.

Heterogeneous bodies, in contrast, are the result of processes that produce local gradients in material properties, but are not described by statistical homogeneity as mentioned above. These bodies may be viewed as composites in the sense that they contain local variations in material properties, but they cannot be represented by a repeated element. Some typical heterogeneous bodies include laminates, functionally graded materials, cracked media and welded structures. In the case of laminates, heterogeneity is the result of manufacturing using known components. For the other examples, the components are products of processing or loading (i.e. cracks). When the components are known, and readily produced, determining the constitutive behavior is a simple task and this information may be utilized to enhance understanding of the overall behavior of the heterogeneous body. However, when the components are unknown and unique to the processing, constitutive behavior is much more difficult to come by. This is particularly the case for welded structures.

Welding, in general, is a tool used for joining structural components and has found widespread application in ferrous and non-ferrous metals [10-12]. Welding methods may be broadly categorized as either fusion processes or solid-state processes

and the selection of one process over the other is largely dependent on the materials to be used. Regardless of the method, the result of a welding process is the production of a heterogeneous structure consisting of locally homogeneous "zones" [11, 12]. Terms typically associated with welding are nugget or fusion zone, heat-affected zone and thermo-mechanically affected zone and it is these zones that govern the overall behavior of the welded structure. Therefore, it is necessary to understand and be able to predict the constitutive behavior of these zones in order optimize the process and improve the overall product.

2.2 Friction Stir Welding

Welding has been an integral part of the technological progress that continues in industries ranging from commercial construction to aerospace. With the ever-present advances in material science and technology, new welding techniques must be developed and existing techniques improved in order to accommodate new materials and achieve new standards. One of the most recent and appealing developments in the welding arena is friction stir welding (FSW). The solid-state process, derived from conventional friction welding, was invented in 1991 by The Welding Institute and arose primarily out of interest in joining the often difficult to weld aluminum alloys [13]. Friction stir welding poses a number of advantages over other welding techniques as well as some disadvantages. Welding can be performed on a standard milling machine and requires no specialized operator skill, equipment or surface preparation. As a solid-state process, there is no need for filler metal or shielding gas for aluminum and the problems of porosity, cracking and distortion associated with fusion welds may be avoided. However,

the forces needed to accommodate the frictional heating and plastic deformation require large reactive forces and support. In addition, the process may prove slower than other techniques and in some situations require additional welding techniques to fill the hole left at the end of the weld.

Detailed descriptions of the process [13-16] describe it as a combination of extrusion and forging. A rotating cylindrical tool is plunged into the material and traversed along the joint line. The tool is designed with a large diameter shoulder and a concentric smaller diameter pin. Figure 2-1 shows a schematic of the process and some associated nomenclature. Frictional heating caused by the relative motion of the pin and shoulder with the work piece creates a volume of plasticized material under the tool. The temperatures achieved during welding are lower than the material melting point, but high enough to reduce the material flow stress so that as the tool is rotated and moved along the joint, the softened material is extruded around the pin and then forged behind the pin under the downward force of the shoulder. Although the actual material flow is not completely documented, FSW produces defect free welds with exceptional mechanical properties. As with any new process development however, a great deal of research is required to advance the knowledge and understanding of the FSW technique. Current efforts in friction stir welding are focused on process modeling, material flow behavior, microstructure, and mechanical properties.

The development of process models is necessary for understanding the physics of the process and providing useful feedback for future improvements. Efforts in this area are paralleled by experimental techniques designed to provide evidence of the actual material flow. Reynolds et al. [17] describe a marker insert technique for post-weld flow

visualization. This technique utilizes markers of a material different than the weld metal inserted in the weld path at various locations through the weld thickness. After welding, a slice of the surface is milled off and etched to reveal the location of the deformed markers. The surrounding region of each marker is then captured in a digital image.

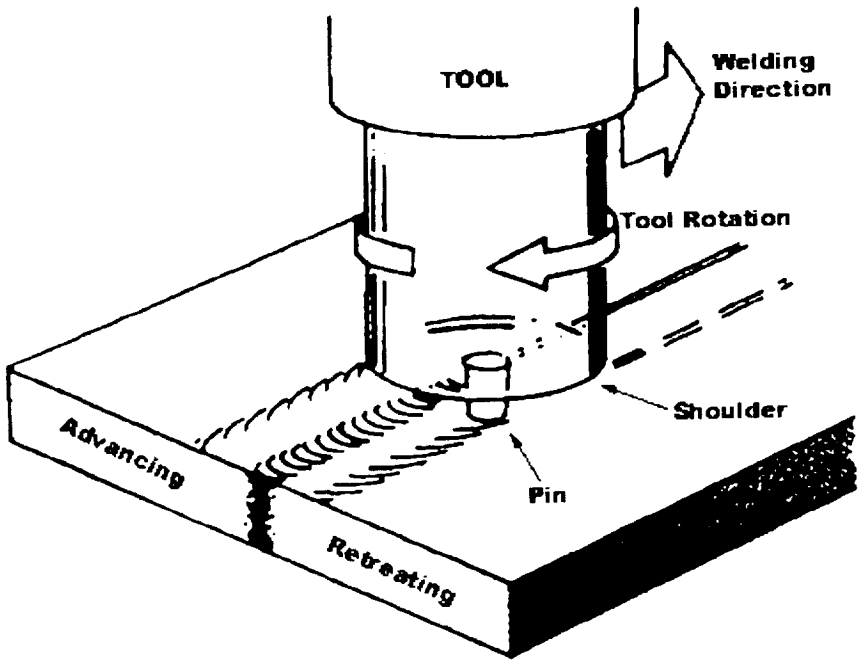

Figure 2-1 Schematic of the Friction Stir Welding process and some of the associated nomenclature.

This process is repeated until the entire weld thickness has been removed so that a three-dimensional image of the deformed material is created. A similar method demonstrated by Bernstein and Nunes [18] uses an array of copper wire markers inserted in the contact surfaces. Radiographs of the deformed markers show the general appearance reported by Reynolds et al [17]. Colligan [15] utilizes a shot tracer technique in which steel shot is

placed in a machined groove along the faying surface. Welding is carried out and then stopped prematurely so that there is undisturbed shot ahead of the weld end. The weld is then radiographed to reveal the location of the tracer material. The welding of dissimilar materials is another method used by Li et al. [19,20] to reveal material flow patterns in FSW. This technique relies on the different etching characteristics of the materials to reveal the complex features characteristic to this process. Experimental flow data and temperature profile data are needed to develop and validate the various process models that are currently being developed. Chao and Qi [21] outline thermal and thermo-mechanical finite element models to investigate the temperature fields, residual stresses and distortion associated with FSW. The thermal model uses experimental temperature data to calculate the thermal history for the particular FSW parameters, and then the thermal history is used as input for the thermo-mechanical model. Smith et al. [22] use a fluid mechanics based model to study the heat generation and material flow in FSW. This approach was adopted from previous efforts in modeling friction welding and aluminum extrusion processes.

As a solid-state process FSW does not involve melting, however, the base metal microstructure is altered and shares some similar characteristics with fusion welds. Figure 2-2 shows a typical FSW and the associated microstructural regions. The nugget or dynamically recrystallized zone, DRZ, and the region directly above (flow arm), which corresponds to the fusion zone, contain recrystallized grains as a result of high temperatures and extreme plastic deformation. Adjacent to the DRZ and flow arm is a region, the thermo-mechanically affected zone (TMAZ) as described by Mahoney et al. [14], that has experienced high temperatures and plastic deformation, but to a lesser

degree than in the DRZ. The heat-affected zone (HAZ), the region that has experienced high temperatures only, extends from the boundary of the DRZ and TMZ and transitions to the base metal with little noticeable change in microstructure at magnifications achievable with the optical microscope.

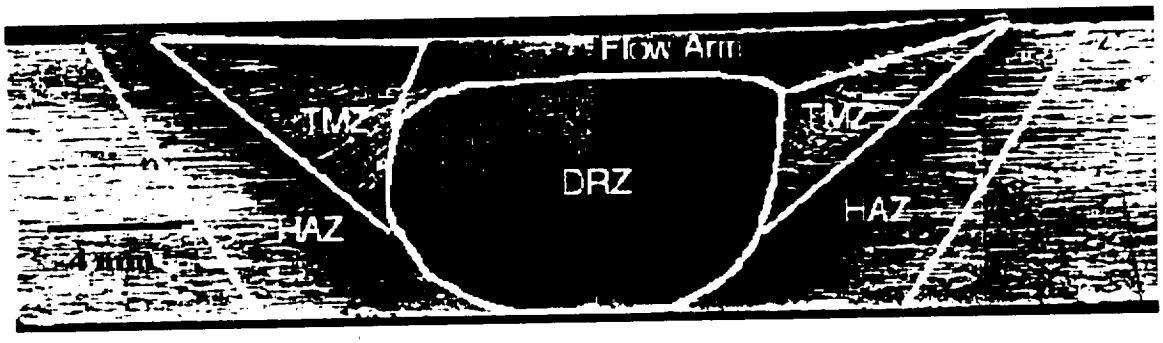

Figure 2-2 Typical microstructure of a Friction Stir Weld showing several distinct weld regions.

It is obvious from Figure 2-2 that FSW creates a heterogeneous structure composed of nominally homogeneous regions (i.e. Base metal, HAZ, TMZ, DRZ). Each zone has experienced some form of thermal or thermo-mechanical cycle and as a result there exists property gradients in both the thickness and transverse directions. The property gradients are undoubtedly related to the microstructural gradients and because the property gradients govern the overall mechanical behavior of the weld, these two issues should be examined together. However, much of the work in microstructural characterization is centered on defining the characteristics of the local weld regions and the corresponding microhardness. This is demonstrated in a number of papers [14,23-26] in which microstructures associated with hardness profiles are characterized for several alloys utilizing transmission electron microscopy (TEM) to identify grain sizes,

precipitate distributions and dislocation densities. Although microhardness is a property, it gives only a qualitative measure of the materials resistance to plastic deformation. The local stress-strain response is needed to determine the local material properties and most of the studies examining mechanical properties are focused primarily on the overall mechanical response in tension and fatigue.

Bussu and Irving [27] and Biallas et al. [28] examine the fatigue performance of friction stir welds in AA2024-T3 to observe the role of surface features and hardness in fatigue initiation. Kinchen et al. [29] study the tensile properties, at room and cryogenic temperatures, and fracture toughness of AA2195-T8 FSW. Mahoney et al. [14] evaluate the effects of FSW and a post weld aging treatment on the tensile properties of AA7075-T651. Longitudinal specimens containing only nugget material were tested in the as-welded and post-weld aged conditions to compare nugget and base metal properties. Transverse specimens containing the entire weld were also tested in as-welded and post-weld aged conditions for comparison with base metal properties. In addition, the local normal strain distribution at failure, within the different zones, was examined by measuring the displacement of finely spaced parallel lines applied to the specimen surface. For the most part, the studies of the mechanical properties of friction stir welds, and heterogeneous materials in general, are concerned with overall or global properties because it is difficult to examine the different components separately. However, because of the link between the local and the global mechanical behavior, it is necessary to develop methods of determining the local constitutive properties in order to improve the product and the process.

2.3 Constitutive Property Determination Techniques

The ability to effectively determine the material behavior of the homogeneous components of heterogeneous structures is a difficult but necessary task for the complete understanding of the overall mechanical response. The difficulty arises due to the limited sizes of the component regions and the fact that in many cases the regions are the result of the processing and cannot be duplicated individually. The necessity for this information has however, led to the development of several techniques designed to measure the local material response of heterogeneous structures.

2.3.1 Microtensile Specimens

The most common method for determining the mechanical response of a material is the tensile test. Typically this requires bulk material from which tensile specimens are machined. In the case of heterogeneous materials, such as welds, the bulk materials of interest are the various weld zones; the sizes of these zones are typically very small and there is no bulk quantity of HAZ or TMZ material available. The idea behind the microtensile technique is to machine small tensile specimens, containing only the desired material, from the various weld regions for use in standard tensile tests. This technique has been applied to the study of several different welded structures and welding processes.

LaVan [30] examines the microtensile technique in determining the local properties of heterogeneous and anisotropic materials. Microtensile specimens, roughly 0.5mm thick and 0.2mm wide, are extracted from various regions of a GMAW (gas metal arc weld) in a steel plate and tested in a miniature tensile test machine. Specimen

preparation involves first cutting 0.5mm thick slices from the weld using wire-EDM. Individual "bow-tie" samples, designed to fit specialized grips to avoid specimen deformation during clamping, are then cut and polished. Specimen strain is measured directly on the sample using a laser interferometry technique, which involves measuring the interference fringes created by the laser reflection from two mirohardness indents. The stress-strain response from each weld region is measured directly from the tensile test and subsequent material properties are determined. Cam et al. [31] utilize microtensile specimens for determining the local mechanical properties of laser beam welded joints in steel. A block of material with the weld in the middle is first removed and then flat specimens (0.5mm thick and 2mm wide) are cut, parallel to the weld, from the base metal, HAZ and weld metal using a spark erosion cutting technique. Tensile tests are carried out on a screw-driven universal test machine and special loading, using high strength pins at the specimen shoulders, is introduced due to the small specimen size. The microtensile technique is then verified by comparing the stress-strain response of base metal microsamples with the response of standard size round base metal samples. Rak and Treiber [32] study the local strength variations in SAW (submerged arc weld) in steels. Miniature tensile specimens machined from different locations within the weld are tested in order to compare local material properties with base metal data. Von Strombeck et al. [33] examined the local mechanical properties of FSW in 2xxx, 5xxx, 6xxx and 7xxx series alloys using microtensile specimens machined from the various weld zones.

The ability of the microtensile technique to provide the local stress-strain response from heterogeneous structures is an obvious benefit. However, the technique has some drawbacks. The technique is destructive and a complete description of the

property gradients associated with a heterogeneous structure involves multiple tests. Specimen preparation requires specialized equipment, operator skill and time, and if very high property gradients exist in the weld there may be no guarantee that the specimen is homogeneous. Special fixturing is also needed for loading and gripping in order to avoid damaging the specimen and in some instances special methods for strain measurement must be employed.

2.3.2 Instrumented Ball Indentation

Hardness measurements are widely used as a measure of a materials resistance to plastic deformation. The small size of typical indenters is well suited for determining a qualitative picture of material property gradients in heterogeneous materials. This is the premise behind the development of an automated ball indentation (ABI) technique for determining the mechanical behavior of heterogeneous materials.

According to Mathew et al. [34], the ABI technique is based on the initial work of D. Tabor in which the correlation of spherical indentation hardness and strain with uniaxial tensile results is developed. The correlations are founded on the assumptions that the monotonic true stress-true plastic strain curves from tension and compression tests are similar; indentation strain correlates with true plastic strain in uniaxial tension; and mean indentation pressure correlates with true flow stress in uniaxial tension. The technique involves a series of indentation cycles, loading followed by partial unloading, made at a single location and the corresponding measurement of load and penetration depth. Elasticity and plasticity theories, in conjunction with semi-empirical formulas describing material behavior under multiaxial indentation loading, are then used to calculate the

incremental stress-strain values from the load-depth data. Mathew et al. [34-36] employ the Stress-Strain Microprobe (SSM) system, based on the ABI technique, for fully automated determination of material properties in steel, molybdenum and a superalloy.

Mechanical property gradients in steel welds were determined by Murty et al. using the ABI technique to investigate the degree of embrittlement in rector pressure vessels [37]. Tests are conducted over a wide temperature range and the ABI results are compared to results from tensile tests on micro-tensile specimens and correlated with observed microstructural gradients. Malow and Koch [38] and Malow et al. [39] examine the mechanical behavior of nanocrystalline materials using the ABI technique. Several grain sizes in nanocrystalline iron, corresponding to different compaction parameters and annealing temperatures, are tested to determine the effect of grain size on the tensile and compressive mechanical behavior. A similar study by Huber and Tsakmakis [40] outlines the use of neural networks in determining material constitutive properties from spherical indentation data. Hysteresis loops in the indentation load-depth data are used as a measure of material hardening and associated with material constitutive parameters. Neural networks are then used to solve the inverse problem of determining the constitutive parameters from the load-depth data.

Techniques employing spherical indentation data are relatively non-destructive; they can be fully automated; and provide a method for determining point-to-point variations in mechanical properties. The technique does require several assumptions involving material behavior and the relationships between indentation stress and strain and uniaxial tensile stress and strain, as well as semi-empirical formulas for determining the true stress and true strain values. In addition, residual stresses, which may be

significant in welded materials, are not accounted for. Depending on the magnitude, variation and sign, either tensile or compressive, residual stresses would greatly affect the indentation response of the material.

2.3.3 Weld Thermal Simulation

An alternative approach to testing small volume samples, such as weld metal, HAZ material etc., is to develop a technique for creating bulk material that simulates the actual material. The weld thermal simulation method relies on the idea that the welding process essentially produces the various weld zones through different heat treatments. Therefore, using temperature measurements from the actual welding process, thermal cycles can be developed and used as guidelines to create simulated weld materials.

The basic assumption in weld thermal simulation, according to Zuniga and Sheppard [41] is that if the real and simulated materials have matching hardness and grain sizes, then the mechanical responses will match. Zuniga and Sheppard utilize the thermal simulation technique in determining the HAZ constitutive properties for resistance spot-welds in steel. Simulated HAZ material is created using the same resistance spot welder that created the actual weld. Using a modified electrode, simulated samples are created using a trial and error process of weld current and time combinations. Samples are tested for microstructure and hardness until the desired results are obtained. Tensile specimens, machined from the simulated material, are tested to determine the material response. Hval et al. [42] apply the weld thermal simulation technique to determining the constitutive properties of the various zones in an aluminum weldment. Material simulation was performed using a Gleeble 2000 weld thermal simulator and

followed by hardness measurements to show correspondence with the real weld material. Tensile tests are performed on the simulated specimens to develop true stress - true strain curves for each material. Wang [43] describes an in situ technique for observing dynamic fracture and damage microprocesses using microtensile specimens machined from simulated weld material. A Gleeble 1500 thermal simulator is used to simulate the coarse-grained heat affected zone (CGHAZ) material found in high strength low alloy steel welds. Tensile tests are performed in a scanning electron microscope outfitted with a tensile platform and damage and fracture processes are recorded on photographs. A similar study on the CGHAZ material of steel welds by Rak et al. [44] is used to examine the effect of welding on material toughness. The simulated material is made using a Smitweld thermal cycle simulator. Subsequent tensile tests are run to determine mechanical properties and material toughness is measured using Charpy impact and CTOD tests.

Thermal simulation provides bulk material for mechanical testing thereby eliminating the need for specialized machining and cutting. However, the technique does require thermal simulation machines and detailed information regarding the thermal history associated with the welding process in order to develop the proper thermal cycles. In addition, each sample must be examined for microstructural characteristics and hardness values to determine whether or not the simulated material matches the real material. This often results in a trial and error process of simulation and examination until the desired results are obtained. Furthermore, in relation to the applicability of this technique to friction stir welding, the microstructures produced by friction stir welding

result from both mechanical and thermal cycles and may not be reproducible solely through thermal simulation.

2.3.4 Digital Image Correlation Technique

The technique proposed in this study is designed to provide an accurate, efficient and relatively fast method for determining the local constitutive behavior of heterogeneous materials from a single transverse tensile test using digital image correlation and numerical modeling. It is a continuation and development of previous work by Reynolds and Duvall [45] on the determination of weld and base metal constitutive behavior using digital image correlation. Motivation for the development of this technique arises from the obvious effects of local property gradients on global mechanical behavior and from the need to understand and accurately predict the mechanical response of heterogeneous materials.

The proposed method relies on an image analysis technique to determine full field displacement measurements as a function of global applied tensile loading. Digital image correlation (DIC) is an optical, full field displacement measurement technique that has been used to successfully measure surface displacements in homogeneous materials [46-48]. As the name suggests, DIC involves comparing digital images to determine the relative displacement of surface features between "un-deformed" and "deformed' images. Different "gray levels" represent surface features in the digital images and in order to obtain correlatable images the specimen surface must have sufficient contrast. This is accomplished by the application of a random speckle pattern using black and white spray paint. The task of correlation amounts to comparing "subsets", small windows within the

digital images, to determine the relative displacement between deformed and un-deformed states and requires a method of error measure for gray level comparison and a search method to define a unique pattern of comparison [49].

Cross correlation, a standard method of error measure used in DIC, uses a correlation function to provide an error measure between 0 and 1 with 0 representing a best match [47]. A typical correlation function is shown in Eq. (2.1):

$$S(x, y, u, v, \frac{\partial u}{\partial x}, \frac{\partial u}{\partial y}, \frac{\partial v}{\partial x}, \frac{\partial v}{\partial y}) =$$

$$1 - \left[\frac{\left(\sum Gray(x, y)_{undeformed} * \sum Gray(x', y')_{deformed} \right)}{\sqrt{\sum Gray(x, y)^2_{undeformed} * \sum Gray(x', y')^2_{deformed}}} \right] \quad (2.1)$$

where $Gray(x,y)_{undeformed}$ and $Gray(x',y')_{deformed}$ refer to the gray levels of a pixel in the undeformed and deformed images, respectively; u, v, $\frac{\partial u}{\partial x}, \frac{\partial u}{\partial y}, \frac{\partial v}{\partial x}, \frac{\partial v}{\partial y}$ are the deformation parameters; and (x,y) and (x',y') are coordinates related to the deformation the object experienced between acquisition of the undeformed and deformed images. In order for the displacement measurements to have any physical meaning, a relationship between the change of intensity patterns and the deformation of the real object must be assumed [50]. The assumption states that each subset in the deformed image is related by a homogeneous linear mapping to a subset of the same size in the undeformed image and also that the subsets deform as the actual object deforms as long as the motion of the object is parallel to the image plane. The linear relationship between the deformed and undeformed subsets is given by Eq. (2.2):

$$x' = x + u + \frac{\partial u}{\partial x}\Delta x + \frac{\partial u}{\partial y}\Delta y$$
$$y' = y + v + \frac{\partial v}{\partial x}\Delta x + \frac{\partial v}{\partial y}\Delta y \qquad (2.2)$$

where (x',y') and (x,y) are the deformed and undeformed position, respectively, of an arbitrary point; u and v are the displacements of the subset center and Δx and Δy are distances from the subset center to the arbitrary point.

Based on the description above, the goal of image correlation is to determine the deformation parameters that minimize the correlation function, which requires a search method. Early techniques employed a coarse-fine search method that tried many possible combinations of the deformation parameters within a given range and compared the result for each combination. This method, however, was computationally expensive due to the large number of calculations required. A much more robust technique utilizing the Newton-Raphson method involves the calculation of corrections for initial guesses in an iterative process that greatly improves convergence and reduces computational costs [47].

By correlating numerous points in an image, a displacement field for the image can be produced. The process is automated by the use of software, which was developed at the University of South Carolina. The software allows the user to define the subset size and correlation area, among other things, based on the un-deformed image. Therefore, correlation is limited to surface features that are present in all images.

Digital images of a specimen are acquired before (un-deformed) and during (deformed images) the tensile test at specified intervals of global applied load or specimen strain using an image acquisition system. Each deformed image is correlated with the un-deformed image and the displacement field is determined. Once the full field

displacements are known, full field strain data may be determined in any number of ways. Reynolds and Duvall [45] use a simple method of fitting a polynomial function to a plot of the displacement versus position in the loading direction for a particular line of interest on the specimen. The first derivative of the fitting function with respect to the loading axis determines the strain in that direction, the normal strain in this case. An alternative method involves fitting a surface to the u, v displacement field and then computing the gradients of the displacements to determine the normal and shear strains at any chosen location. Reynolds and Lockwood [51] demonstrate this method in examining the full field strain development of friction stir welded aluminum alloys under uniaxial tension.

In order to construct the stress-strain response using the proposed technique, a simplifying assumption must be made regarding the loading conditions. For a homogeneous material with constant cross-section under uniaxial loading, the applied load, and hence stress, is the same at every cross-section, perpendicular to the loading direction, within the material. However, for heterogeneous materials the local stress is not necessarily constant at every cross-section if property gradients exist such that every cross-section normal to the loading direction is not homogeneous, as is the case with welded structures. Therefore, the assumption that must be made is that the material is treated as a composite material undergoing a nominally iso-stress loading condition. Using this assumption the engineering stress, calculated from the global applied tensile load and original cross-sectional area, is known at every specified load or strain interval and is constant at every location within the specimen. Stress-strain curves are then constructed by extracting the local strain and global stress data, at each interval, from

virtually any point of interest. Once the material behavior is determined, relevant material properties such as elastic modulus, yield strength and tensile strength are readily obtainable. These properties can then be examined as a function of position within the material and eventually related to the material microstructure.

The proposed technique displays many advantages compared to the other methods described above. The potential for detailed local strain analysis at any point in the material is limited only by the spatial resolution of the imaging system and the applied speckle pattern. In contrast to weld thermal simulation, there is no uncertainty regarding whether the material being tested is representative of the real material because the material being tested is the real material. Since material behavior is determined directly from tensile testing, no prior knowledge of material properties is required as in the ABI technique. Finally, in contrast to the micro-tensile method, all the necessary information for obtaining the local constitutive behaviors of a heterogeneous material may be determined from a *single* transverse tensile test.

As with any experimental technique, there are some associated disadvantages. The loading condition must be assumed to be iso-stress in order to construct the stress-strain curves from the global applied load. Therefore, the accuracy of the measured constitutive behavior is determined by the degree of non-homogeneity at all cross-sections to which the load is applied. In addition, the strain range over which the constitutive behavior of a particular region is measured is limited by the strength of the weakest region.

2.4 Modeling

Analytical and numerical models play an important role in the study of many physical problems, especially in the area of welding. Models are used as tools to gain insight into the physical processes of the problem being studied that would otherwise be too costly or impossible to obtain through experimental procedures. In the study of welded components, much of the current work is involved in failure analysis and in the determination of the mechanical properties of the various zones that comprise a weld.

Several studies have been performed regarding the effect of yield strength mis-match on the fracture behavior of welds that incorporate both analytical and numerical models. Hao et. al. [52] and Kim and Schwalbe [53, 54] examine the effect of yield strength mismatch in the determination of the limit load, which is an important parameter in estimating crack driving force, for several specimen geometries containing an idealized weld and a crack. In their analyses, the weld is viewed as a bi-material system consisting of elastic-perfectly plastic base and weld materials. Analytical solutions for the limit load of several specimen geometries are developed using slip-line field analysis and compared with 2-D and 3-D finite element solutions.

Hval et al. [42] studied ductile fracture in aluminum welds using finite element models that incorporated a micro-mechanics model for simulating growth and coalescence of microvoids. Two-dimensional and 3-D models are used to simulate the transverse tensile response of an aluminum weld containing base material, weld metal and four HAZ materials arranged in series. A user-defined subroutine is used to define the material behavior demonstrated by experimental results of thermally simulated tensile specimens. The axisymmetric model employs a non-uniform mesh to approximate the

orientation of the weld metal/base metal boundary, a reduced diameter around the weld to insure necking, and contains a grip section at the edge of the gage length.

Matic and Jolles [55] examine failure prediction in steel welds using finite element analysis and critical strain energy density concepts. They describe a 2-D model of a transversely loaded steel weld consisting of base metal, weld metal and four HAZ materials arranged in series. Base metal and weld metal behavior are determined from tensile data on the respective materials, while the different HAZ material behaviors are constructed from base metal data.

Local material properties within the heat affected zone of a resistance spot weld are determined by Zuniga and Sheppard [41] using finite element analysis. A 3-D, axisymmetric model is constructed for extracting flow curves from notched-bar transverse tensile test data for thermally simulated weld metals. An iterative correction procedure is developed to adjust the uniaxial tensile stress to compensate for the triaxial stress state associated with necking. Models of the simulated materials contained two material zones; one modeled as linear elastic and the other modeled as elastic plastic.

The numerical modeling component of the proposed technique serves a dual purpose. A certain amount of error, associated with the iso-stress assumption, is to be expected in the material properties determined using this technique. Finite element analysis is used to verify these properties by providing a tool for simulating the mechanical behavior of a material with known properties. The heterogeneous material is modeled using the measured property distributions and the simulated tensile test is run. Model results, in terms of local and global mechanical response, are compared to the experimentally determined results to gauge the accuracy of the measured properties and

demonstrate the models predictive capabilities. Once the material properties have been accurately determined, the model then becomes a predictive tool that may possibly be used to examine a number of interesting topics. Such topics may include studies on the effects of varying the property gradients, which could be coupled with microstructural development models to provide invaluable information for process development; studies on the effects of defects on the mechanical response; examination of the actual stress state in the vicinity of failure; and the mechanical response under different loading conditions. The finite element model proposed in this study is designed to simulate the mechanical response of a heterogeneous, transversely loaded tensile specimen using the ABAQUS finite element software. The specific heterogeneous material for which the model is applied is a friction stir weld in aluminum alloy 2024-T351.

The degree of heterogeneity produced by the FSW process is evident from the macrograph of the typical FSW specimen shown in Figure 2-2. Material property and microstructural gradients exist in the transverse and thickness directions and there is noticeable lack of symmetry about the weld centerline. Therefore, discretization of the domain is based on the desire to accurately model the property and microstructure distribution associated with the FSW sample. Tensile specimen dimensions, corresponding to the gage section, are used to define the domain boundary and a uniform mesh is created in order to achieve the necessary resolution required to capture the microstructural and property gradients in the weld. The material behaviors assigned to the various weld regions come directly from the experimentally measured material properties and define the elastic and plastic response of each material.

2.5 Summary of Literature Review

A review of the literature has shown that, in the study of the mechanical behavior of heterogeneous materials, a definite interest and need exists for the accurate determination of local material properties. This need has given rise to the development of many techniques designed to provide this information, each of which is applicable to a particular scale of heterogeneity. For the case of material heterogeneity on a global scale, which includes structures produced by welding processes, the current techniques used to determine local material properties include testing of microtensile specimens, testing of thermally simulated materials, instrumented ball indentation and the proposed image correlation technique.

The information presented in the literature provides a good description of the different techniques and demonstrates the advantages and disadvantages associated with each. Most of the applications of these techniques involve welds and determining the properties of a few of the weld regions, and in some cases the local results are compared to experimental results from testing of simulated material or microtensile specimens. Verifications of the locally measured properties, through simulation of the global response of the heterogeneous materials, are only demonstrated in a few cases. The finite element models that do present global behavior display good results, however, the descriptions of the welds are relatively simple in terms of the number of weld materials and the weld geometry and comparisons with more detailed models were not provided. Also lacking in the literature is a comparison of results, for a given heterogeneous material, from all of the different techniques. Due to the unique nature of the materials

investigated and the specific equipment required for the individual techniques, this may prove difficult to come by, but it would provide a valuable comparison.

Chapter 3 Materials and Experimental Procedures

3.1 AA-2024 T351

In this work friction stir welds in aluminum alloy 2024 T351 have been chosen as a representative heterogeneous material. This alloy is a precipitation hardened aerospace material with a nominal composition (wt.%) of 4.4Cu-0.6Mn-1.5Mg-balance aluminum. Base metal microstructure, shown in Figure 3-1 consists of recrystallized, slightly elongated grains. The base material is supplied as 9.53 *mm* thick plates in the T351 condition, a temper in which the material is solution heat treated, stretched and naturally aged. Base metal mechanical properties are listed in Table 4-1.

3.2 Welding Procedure

All welded specimens used in this study were produced at the University of South Carolina on either a vertical milling machine or on the FSW Process Development System (PDS), a "milling" machine designed specifically for friction stir welding by the MTS Corporation. The vertical mill is a standard milling machine with a tilting head capability, 15 HP spindle motor and manual and automatic x, y, z controls. This setup enables welds to be made in displacement control only, meaning that the FSW tool is fixed at a constant position throughout the welding process.

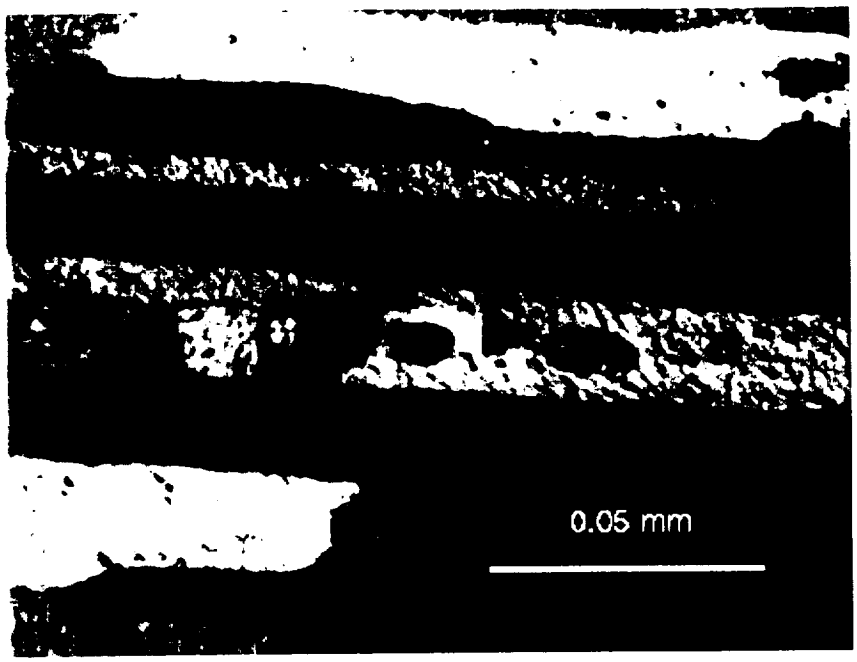

Figure 3-1 AA 2024 Base metal microstructure.

The PDS is a computer controlled friction stir welding machine equipped with z-axis load cell, tilting head capability and a complete data acquisition system. This setup allows operation in either displacement or load control and allows for much greater control and feedback of process variables. Regardless of which machine was used, the process parameters were consistent in producing welds of equal quality and characteristics. A single FSW tool was used for all of the welds. The FSW tool, fashioned from oil hardened tool steel, has shoulder and pin diameters of 25.4 *mm* and 10 *mm* respectively (see Figure 3-2).

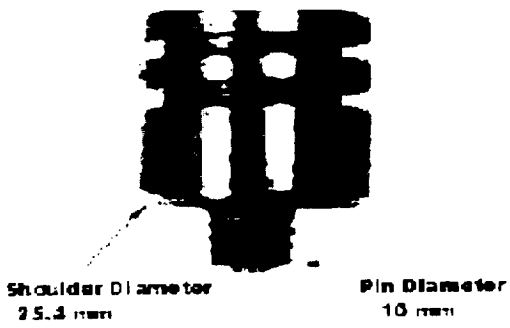

Figure 3-2 Friction Stir Welding Tool.

Weld preparation for both machines was identical and is described below. The mill table contains a recessed section to hold the steel backing plate used to constrain the material from flowing out the bottom of the weld, several T-slots used to hold the clamping fixtures, and centering pins to act as guides for plate alignment. Prior to welding, the original plates were machined to a nominal thickness of approximately 8.1 *mm*. The two plates to be welded were cleaned with a de-greaser and placed on the backing plate in a butt-weld configuration. Using a scrap block of material, the tool was firmly seated in the milling chuck by applying suitable pressure to the shoulder surface. The tool pin was centered on the joint line at one end and traversed the length of the weld to ensure proper alignment of the plates. Clamps, spaced evenly along the length of each plate, were tightened with a torque wrench to apply sufficient restraint so that the plates did not move during welding. For a given tool, the depth of shoulder penetration determines the forging pressure. The forging pressure controls the weld consolidation between the pin and backing plate and hence the type of weld produced, either full or

partial penetration. Shoulder penetration was set prior to welding using a feeler gage to fix the pin/backing plate clearance.

The welds produced for this study were all single pass welds made using the tool and setup described above. Tool-to-workpiece angle was fixed at 2.5°, and the spindle speed and feed rate, measured in revolutions per minute (RPM) and inches per minute (IPM) respectively, are selected. The labeling schemes for the welds in this investigation were based on the specific weld energy or energy per unit weld length (EPUWL) required to make the weld. For example, a set of parameters is chosen to make the baseline, or "*nominal*" weld, and then the parameters are changed accordingly to produce higher energy input ("*hot*") or lower energy input ("*cold*") welds. The welding schedule listing the actual weld parameters is shown in Table 3-1.

Once the setup was complete and the parameters set, the rotating tool was plunged into the joint at one end of the plates. Plunging was done slowly to avoid possible damage to the tool and allow for some temperature increase to develop in material surrounding the pin as a result of frictional heating between the pin and the work. When the desired shoulder penetration was reached, the tool was traversed along the joint line at the set feed rate. After welding, the tool was removed from the work and the clamps were removed. Each welds was then inspected for visible flaws and labeled.

Weld Designation	Weld Number	RPM	IPM	EPUWL (J/mm)
Nominal	172	360	4 7/16	1143.848
Hot	180	360	2 5/8	1940.998
Cold	219	215	7 11/16	967.750

Table 3-1 Weld schedule for AA 2024 Friction Stir Welds

3.3 Mechanical Testing

The mechanical testing carried out during this study consisted of tensile tests that either did or did not include the simultaneous acquisition of images for the DIC tests. Although the test equipment was the same in both cases, the preparation and procedures for the non-DIC and DIC tensile tests were different and are described below.

3.3.1 Non-DIC Tensile Testing

Standard size transverse tensile specimens [56] were machined from the welded plates for testing in a 100-kN servo-hydraulic universal test machine. These dogbone specimens were 210.82 mm long with a gage length of 58.42 mm and a gage width of 12.7 mm. A fillet radius of 12.7 mm was used for the transition to the gage section. All specimens were made with the weld centered in the gage section and oriented so that the load was applied normal to the welding direction.

A PC based data acquisition system was used to control machine operation and data recording. The control and acquisition software was written using LABVIEW, and the inputs and outputs from the computer to the test machine were connected through a BNC board. Three input channels, corresponding to load, displacement and strain were

monitored throughout the test. All tests were performed at ambient temperature in displacement control with a nominal, initial strain rate of 10^{-3} s^{-1}. Global specimen strain was measured directly with a 25.4 *mm* gage length extensometer.

Non-DIC tensile tests were performed in the following manner. (1) The cross-sectional dimensions are measured. (2) With the machine running, the specimen is placed in the spring-loaded grips. (3) The extensometer is attached to the through-thickness surface of the specimen such that the extensometer gage length spans the width of the weld. (4) The strain transducer is zeroed and (5) the test is started. (6) Load, displacement and strain data are recorded continuously until the specimen fails and the test is completed.

3.3.2 DIC / Tensile Testing

The DIC tensile test procedure involves some specimen preparation and a second acquisition system for recording images, but otherwise follows the same procedures as the non-DIC tensile test. (1) The specimen is measured for cross-sectional dimensions and then prepared for application of the speckle pattern by cleaning and drying the surface to be viewed. (2) A background coat of white spray paint is applied, completely covering the surface, and then followed by an over-spray of black paint. The scale of the pattern depends on the spatial resolution desired and hence, the magnification used to view the pattern. (3) Two marks are placed on the specimen using a permanent marker, typically at the edges of the weld representing the shoulder diameter, to indicate the image magnification.

The image acquisition system consists of a black and white, 8-bit CCD digital camera with a 768x484 pixel sensor array and 200 *mm* telephoto lens mounted on a tripod equipped with translation stages, and a PC with imaging software for recording the images (see Figure 3-3). The camera is positioned as far away from the specimen as possible to maximize the working distance and minimize the effects of out-of-pane motion. In each test the camera is oriented with the long axis of the image corresponding to the length of the specimen, thereby maximizing the available field of view. The prepared specimen is placed in the grips and the camera is positioned so that the image contains the desired field of view. All specimens are placed in the grips so that loading and orientation in the images is consistent between tests.

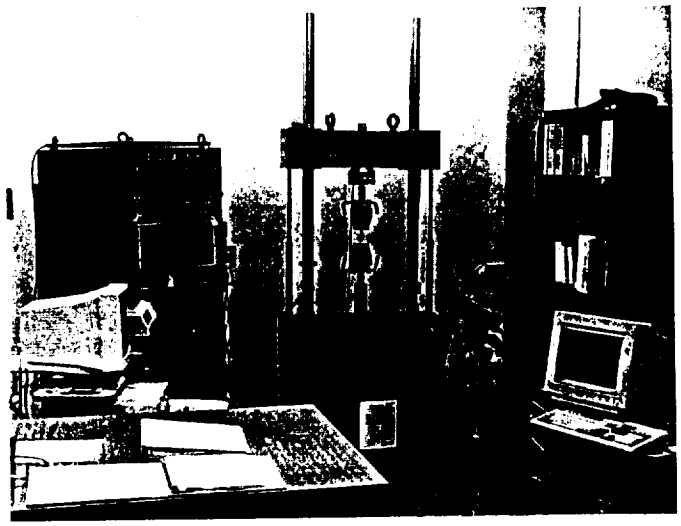

Figure 3-3 Mechanical testing lab with data and image acquisition systems.

Due to the nature of the DIC test, namely the measurement of in-plane surface displacements, the line of sight of the camera must be normal to the specimen surface. By viewing the live image of the specimen, the misalignment is determined by the amount of

specimen visible in the depth direction (i.e. normal to the image plane, see Figure 3-4) and then corrected by rotating the tripod and translating the camera. Once the camera and specimen are properly aligned, the initial, "un-deformed" image is captured. In order to maintain as much of the original field of view as possible during the test, a landmark is chosen at the center of the image and kept roughly in its original position by translating the camera, in a direction parallel to the motion of the landmark, when necessary. The tensile test is started and the subsequent "deformed" images are captured at specified load or displacement intervals until the specimen fails or the speckle pattern breaks down. Global specimen strains are determined from the measured displacement fields.

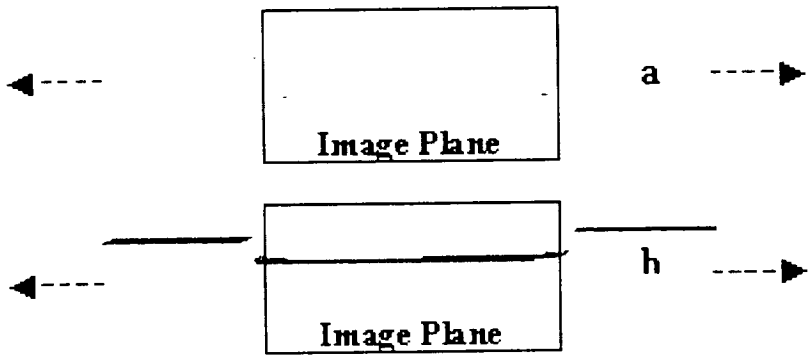

Figure 3-4 Camera-Specimen Alignment. (a) Aligned, (b) Misaligned

3.3.3 Full Thickness and Reduced Thickness Specimens

One of the major benefits of the proposed technique described previously is the ability to obtain local constitutive data from a heterogeneous material using a single transverse tensile test. In the development of this technique, however, it was necessary to examine two different specimen configurations; full thickness and reduced thickness

specimens. Although the specimen thickness varied between the two configurations, in both cases the entire weld region was maintained so that each specimen contained all of the various weld zones.

In order to completely capture the local effects associated with the heterogeneous material from a single test, full size or full thickness specimens were required. Full size refers to the dimension corresponding to the plate thickness and, hence, these specimens included both the top (crown) and bottom (root) of the weld. Standard dogbone specimens were machined from each weld, with a transverse orientation as shown in Figure 3-5.

As a part of the requirement to justify the iso-stress assumption used in the technique, reduced thickness specimens were machined from full size *nominal* weld specimens to provide a more accurate representation of the iso-stress loading condition. The goal was to reduce microstructural gradients from the top to bottom of the specimen, thereby improving the chances of obtaining true homogeneous cross-sections throughout the specimen. Three reduced thickness specimens were machined from full size specimens at locations near the top, middle and bottom of the weld as shown in Figure 3-6. Due to the undermatched nature of the welds, which implies the weld strength is lower than the base metal strength, straight-sided specimens were used rather than dogbones without the danger of failure outside the gage length.

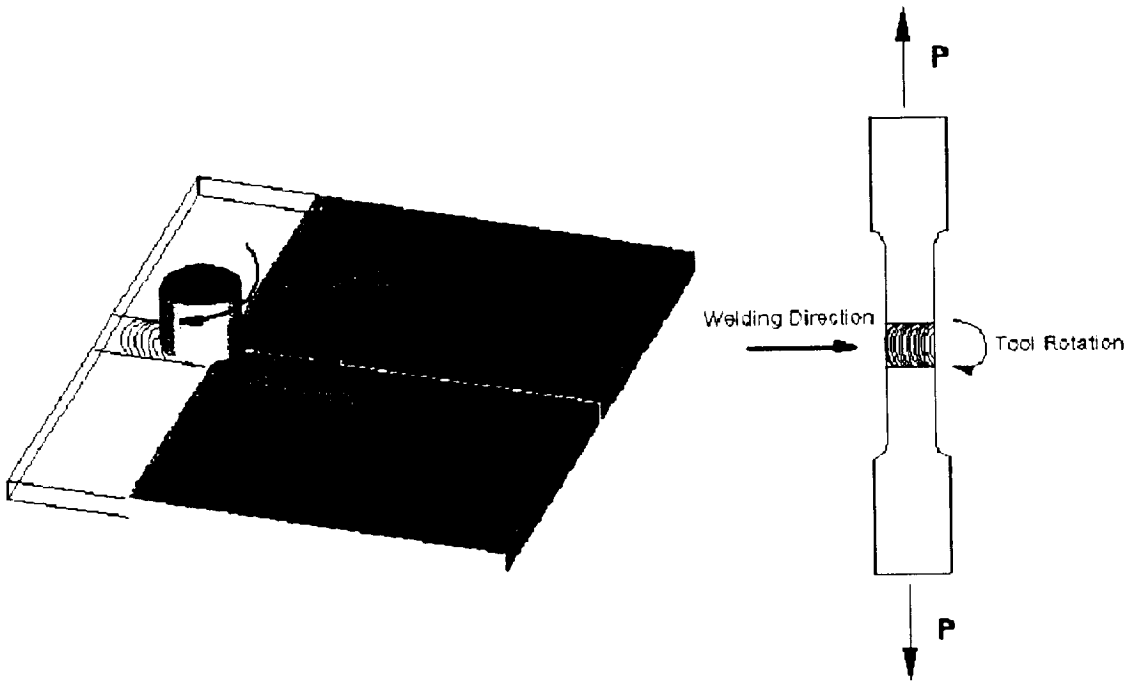

Figure 3-5 Full thickness specimen cut from welded plate. Specimen is oriented so that loading is transverse to the welding direction.

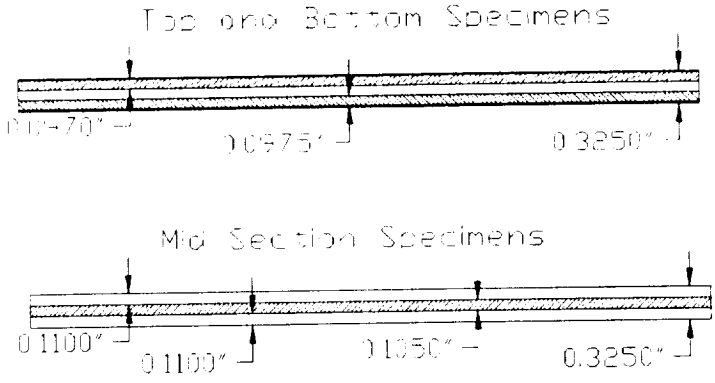

Figure 3-6 Reduced Thickness Specimens.

3.4 Data Reduction

3.4.1 Image Correlation

The undeformed and deformed images are loaded into the image correlation software. As mentioned previously, the undeformed image is the reference in the correlation process; therefore, the region to be correlated (termed AOI, for area of interest) must be present in all of the deformed images. Subset size and step size are chosen, based on the scale of the pattern, so that each subset contains a sufficient number of features and so that the desired spatial resolution is achieved. The AOI is selected in the undeformed image as shown in Figure 3-7. An initial guess is provided by the user for each undeformed / deformed image pair by manually selecting a feature in the undeformed image (seed point) and locating the same feature in each deformed image. The initial guess is used to speed up the correlation process by reducing the number of iterations required to minimize the correlation function (i.e. find the best match). After the best match is found for a particular subset, the displacements (u,v) of the subset center are returned, the next subset is stepped, relative to the previous one, using the step size and the correlation process is repeated until all the subsets in the AOI have been correlated. The resulting displacement fields are smoothed and then post-processed to determine the full field strains.

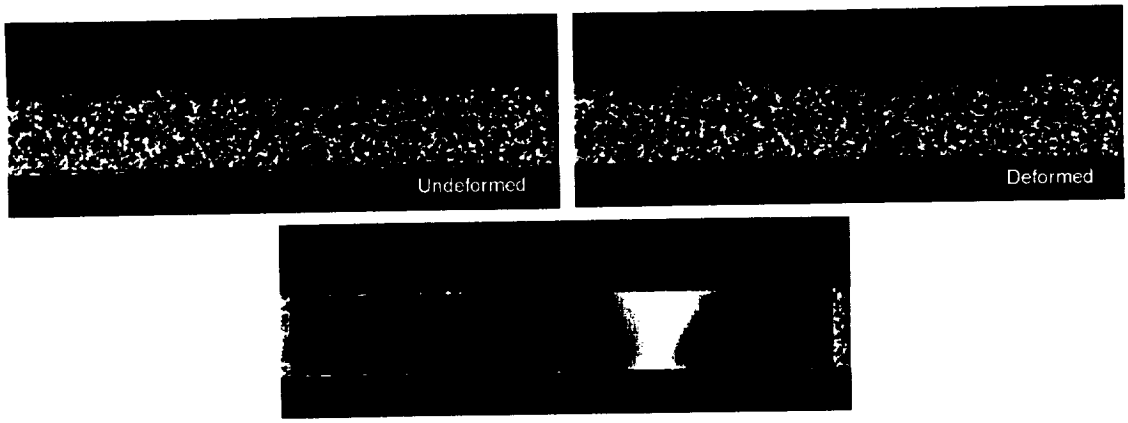

Figure 3-7 Image correlation process showing selected area of interest (AOI), subset location in un-deformed and deformed images, and the resulting displacement field.

3.4.2 Strain Determination

The output files from the image correlations contain the smoothed u and v displacement fields. Each file is post-processed using a program that fits a surface to the total displacement field and computes the gradients of this surface. The displacement gradients on the surface correspond to the strains in any chosen direction and so the normal and shear strains are obtained at each position in the AOI.

A common reference system must be created to relate the image coordinates to the positions in the actual weld so that comparisons can be made between strain data and other results, such as hardness or model simulation data. Image magnification in the x-direction (pixels/*mm*), determined by dividing the distance, in pixels, between the two marks placed at the edges of the weld by the known shoulder diameter, in *mm*, is used to convert image coordinates from pixels to *mm*. Similarly, the magnification in the y-

direction is determined by measuring the specimen thickness, in pixels, and dividing by the known thickness, in *mm*. The weld centerline is chosen as the common reference and the strain data is altered so that the origin of the abscissa corresponds to the location of the weld centerline in the image. Absolute position in the thickness direction can be determined by noting the coordinate position of the data relative to the coordinate position of top or bottom of the weld in the image and making the appropriate conversions.

3.4.3 Stress Mapping

One of the major assumptions underlying the proposed technique is that loading of the heterogeneous material in question may be approximated by an iso-stress condition. This assumption is required so that the global stresses may be mapped to the local strain data measured using the image correlation technique. The iso-stress concept may be understood by considering the uniaxial loading of an idealized heterogeneous specimen, of constant cross-section, comprised of different layers of material arranged in series as shown in Figure 3-8. When the specimen is loaded such that the force acts normal to the cross-sectional area of each material (Figure 3-8(**a**)), i.e. the cross-section normal to the force at any point in the specimen is comprised of a homogeneous material, then the loading is considered iso-stress. The alternate scenario, termed iso-strain, occurs with the loading and orientation shown in Figure 3-8(**b**). In this case, each material in the heterogeneous body experiences the same strain. The idealization that uniaxial loading transverse to the friction stir weld represents an iso-stress condition provides the

necessary approximation for determining the local stresses based on the globally applied loading.

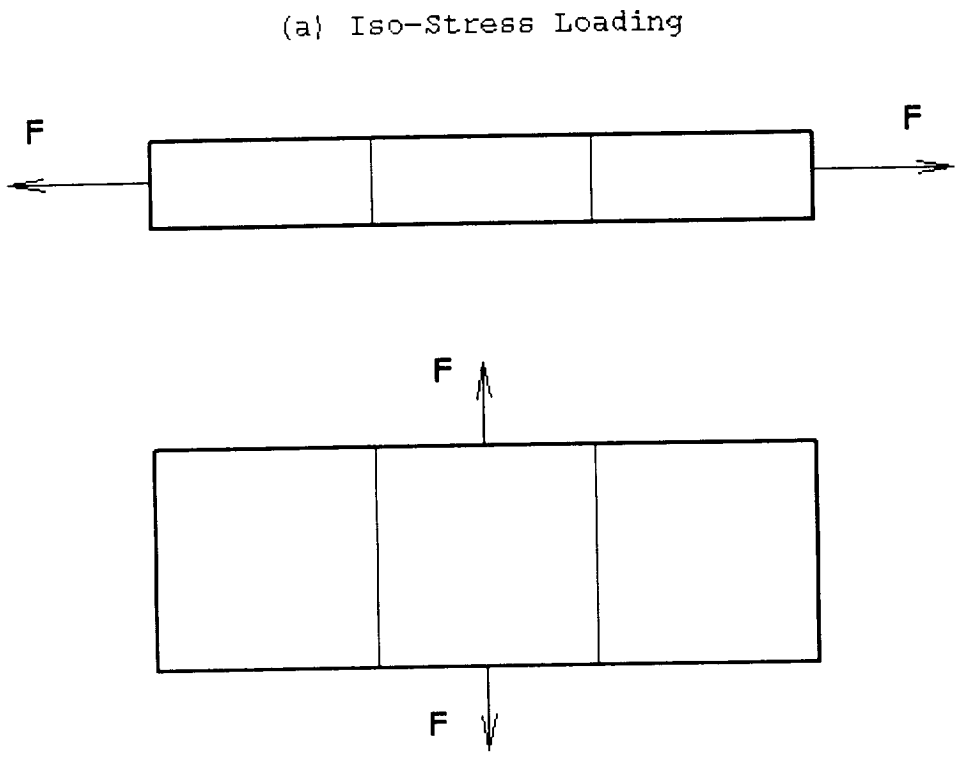

Figure 3-8 Idealized loading conditions of a heterogeneous body. (a) iso-stress and (b) iso-strain.

Chapter 4 Experimental Results and Discussion

The mechanical response of friction stir welds in aluminum alloy 2024 has been examined experimentally using standard tensile testing procedures and digital image correlation. Several specimens, corresponding to different welding conditions and specimen types, were used to determine both the local and global responses and also to study the validity of the iso-stress assumption. The individual cases examined include full size specimen testing of the *nominal*, *hot* and *cold* welds and reduced thickness specimen testing of the *nominal* weld. Results for each case considered are separated into global response, local response and local constitutive behavior.

The global response for the individual welds is presented in terms of the overall stress-strain response. Although the intent of this study is not to provide a detailed account of the effects of welding parameters on the global mechanical response of friction stir welds, the global behavior is needed to demonstrate the viability of the proposed technique and provide one measure of comparison for the numerical model.

Information provided by the global response is useful in terms of gauging the overall quality of the weld, however, due to the local interactions occurring within the heterogeneous material nothing of substantial importance can be determined that would lead to insight into the relationships between process parameters and weld performance. This type of information can only be determined through investigation of the local

behavior. Again, it is not the intent here to provide correlations between process parameters and weld performance. The focuses of the investigation into local mechanical behavior are threefold: (1) Provide a means for determining the material distribution within the weld. (2) Provide the necessary information for extracting the local constitutive behavior of the various weld materials. (3) Provide a measure of comparison for the numerical model.

The primary goal of this study is the accurate description of the local constitutive behavior of heterogeneous materials. Together with material distribution data mentioned above, this information provides the foundation for the development of the numerical model. The constitutive behavior for the various weld materials is presented in terms of the stress-strain response.

4.1 Global Mechanical Response

Using the procedures outlined in Section 3.3.1, standard full size specimens for each of the three welds were tested to determine the overall responses. The stress-strain responses for the *nominal*, *hot*, and *cold* welds are shown together with the all base metal response in Figure 4-1.

A standard metric for judging the quality of a weld is the joint efficiency. The joint efficiency provides a means for comparing various material properties of the global weld response with associated material properties of the base material. Common properties used in this type of comparison are yield strength, ultimate strength and total elongation. These material properties and the corresponding joint efficiencies for the *nominal*, *hot* and *cold* welds are found in Table 4-1.

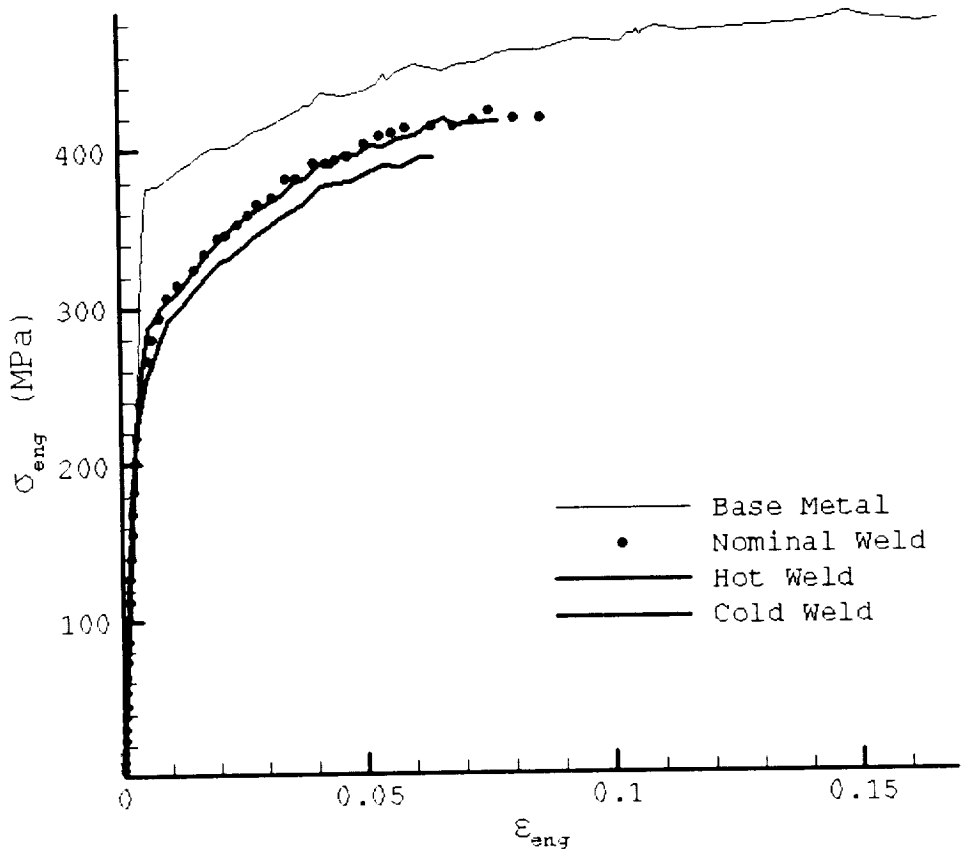

Figure 4-1 Global stress-strain responses for AA 2024 Base metal and AA 2024 Friction Stir Welds.

Material	0.2% Yield Strength (Mpa)	UTS (Mpa)	Total Elongation (%)
Base	**380**	**490**	**17**
Nominal Weld	272 (72%)	426 (87%)	8.6 (51%)
Hot Weld	255 (67%)	401 (82%)	6.4 (38%)
Cold Weld	286 (75%)	425 (87%)	7.9 (46%)

Table 4-1: Material properties for AA 2024 Base material and Friction Stir Welds. Joint efficiencies are shown in parentheses.

The properties for the welds listed in Table 4-1 should be clarified to avoid any confusion regarding performance. The yield strengths are determined by the intersection of an offset line and the stress-strain curve, where the offset line originates at a strain value of 0.2% and has a slope equal to the elastic modulus of the material. Yield strengths defined this way for homogeneous materials are then representative of the onset of yielding in the material. For heterogeneous materials, however, yield strengths defined this way are misleading because they do not account for localized yielding in the lower strength constituents, where strains may be significantly higher than the 0.2% global strain level. Therefore, the values listed for the welds are fictitious in that they overestimate the stress at which actual yielding occurs. Unfortunately, there is no way to determine the stress corresponding to local yielding from the global stress-strain curve so these values must suffice for making quantitative comparisons with base metal values.

In addition to the yield strengths, the total elongations listed are not entirely indicative of the heterogeneous welds. Compared to the base metal, the total elongations of the welds suggest that they behave in a brittle manner. What is not revealed by this global description, though, is the presence of localized regions within the weld that experience significantly higher strains than those listed in Table 4-1. Again, this information is not available from the global stress-strain curve so the global values are used for comparison purposes.

In terms of joint efficiency, given as a percentage of the base metal values, all of the welds exhibit good yield strength, ultimate strength and ductility. However, there is a noticeable difference between the responses of the welds and that of the base material. Due to the thermal cycles and mechanical deformations experienced during welding, a

heterogeneous material consisting of several microstructural regions having mechanical properties different from the parent material exists. It is the local material properties within the weld that govern the global response of the transversely loaded weld. Much of the current effort in the area of analysis of weldments focuses on the effects of yield strength mismatch, arising from variations in parent metal and weld properties, on the mechanical behavior and fracture of welded joints [52-54].

The thermal and mechanical deformation cycles accompanying the welding process create gradients in microstructure and properties that are observable in both the transverse and through-thickness directions. It is the through-thickness gradient, evident from the crown of the weld to the root of the weld, which is the primary reason that the iso-stress assumption is simply an approximation. The validity of this assumption, as it was stated earlier, is examined by testing reduced thickness specimens.

Three specimens were machined from full thickness, *nominal* weld specimens, corresponding to locations near the top, middle and bottom of the weld, and tested using the procedures outlined in Section 3.3.2. The global responses for the three reduced thickness specimens are shown in Figure 4-2 along with the full thickness *nominal* weld response. Since an extensometer was not used to measure global specimen strains directly, these values were determined from the measured displacement data obtained via image correlation. Using the magnification markers placed on the specimens, the DIC data was processed to convert the image coordinates to actual specimen coordinates. In this manner it was possible to construct an artificial gage length, consisting of two points located on either side of the weld centerline and 25.4 *mm* apart, for direct comparison with the strains measured by the extensometer.

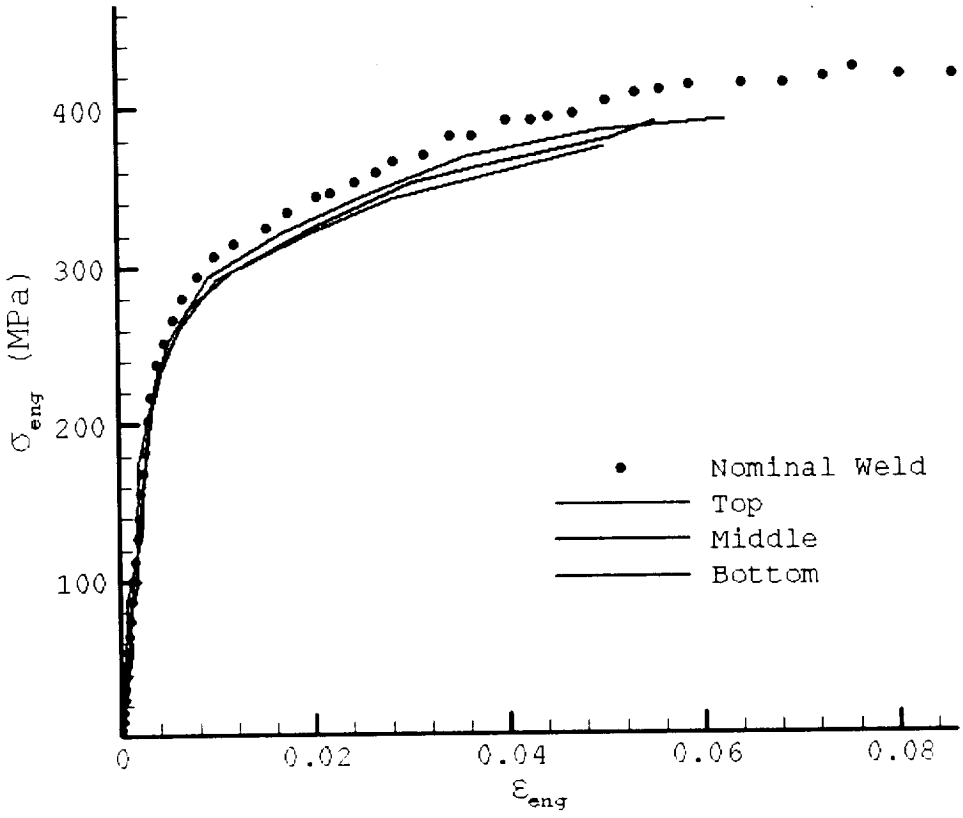

Figure 4-2 Global stress-strain response for the AA 2024 Nominal FSW. Top, Middle and Bottom refer to reduced thickness specimens machined from full thickness nominal welds.

Although the through thickness gradients were not completely eliminated by reducing the specimen thickness, the effect of reducing them is noticeable in the global response of the reduced thickness specimens. Yielding is fairly consistent among all of the specimens and the post yield behaviors all show the same trends. Global stress levels and ductility, however, drop according to specimen location relative to the full thickness weld. The *top* specimen demonstrates higher stress levels and ductility overall while the *bottom* specimen demonstrates minimum stress levels and ductility and the *middle* specimen falls in between.

It is possible that a qualitative understanding of these results, and the results shown for the full thickness specimens, may be provided by a simple rule of mixtures approach. Neglecting the locally defined zones in the FSW macrograph shown in Figure 2-2, the weld possesses a general V-shape that is typical of many welding processes. Microhardness provides a qualitative description of a materials resistance to plastic deformation and several studies conducted on the mechanical properties of friction stir welds in various aluminum alloys [57-60] have shown that microhardness variations in the transverse direction, spanning the width of the weld, exhibit a typical W-shape as seen in Figure 4-3.

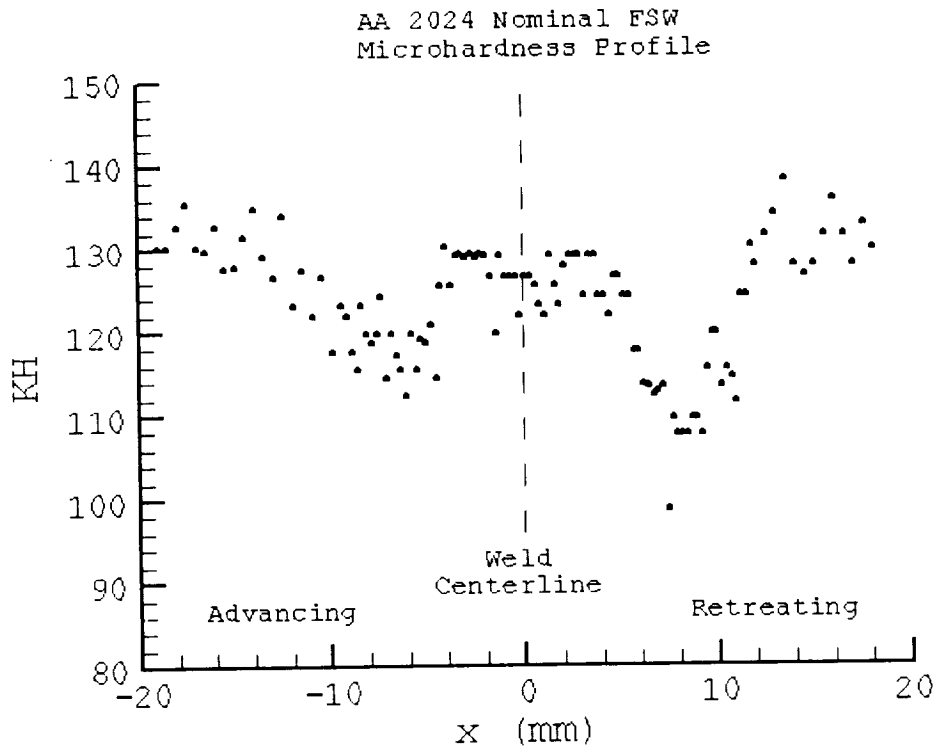

Figure 4-3 Microhardness profile for the Nominal FSW. Note the W-shape.

This microhardness profile was taken from a *nominal* friction stir weld in AA 2024, midway between the crown and root of the weld, and shows the typical characteristics of high hardness in the nugget region accompanied by hardness minima in the adjacent heat affected zones and a return to base metal hardness outside of the weld. Similar profiles taken from near the top and bottom of the weld show the same shape, but the hardness minima are shifted towards the weld centerline moving from top to bottom and the widths of the nugget and heat affected zones decrease moving from top to bottom.

A simplified view of the weld as a composite, based on the hardness profile, is shown in Figure 4-4. There is a medium strength region (nugget) in the center of the weld bordered on each side by a low strength region (HAZ), which is in turn bordered by the high strength base material. Considering the V-shape of the weld and the variation in size of the different zones from the top of the weld to the bottom, it is clear that the relative amounts of the constituents vary between the three reduced thickness specimens.

Qualitatively, the rule of mixtures is a method that can be used to examine characteristics of the response of a composite material based on the volume fractions of the constituents [61]. It basically states that the composite behavior will fall somewhere between the behavior of the individual components. Since the friction stir weld is undermatched with respect to the base metal strength, the tensile response of the heterogeneous specimen is almost solely governed by the weld and is, therefore, related to the relative amounts of the materials comprising the weld.

To demonstrate the use of the rule of mixtures, consider the transverse loading of the composite FSW. Assuming iso-stress loading conditions, the stress in the composite is equal to the stress in each component:

$$\sigma_c = \sigma_{HAZA} = \sigma_{HAZR} = \sigma_{Nugget} = \sigma_{Base} \tag{4.1}$$

where HAZA and HAZR refer to advancing and retreating side heat affected zones, respectively. The total change in length of the specimen is given as the sum of the changes in length of the individual components:

$$\Delta L_c = \Delta L_B + \Delta L_{HAZA} + \Delta L_{Nugget} + \Delta L_{HAZR} \tag{4.2}$$

Since the change in length is related to the strain by $\Delta L = \varepsilon * L$, the composite strain may be written as

$$\varepsilon_c = \varepsilon_B * \frac{L_B}{L} + \varepsilon_{HAZA} * \frac{L_{HAZA}}{L} + \varepsilon_{Nugget} * \frac{L_{Nugget}}{L} + \varepsilon_{HAZR} * \frac{L_{HAZR}}{L} \tag{4.3}$$

where L_i is the length of the component and L is the total composite length. When the cross-sectional dimensions are constant, the line fraction $l_i = \frac{L_i}{L}$ is equivalent to the volume fraction V_i, and the composite strain takes the form:

$$\varepsilon_c = \varepsilon_B * v_B + \varepsilon_{HAZA} * v_{HAZA} + \varepsilon_{Nugget} * v_{Nugget} + \varepsilon_{HAZR} * v_{HAZR} \tag{4.4}$$

Using this approach the composite response can be estimated from the relative amounts of the components.

From Figure 4-4 it is clear that the volume fraction of the medium strength nugget decreases and the volume fraction of the low strength HAZ increases, or remains fairly constant, from the top to the bottom of the weld. The top reduced thickness specimen then contains a greater percentage of higher strength material than the middle and bottom

specimens, respectively, and, conversely, the bottom specimen contains a greater percentage of low strength material than the middle and top specimens. Qualitatively, then, it could be expected that the reduced thickness specimens performed as shown in Figure 4-2.

This same argument can be made for the full thickness *nominal*, *hot* and *cold* weld specimens. The designation, nominal, hot or cold, offers a qualitative description of the energy input to the weld. In relation to the baseline nominal weld, a hot weld receives more energy and experiences higher temperatures and the contrary is true for the cold weld. As demonstrated by the hardness data, the heat affected zone represents a lower strength material than the nugget. Assuming that the size of the HAZ is directly related to the thermal cycle experienced during welding and that the size of the nugget is fairly constant for a given tool, it can be concluded that the hot and cold welds contain a higher and lower percentage of low strength material, respectively, than the nominal weld. Referring back to Figure 4-1, the *hot* weld, in fact, performs worse than the *nominal* and *cold* welds. Although the responses of the *nominal* and *cold* welds are very similar, this is most likely due to negligible difference in energy input associated with the prescribed changes in welding parameters, as shown in Table 3-1.

4.2 Local Mechanical Response

A need to study the local mechanical response of a heterogeneous material was established previously in order to offer some insight into the observed global response and to provide a means for measuring the local constitutive behavior. Using the techniques and procedures outlined in Section 3.3.2, the local response of the three

friction stir welds was examined. The results are presented as contour plots of the full field strain measurements obtained via the image correlation technique. The coordinate system adopted for presenting these results is slightly different for the full thickness and reduced thickness specimens. In both cases the x-axis is oriented with the global tensile loading axis and the associated strain in this direction is labeled ε_{11}. For the full thickness specimens, the y-axis corresponds to the plate thickness with the crown of the weld at the top of each contour, and the welding direction is into the page. For the reduced thickness specimens, the y-axis represents the welding direction and the plate thickness is the out of plane dimension.

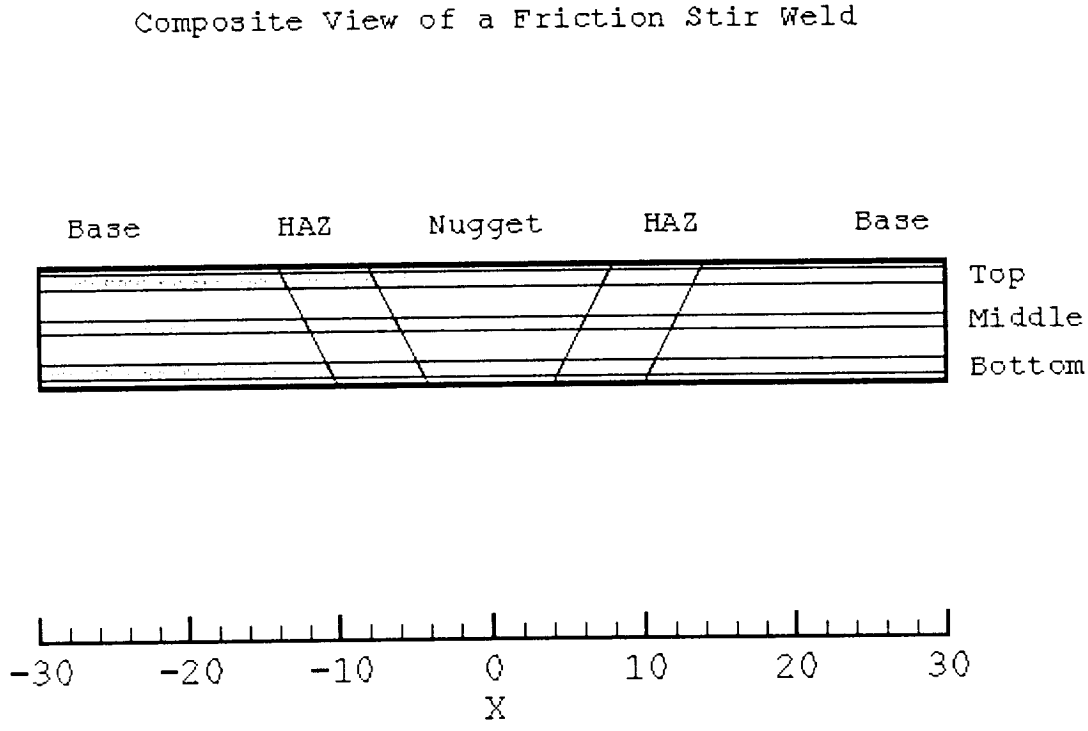

Figure 4-4 Simplified view of a FSW as High, Medium and Low strength materials arranged in series. Reduced thickness specimen locations indicated as Top, Middle and Bottom.

One of the advantages afforded by the experimental technique is that it can be used to capture the mechanical behavior at various stages. As a result, a history of the deformation is obtained that allows for identification and tracking of interesting local effects. The local response for the *nominal* weld is shown in Figure 4-5 at three different levels of global specimen strain. The contour plots show the normal strain (ε_{11}) as a function of position within the weld. At a global strain of 0.5%, corresponding to a global stress of approximately 267 MPa, strain localizations are evident in the regions corresponding to the HAZ, with slightly higher localizations occurring on the retreating side of the weld. In relation to the overall response, this stage is indicative of the onset of global yielding, which is identified in Table 4-1 as 272 MPa. Note that the strain in the HAZ is approaching 1%, signifying yielding has already occurred and suggesting that the stated yield strength is a fictitious yield strength. The remaining regions of the weld exhibit fairly uniform deformation. Later on in the loading, at global strains of 2.5% and 4.7% and global stresses of 355 MPa and 396 MPa, the strain localizations within the HAZ have increased in magnitude, however, the specimen continues to strain harden as indicated by the significant strain development in the nugget and regions surrounding the HAZ. Beyond roughly 5% global strain, as seen in the global response, the specimen continues to strain with relatively little increase in load and it could be presumed that the retreating side HAZ localization became the dominant factor in the specimen failure. However, since no full field information was collected after the 4.7% strain level and the specimen actually failed in the nugget, this appears not to be the case. It is possible that there was a very small defect in the weld, such as a lack of penetration (LOP) defect that was not observed in the optical microscope, or it may be that the nugget material is too

brittle to withstand the strain. Results from the reduced specimen tests, discussed later in this section, seem to indicate the former.

The local response for the *hot* weld is shown in Figure 4-6 at global strain and stress levels of 0.7% (271 MPa), 3.0% (350 MPa) and 5.4% (389 MPa). At 0.7% strain and 271 MPa, which occurs slightly after global yielding indicated by the 255 MPa yield stress, localizations are observed in the advancing and retreating side HAZ. These localizations continue to develop throughout the loading and the retreating side HAZ localization eventually becomes the dominant factor in failure, as indicated by fracture of the specimen in this region.

As was the case in both the *nominal* and *hot* welds, the *cold* weld demonstrates similar characteristics in local response at the early stages of loading, as seen in Figure 4-7. Localization is observed at a global strain of 0.6% and this occurs at a global stress of 290 MPa, which is very near the yield strength for this weld. An additional localized region is seen developing near the centerline of the weld at a strain of 2.0%, an effect usually indicative of a lack of penetration defect. This localized region becomes dominant, as shown by the response at 3.1% strain, and the specimen fractures through the nugget. The presence of the defect was not observed in the optical microscope, however, the fracture surface did show signs indicating this type of defect. It is interesting to note that although the nugget material experiences highly localized strains, approximately 17%, the weld continues to strain harden and withstands a maximum global strain of almost 8.0%.

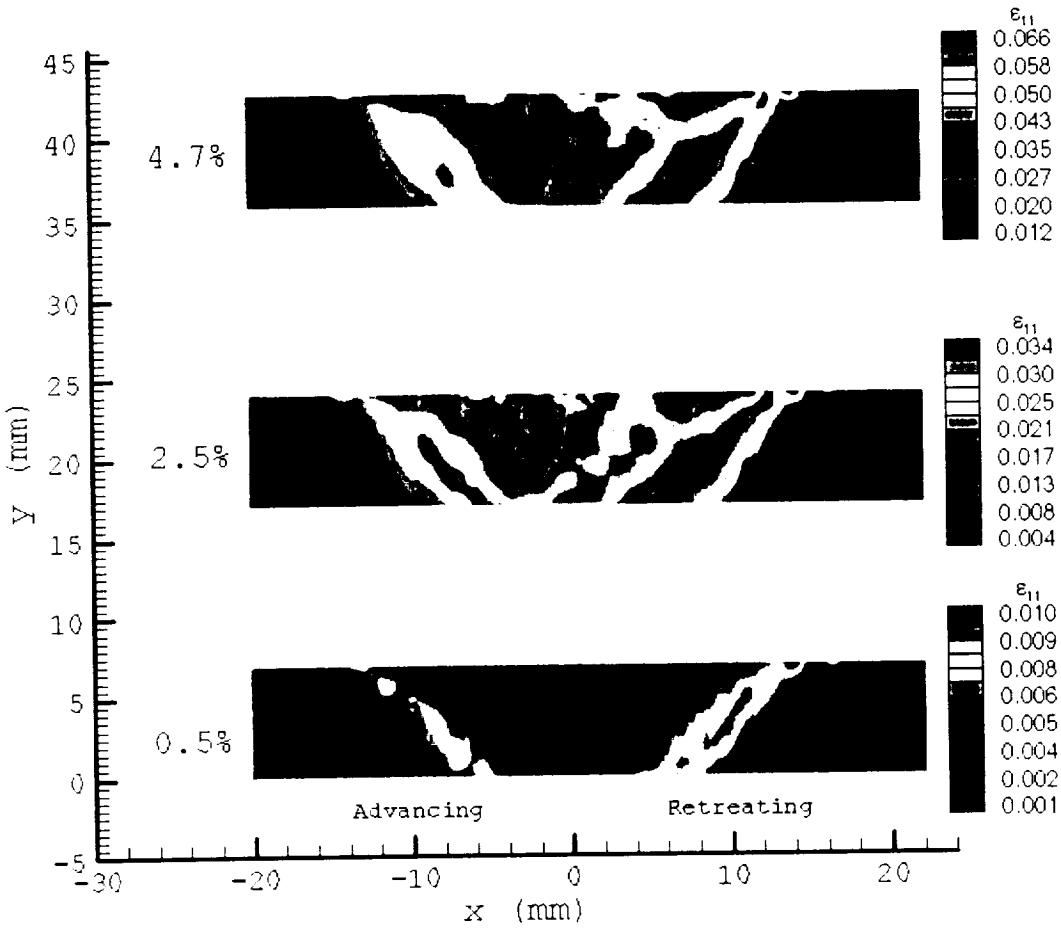

Figure 4-5 Local Response in AA 2024 Nominal FSW. The top middle and bottom plots represent global strain levels of 4.7%, 2.5% and 0.5%, respectively.

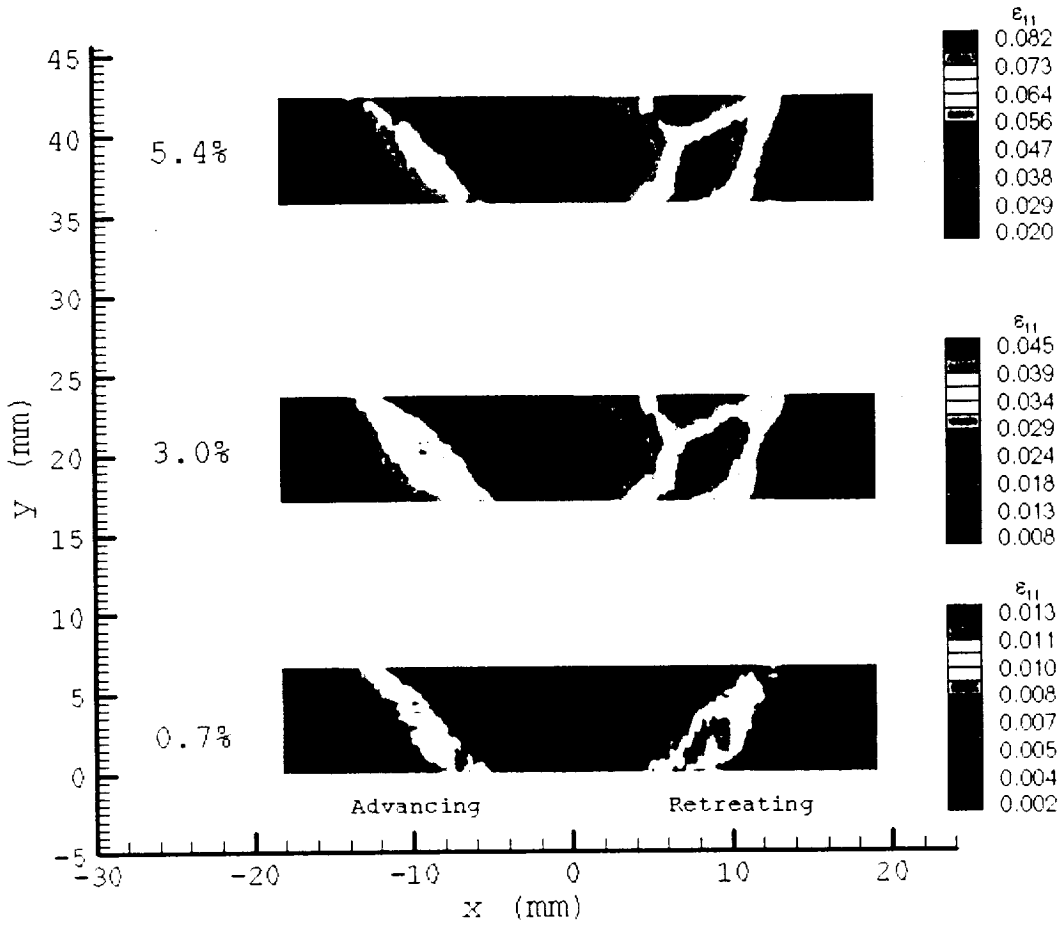

Figure 4-6 Local Response in AA 2024 Hot FSW. The top middle and bottom plots represent global strain levels of 5.4%, 3.0% and 0.7%, respectively.

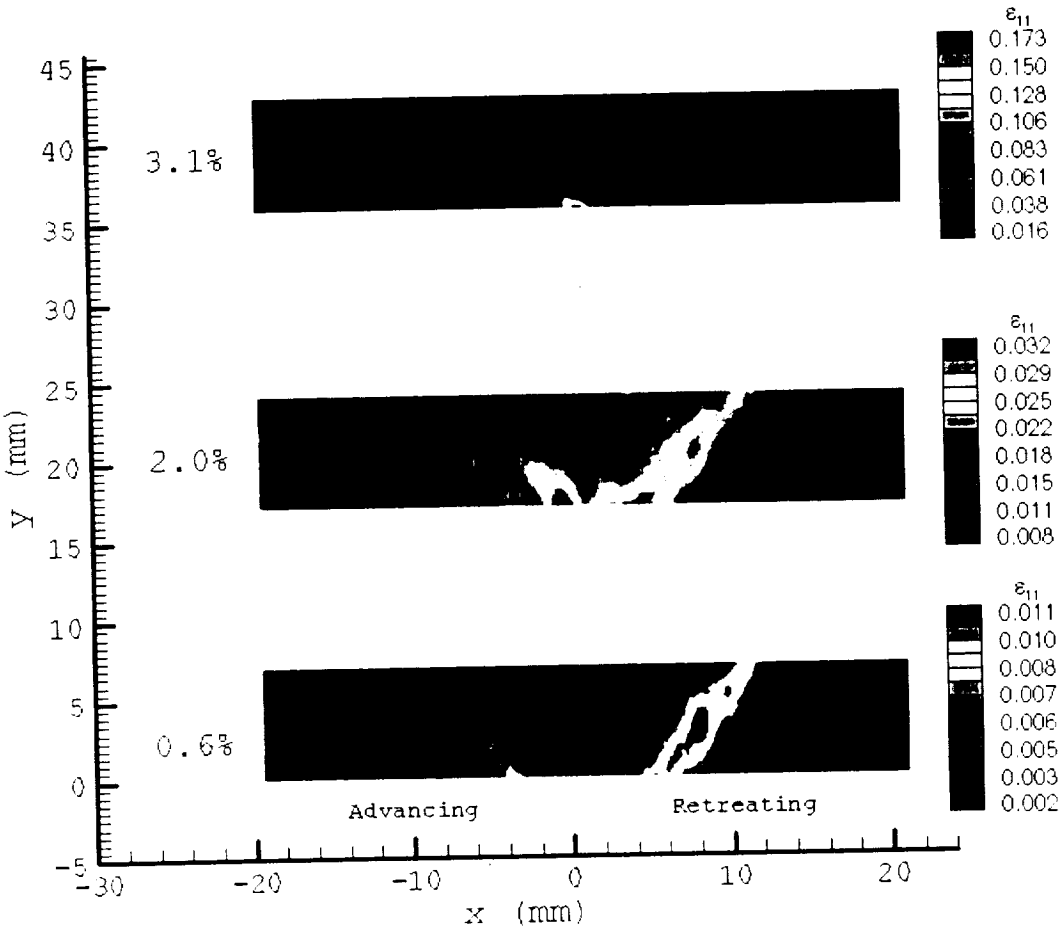

Figure 4-7 Local Response in AA 2024 Cold FSW. The top middle and bottom plots represent global strain levels of 3.1%, 2.0% and 0.6%, respectively.

Reduced thickness specimens machined from *nominal* weld specimens were tested and examined using the DIC technique. The results are presented in the same fashion as the full thickness specimens, with the exception that the surface viewed was normal to the plate thickness direction as opposed to normal to the welding direction.

The full field contour plots for the top, middle, and bottom specimens are shown in Figure 4-8, Figure 4-9 and Figure 4-10, respectively. Each figure contains the local response of the specimen at different global strain levels. As for the full thickness *nominal* weld specimen, the reduced thickness specimens show the same characteristic strain localizations developing in the HAZ regions with maximum normal strains occurring on the retreating side. It was mentioned previously that failure in the full thickness specimen was expected to take place in the retreating side HAZ due to the localized effects, but the specimen actually failed in the nugget most likely because of an unseen defect. All of the reduced thickness specimens failed in the retreating side HAZ, which seems to support the presence of the LOP defect at the bottom surface. Based on the amount of material removed from the bottom surface of the *bottom* specimen, the size of the defect can be estimated at 0.25 *mm*.

One of the interesting features of all three specimens is the relatively uniform deformation of the individual regions in the welding direction (y-direction) indicating that the materials representing the weld are homogeneous in this direction. This is a generally accepted feature of the FSW process under steady state conditions and one that supports the assumption that the mechanical response of a friction stir weld can be modeled as a two dimensional problem.

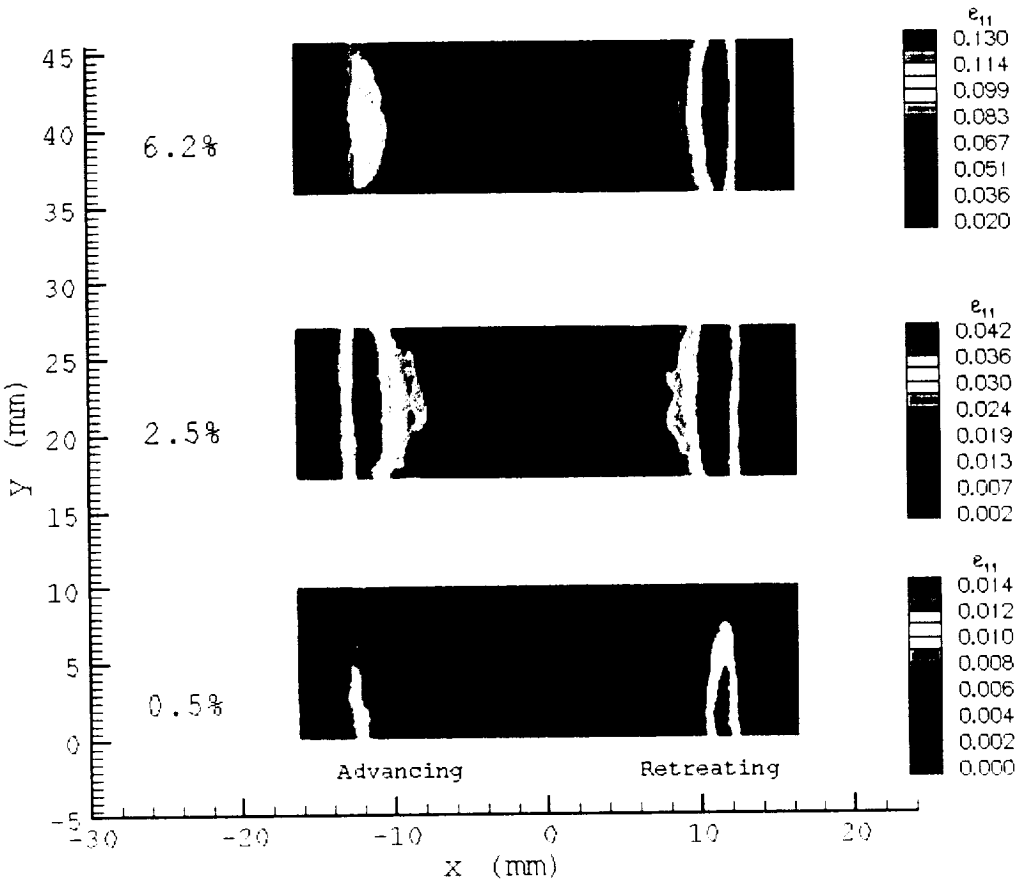

Figure 4-8 Local Response for Top Reduced Thickness Specimen.

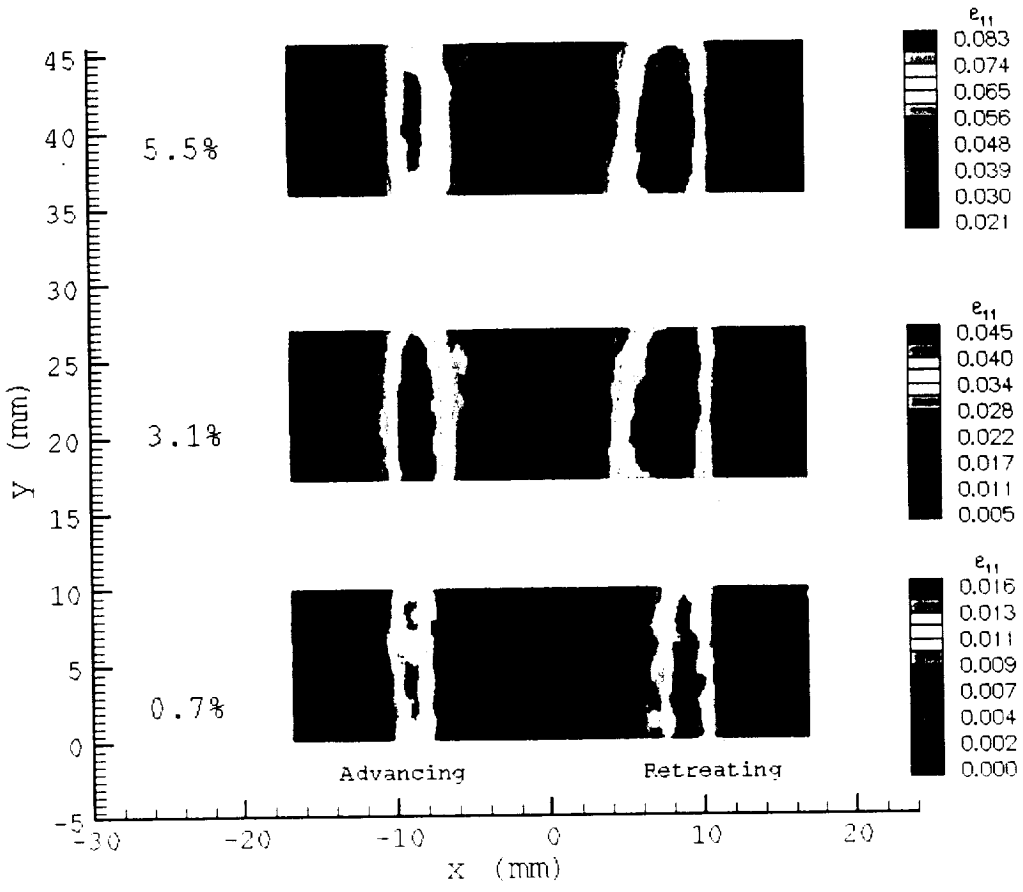

Figure 4-9 Local Response for Middle Reduced Thickness Specimen.

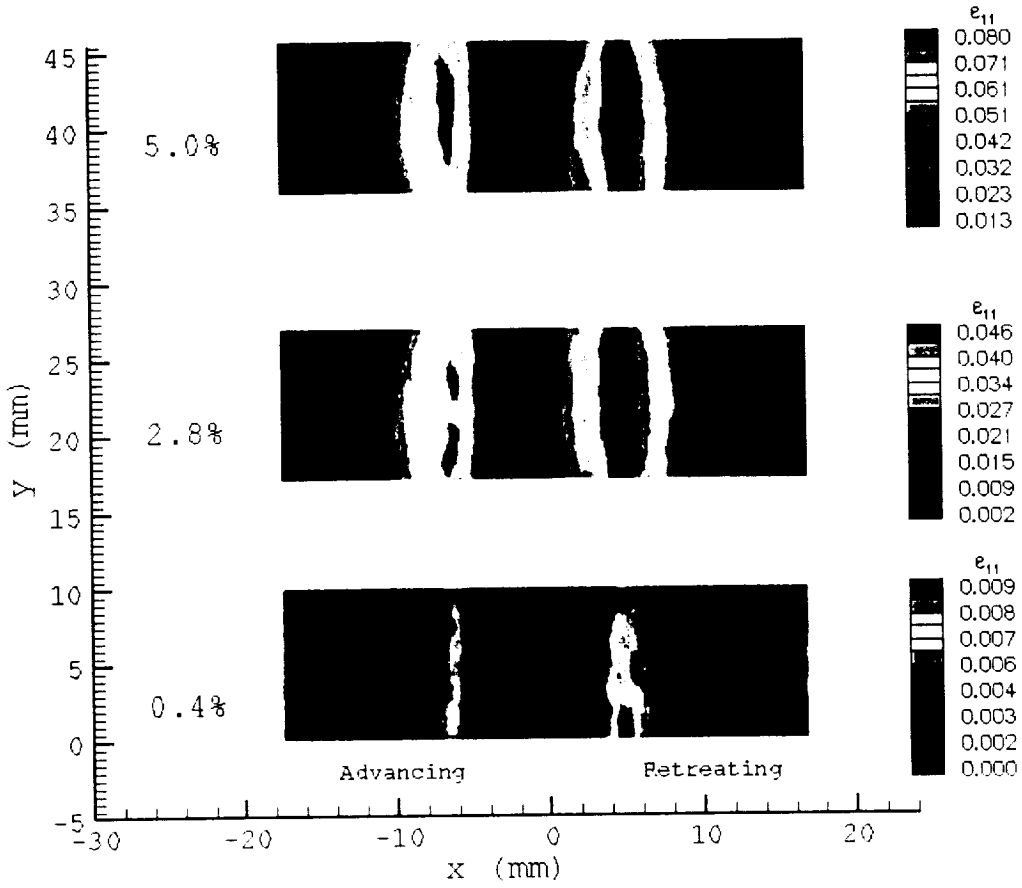

Figure 4-10 Local Response for Bottom Reduced Thickness Specimen.

4.3 Local Constitutive Behavior

Ultimately, the goal of the experimental technique is to provide the information necessary for developing the finite element model: (1) the local constitutive behavior, given by the uniaxial stress-strain response, of the various materials that make up a friction stir weld; (2) the number of materials to be used in defining the weld; and (3) the distribution of these materials within the weld.

As stated previously, capturing and correlating images at different stages of loading provides a history of the local mechanical response. By assigning the global stress, corresponding to the load at which a particular image was recorded, to the local strains extracted from the full field data for that image, the constitutive data for virtually any point in the weld can be constructed. In order to define the constitutive data for the weld materials, the number and distribution of these materials must be decided upon. Based on the results demonstrating the local mechanical response, a description of the weld in terms of constituents could be presented by any number of different materials. An attempt to distinguish every possible difference in material behavior would not only be overly time consuming but also impractical. Therefore, a reference must be chosen to use as a basis for separating the weld into a manageable number of materials. Towards this end, the offset yield stress is used to characterize the weld materials and provide a map for choosing the number and distribution of these materials.

Yield stress maps for the *nominal*, *hot* and *cold* welds are shown in Figure 4-11, Figure 4-12 and Figure 4-13, respectively. These maps show the yield stress as a function of position in the weld. Each map was constructed from the manually determined 0.2% offset yield stresses of several hundred stress-strain curves extracted from the full field data. In order separate the weld into a reasonable number of distinct materials, five contour levels were used to display the data. Trends in the yield stress distributions exhibit the same characteristics as the typical hardness profile shown previously. A medium strength nugget region is bordered by lower strength HAZ regions, which transition towards the high strength base metal outside the weld.

The material distribution provided by the yield stress map is subject to interpretation, however, only those regions that extend from the top to the bottom of the weld are selected as individual materials. Local stress-strain curves are extracted from the positions indicated on the maps and used to describe the constitutive behavior for the corresponding materials. In addition to determining the number of materials and their constitutive behavior, the boundary locations are measured relative to the weld centerline and used as a guide for establishing the material distribution in the model.

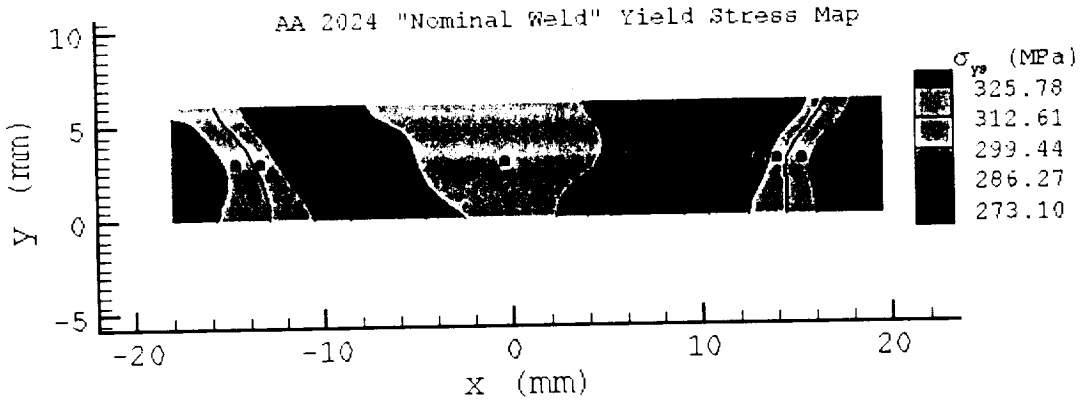

Figure 4-11 AA 2024 Nominal Weld Yield Stress Map.

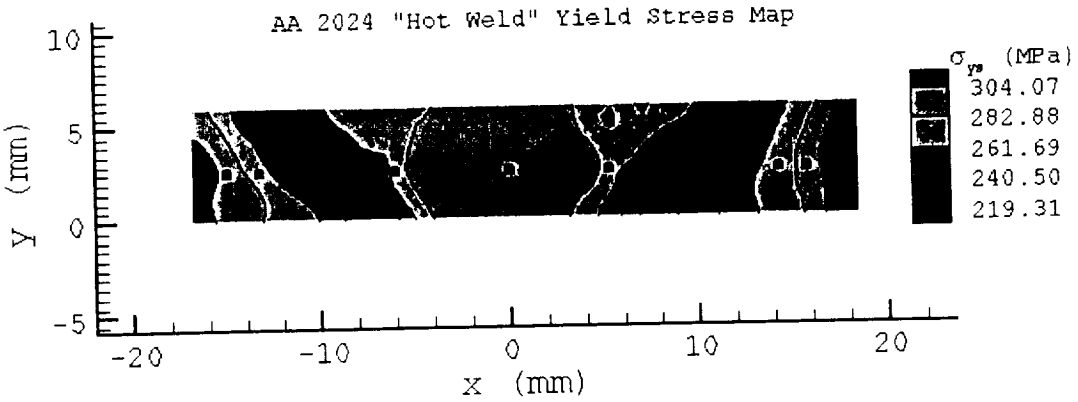

Figure 4-12 AA 2024 Hot Weld Yield Stress Map.

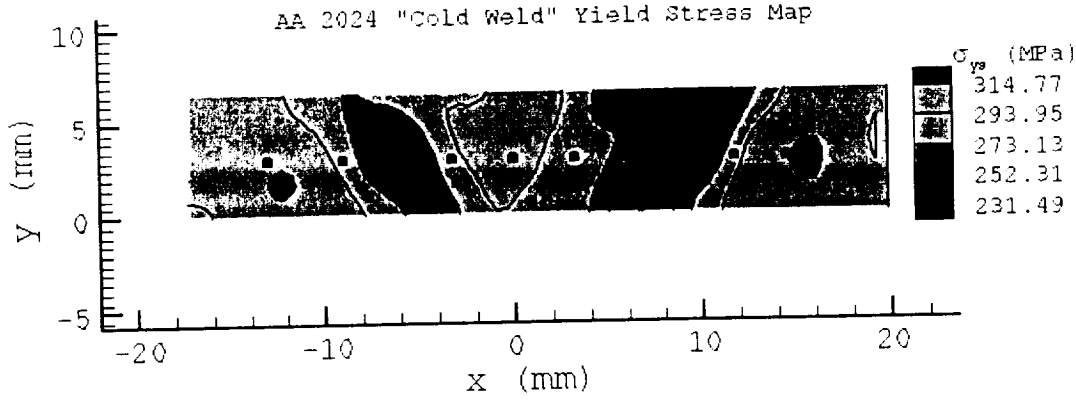

Figure 4-13 AA 2024 Cold Weld Yield Stress Map.

The constitutive data measured from the full thickness specimens was assumed to be representative of the response under iso-stress loading conditions and this assumption was tested using reduced thickness specimens taken from the *nominal* weld. A comparison of the results from the full and reduced thickness specimens is used to verify this assumption.

Stress-strain curves were constructed for each of the materials comprising the weld, excluding the base material, at locations near the top, middle and bottom of the full thickness specimen using the *nominal* weld yield stress map as a guide for determining material positions relative to the weld centerline. Stress strain curves from each thin specimen were also constructed corresponding to the same relative positions in the thick specimen. The 0.2% offset yield strengths, used to compare local constitutive behavior between the thick and thin specimens, are plotted relative to the weld centerline in Figure 4-14. Also shown in Figure 4-14 is the thick specimen yield stress map defining the local material boundaries and the positions for the material property comparisons. Differences in local yield strengths between the thick and thin specimen are most pronounced in the low strength regions of the weld, and in each case the thick specimen yield stresses are higher in these regions. This result was expected due to the iso stress approximation, in which an unrealistically high stress may be assigned to a region that has yielded and redistributed its load to another part of the cross section. Furthermore, the reduction in thickness may have relaxed the material constraint in the low strength regions, providing an additional explanation for the lower yield strengths. Overall, the thick specimen properties closely match the thin specimen properties and seem to justify the iso-stress approximation.

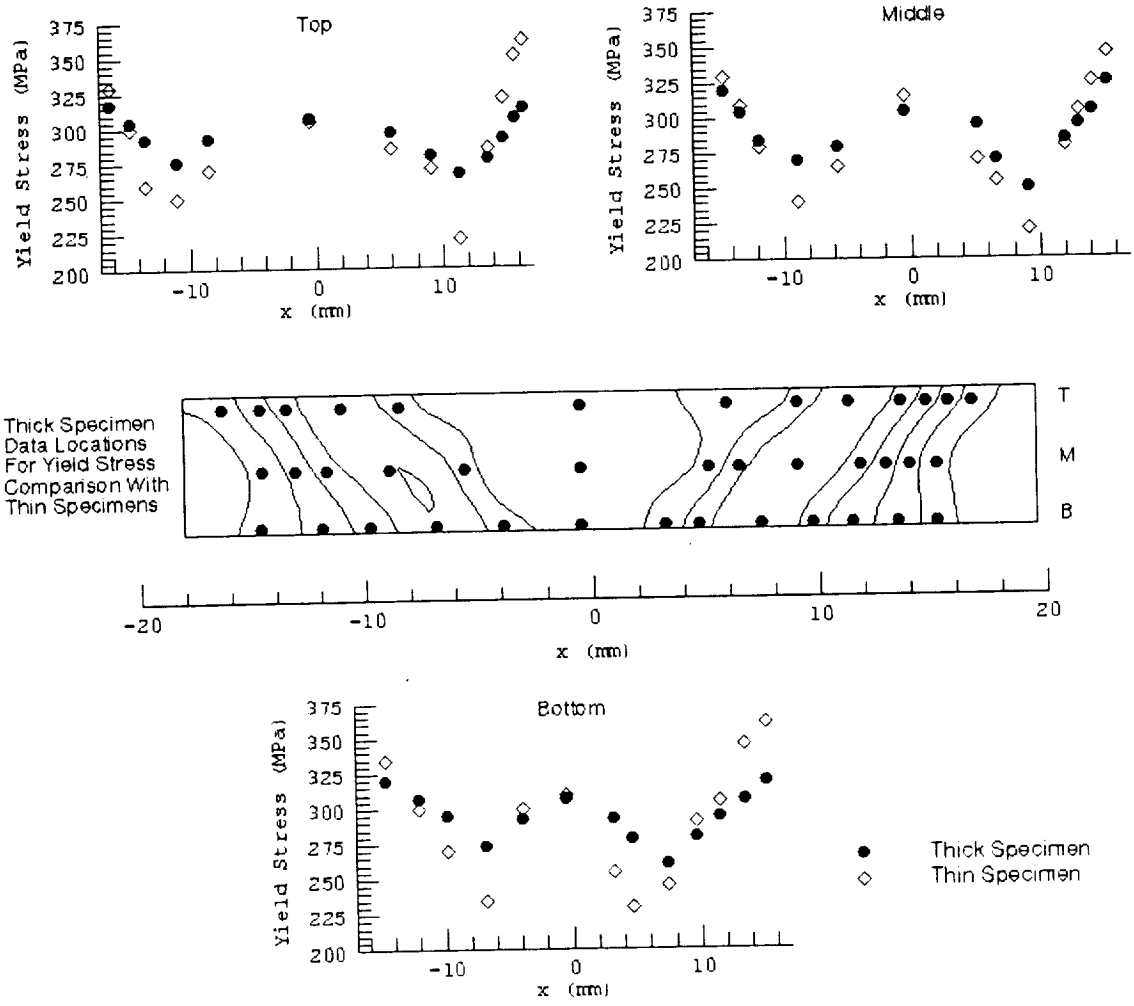

Figure 4-14 Comparison of Full Thickness and Reduced Thickness Specimen Local Constitutive Data.

To summarize, the global and local responses of the various welds and specimen types have been examined using the full field measurement capabilities provided by the image correlation technique. Observed differences in the global responses between parent metal and welded specimens were attributed to complexities arising from interactions among the various materials that make up the heterogeneous weld. Local material behavior was shown at different stages of loading and provided a detailed view of the

highly localized effects that develop throughout the loading history. The number of materials, material distribution and material constitutive data was then established for each weld using the yield stress map as guide. In addition, the iso-stress assumption was justified through a comparison of material constitutive data extracted from full thickness and reduced thickness specimens.

Information gathered from these experimental results provide the foundations for developing the 2-D and 3-D finite element models of the friction stir weld. The accuracy of the models will be gauged by comparing the model results, in terms of both the global and local mechanical response, with these experimental findings.

Chapter 5 Numerical Model

The goal of modeling the mechanical response of the friction weld is to accurately predict the global and local response that is observed experimentally. In doing this, the model serves dual purposes. (1) An accurate representation of the global and local response provides solid evidence that the local constitutive data measured experimentally is valid. (2) An accurate model can be used as a tool to investigate issues relevant to the problem that are otherwise difficult or impossible to determine experimentally. The model may also be used to supplement additional experiments, for example, the effects of different loading conditions, which can often be time consuming and expensive. Two-dimensional simulations are carried out for the three weld specimens using the local constitutive data obtained from the full thickness tests. In addition, the *nominal* weld is modeled using the local data determined from the reduced thickness tests to verify the iso-stress assumption. Three-dimensional models of the full thickness *nominal* weld are run to validate findings from the 2-D model. The finite element model of the friction stir weld is developed using the commercial code ABAQUS.

The finite element method is a numerical technique used to approximate the solution of boundary value and initial value problems over the entire problem domain. The solution of a particular problem is given by a mathematical formulation, often a differential equation, which describes the physical nature of the problem. Depending on

the complexity of the governing equation, the exact solution of a particular differential equation may be difficult to find. The finite element approach to solving the differential equation over the whole domain is to first discretize the domain into subdomains, called finite elements, and then determine an approximate solution over each element using approximation functions [62]. Discretization is accomplished by dividing the original domain into an assemblage of simple geometric shapes, consisting of elements and nodes, so that the geometry and the solution are well represented. The solution to the differential equation is approximated over each element by continuous functions, usually represented by linear combinations of algebraic polynomials. In order to obtain the necessary and sufficient number of algebraic equations required to solve for the unknown coefficients of the approximation functions, the differential equation must be recast in an equivalent integral form using variational methods. Once the element equations are determined, the entire set of equations is assembled and may be solved simultaneously.

Solid mechanics problems are governed by the equations of equilibrium for both forces and moments. For the case of static equilibrium of an arbitrary body, occupying a volume V enclosed by a surface S, the force and moment equilibrium equations are given by [63, 64]:

$$\int_S (\mathbf{n} \cdot \sigma)\, dS + \int_V \mathbf{f}\, dV = 0 \tag{5.1}$$

$$\int_S (\mathbf{r} \times \mathbf{n} \cdot \boldsymbol{\sigma})\, dS + \int_V (\mathbf{r} \times \mathbf{f})\, dV = 0 \tag{5.2}$$

where σ is the stress tensor, $(\mathbf{n} \cdot \sigma)$ and $\mathbf{f}$ represent surface and body forces, respectively, $\mathbf{n}$ is the surface outward normal and $\mathbf{r}$ denotes the position vector. In the absence of body

moments, the consequence of the moment equilibrium equation is the condition of symmetry of the stress tensor, which states $\boldsymbol{\sigma} = \boldsymbol{\sigma}^{T}$. Therefore, by using the symmetric stress tensor, the moment equilibrium equation is automatically satisfied and only force equilibrium need be considered. By transforming the surface integral in (5.1) to a volume integral using Gauss's theorem, the force equilibrium equation for an arbitrary volume may be written as:

$$\frac{\partial \sigma_{ji}}{\partial x_j} + f_i = 0 \tag{5.3}$$

which are the three familiar equations of force equilibrium.

As stated previously, the finite element method relies on approximations to the solution of the governing differential equations and requires an integral representation of the governing equations usually obtained by variational methods. These methods involve multiplying the original differential equation by a weight function and integrating over the domain to obtain a weighted integral statement [62]. The weighted integral statement requires that the approximation be differentiable as required by the original differential equation and satisfy both natural (force) and essential (displacement) boundary conditions. If differentiation can be distributed between the approximate solution and the weight function, the resulting integral represents a *weak* form in that the continuity requirements on the approximation functions are weaker. The *weak* formulation is usually preferable because of this feature and also because it includes the natural boundary conditions. Therefore, the available approximation functions include a larger space of functions and the approximation must only satisfy the essential boundary condition.

In the displacement based finite element formulation, the *weak* form of the equilibrium equation (5.3) is developed using the principle of virtual work (or principle of virtual displacements) [65]. Following the procedure discussed above, (5.3) is multiplied by the weight function, assumed to be a virtual displacement field $\mathbf{u_i}$, and integrated over the volume:

$$\int_V \left(\frac{\partial \sigma_{ji}}{\partial x_j} u_i + f_i u_i\right) dV = 0 \tag{5.4}$$

Using the identity $\frac{\partial \sigma_{ji} u_i}{\partial x_j} = \frac{\partial \sigma_{ji}}{\partial x_j} u_i + \sigma_{ji} \frac{\partial u_i}{\partial x_j}$, (6) may be rewritten as:

$$\int_V \left(\frac{\partial \sigma_{ji} u_i}{\partial x_j} - \sigma_{ji} \frac{\partial u_i}{\partial x_j} + f_i u_i\right) dV = 0 \tag{5.5}$$

Gauss's theorem may then be applied to the first term to transform the volume integral to a surface integral. Noting that the surface force is given by $t = (n \cdot \sigma)$, the result is:

$$\int_V \left(\sigma_{ji} \frac{\partial u_i}{\partial x_j}\right) dV = \int_V f_i u_i dV + \int_S t_i u_i dS \tag{5.6}$$

The left hand side of (5.6) contains the Jacobian matrix $\frac{\partial u_i}{\partial x_j}$ from which the symmetric virtual strain matrix ε and skew-symmetric virtual rotation matrix Ω are obtained. Due to the symmetry of σ and the skew-symmetry of Ω the term $\sigma \Omega = 0$, and (5.6) may be written as:

$$\int_V (\sigma_{ij} \varepsilon_{ij}) dV = \int_V f_i u_i dV + \int_S t_i u_i dS \tag{5.7}$$

This is the familiar form of the principle of virtual work that states that the total internal virtual work, corresponding to the equilibrium stresses and virtual strains, is equal to the total external virtual work done by the surface and body forces and the virtual displacements. Application of the equilibrium equation to the discretized domain results in a system of N equations for N unknown nodal values represented by:

$$[K]\{U\}=\{F\} \tag{5.8}$$

where $[K]$ is the global stiffness matrix, $\{U\}$ is the displacement vector and $\{F\}$ is the force vector. The system of equations is then solved for the displacements, which are then used to compute the element strains and element stresses. This is the general procedure used in the displacement based finite element formulation and is the same used in the ABAQUS finite element code [66].

Modeling the mechanical response of the friction stir weld under uniaxial loading is a nonlinear, static stress-analysis problem due to the nonlinear material behavior. ABAQUS handles the nonlinear problem in an iterative manner by dividing the solution into a number of small increments. The nodal displacements are calculated in each increment and a residual force is computed for comparison with a specified force tolerance. If the tolerance is met, the solution has converged for the increment and the next increment begins. Otherwise, the increment is adjusted and another iteration is computed. In this study the force tolerance and increment step are handled automatically by ABAQUS.

Accuracy and convergence are two important features of any numerical model. The sources of error in the finite element method arise from discretization of the domain, approximation of the solution and numerical computation. These errors can be minimized

by proper selection of mesh, elements and solution method. Since there is no exact analytical solution to this particular problem, the accuracy of the solution cannot be explicitly checked. In this case the accuracy is gauged by comparisons made with the experimental results. Convergence describes the changes in the accuracy of the solution as the model is refined; either by increasing the order of the approximation functions (p-method) or by increasing the number of elements (h-method). An important feature in the development of the *weak* form of the governing equation is that the approximation functions are required to satisfy the conditions of compatibility and completeness to ensure convergence. Compatibility means that the approximation functions must be differentiable as required by the *weak* form. Completeness means that the approximation function must be a complete polynomial to represent the rigid body displacements and constant strain states. Since convergence is assured in this sense, convergence of the friction stir weld model is demonstrated using the h-method of mesh refinement.

Finite element analyses are typically completed in the following stages: pre-processing, simulation, and post-processing. The preprocessor is used to create the input file, which includes model geometry, finite element mesh, material properties, boundary conditions and analysis information. Simulation is the stage in which the analysis package solves the numerical problem described in the input file. The postprocessor is used to visualize the simulation results graphically. Although ABAQUS contains modules for each of these functions, only the analysis and postprocessor packages, ABAQUS/Standard and ABAQUS/POST, are used in this investigation. MSC-Patran is the preprocessor used to create the input file for use by ABAQUS.

In the discussion of the numerical models, the coordinate system is defined as follows. The loading direction, normal to the welding direction and in the rolling plane of the plate, is labeled the 11 axis; the direction corresponding to the specimen thickness is labeled the 22 axis; and for the 3-D model the welding direction is labeled the 33 axis. For all models, it is assumed that the material properties do not vary along the welding direction (this assumption is implicit in the 2-D models).

5.1 2-D Model Definition

Due to the generally accepted notion that the various weld regions produced by friction stir welding are homogeneous in the welding direction, an idea that was supported by the reduced thickness specimen experimental results, modeling the mechanical response of the friction stir weld can be viewed as a two-dimensional problem. Two-dimensional models are constructed for *nominal*, *hot*, and *cold*, full thickness specimens. The model domain for the full thickness specimen is chosen to represent the specimen gage section and measures 60 *mm* long and 8 *mm* thick. Based on the experimental data provided by the yield stress map, used to define the material distribution in the model, the domain for each specimen type is approximated using quadrilateral elements with an edge length of 0.25 *mm* and a unit thickness. This results in a uniform mesh with a spatial resolution sufficient to accurately capture the material distribution. Figure 5-1 shows the mesh for the full thickness specimen. The full thickness mesh consists of 7680 elements and 7953 nodes. For the h-method convergence test, the full thickness mesh is refined using an element length of 0.125 *mm*, resulting in 30720 elements and 31265 nodes.

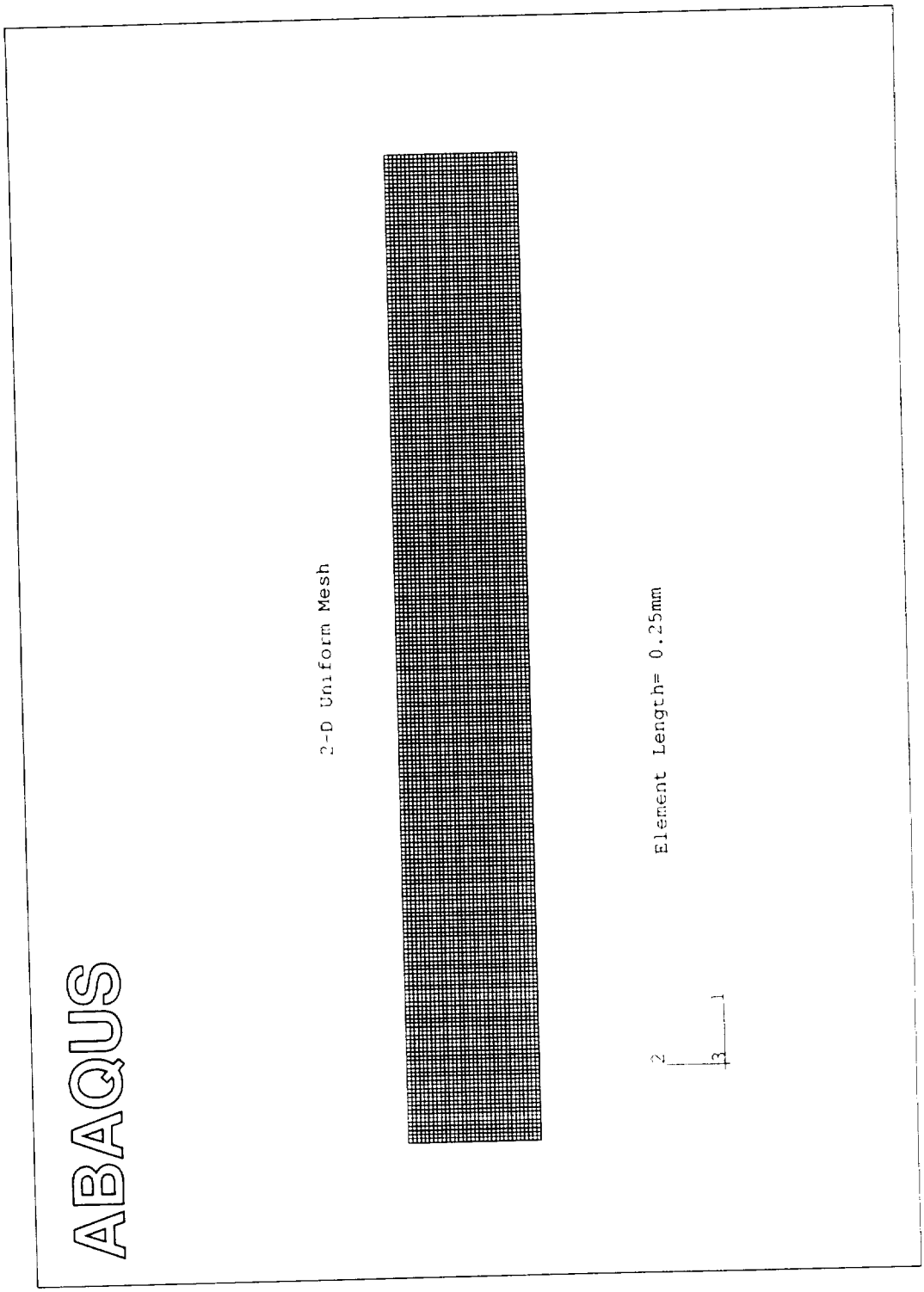

Figure 5-1 Uniform Mesh for Full Thickness 2-D FSW Models.

Material behavior is defined in the model using the *ELASTIC and *PLASTIC options in the ABAQUS input file. These options allow each weld material to be defined in terms of its elastic and plastic properties. Properties for the elastic response are given by the modulus of elasticity (E) and Poisson's ratio (ν) for the material. All of the materials are aluminum alloy 2024, therefore constant values of 73 GPa and 0.3 are chosen for E and ν, respectively. The true stress and corresponding true plastic strain values obtained from the experimentally determined constitutive data define the plastic behavior. The material distributions, provided by the yield stress maps, are created in ABAQUS using element sets. From the yield stress maps, the individual boundaries between the different weld materials were measured relative to the weld centerline. These locations are then used to determine the elements lying within these boundaries, which are subsequently assigned to element sets representing the various weld regions. Figure 5-2 shows the *nominal* weld mesh with the individual element sets indicated by alternating colors.

The boundary conditions imposed on the model are chosen to represent the actual tensile test. In the displacement controlled tensile test, one end of the specimen is fixed and a constant displacement is applied to the other end. As stated previously, the natural or force boundary conditions are included in the *weak* formulation of the equilibrium equation and correspond to the surface forces. For this problem the surface forces are zero. The essential or displacement boundary conditions for this problem are defined at the ends of the specimen. One end was fixed so that the displacements of the nodes at this end are zero in the 11 and 22 directions. A constant displacement in the 11 direction is applied to the nodes at the other end to simulate the tensile test.

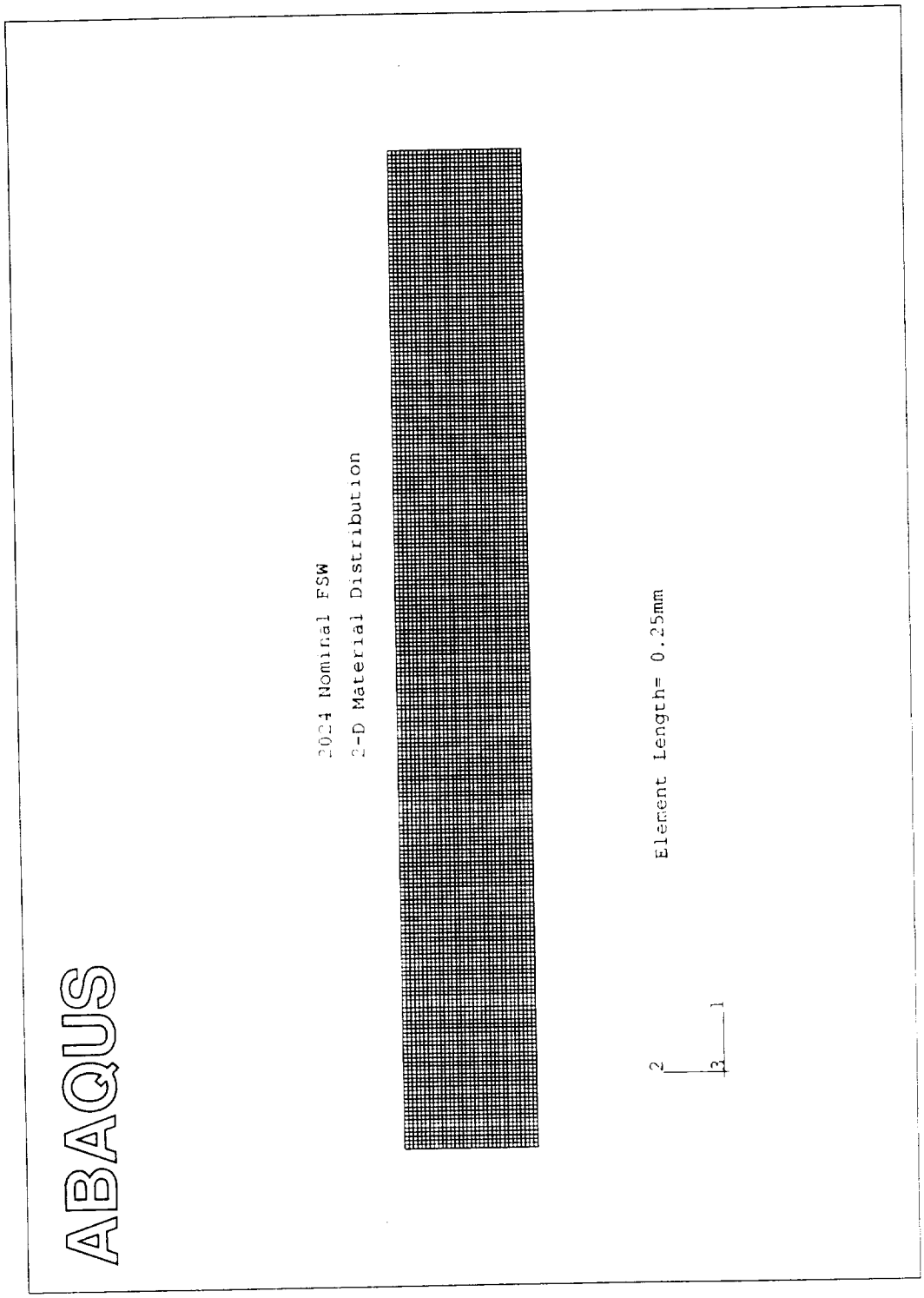

Figure 5-2 Material Distribution in the Nominal Weld. Element sets, indicated by alternating colors, are used to define different material regions.

The two dimensional model provides a method of conducting a limit analysis through the use of plane strain and plane stress elements. These two limiting cases are investigated for the *nominal* weld and, as it will be demonstrated, the actual conditions for the friction stir weld are best represented by the plane stress condition. All of the remaining 2-D models are analyzed under plane stress conditions.

5.1.1 Plane Strain

Plane strain is a 2-D idealization of the state of strain and stress representative of infinitely thick 3-D structures. Deformation is restricted in the out of plane direction, associated with the thick dimension, as a result of the excess material constraining the deformation and the resulting triaxial stress state. The plane strain model is created using the CPE4 elements from the ABAQUS solid element library. These first order continuum plane strain (CPE) elements are 4-node quadrilateral, solid elements with linear interpolation and full integration. The degrees of freedom associated with the nodes are the primary variables calculated during a simulation, in this case the displacements. Linear interpolation is used to calculate the degrees of freedom at any other point in the element. All other quantities are integrated over the volume of the element and evaluated at the integration points. Full integration and reduced integration refer to the number of integration points used in the calculations and depending on the problem, the number of integration points can greatly affect the accuracy of the element by introducing locking or hourglassing problems. Hourglassing is not a problem associated with fully integrated elements and locking is only a concern for first order, fully integrated elements subject to bending loads or when the material is incompressible.

5.1.2 Plane Stress

The opposite extreme to the plane strain condition is plane stress. Plane stress is a 2-D idealization representative of thin 3-D structures. Under plane stress conditions the out of plane stress is zero, therefore, no triaxial constraint can develop. The plane stress model is constructed using the CPS4 element. These first order elements, like the CPE4 elements, are 4-node quadrilateral, solid elements with linear interpolation and full integration.

5.2 3-D Model Definition

The 2-D plane strain and plane stress representations demonstrate the extremes in terms of material constraint. In order to examine intermediate levels of constraint, 3-D models of varying specimen size were constructed. Since the specimen thickness is an experimental constant the dimension that is varied is the width, corresponding to the actual direction of welding and the out of plane dimension in which the constraint is developed in 2-D. One of the assumptions made about the FSW process, which led to the initial 2-D simulations, is that under steady state conditions the resultant material properties are homogeneous in the welding direction. In light of this assumption, the 3-D models are constructed by extending the 2-D model in the welding direction (33), i.e. out of plane dimension. To obtain manageable model sizes and reasonable computational times, the element sizes are increased from 0.25 *mm* to 0.5 *mm* in both the 11 and 22 directions and the element width is defined as 1 *mm* in the 33 direction. Although this results in a slightly coarser mesh, the spatial resolution is still adequate to capture the

detail in the material distribution. The boundary conditions for the 3-D models are the same as for the 2-D model. One end is fixed in the 11 and 22 directions and a constant displacement is assigned to the other end.

Chapter 6 Finite Element Model Results

The purpose of developing numerical models is to provide a tool for making predictions and gaining insight about a particular problem. For this study, the friction stir weld model is used to verify the local constitutive data obtained by the proposed experimental technique and justify the assumption of iso-stress loading conditions. The model development began with 2-D plane strain and plane stress models and led to 3-D models to validate findings from the 2-D limiting cases. All of the work done in developing the 2-D model was based on the full thickness *nominal* weld specimen. This included plane strain and plane stress analyses and eventually led to the conclusion that the plane stress model provided the best representation of both the local and global response. Therefore, only the *nominal* weld was modeled in both plane strain and plane stress. The *hot* and *cold* welds were modeled as plane stress.

Two-dimensional and three-dimensional models simulating the uniaxial tensile response of various friction stir welds have been constructed using experimentally determined local constitutive data. In order to capture both the local and global response that was observed in the experiments, several different materials were identified for each weld and their distributions within the model were established using the yield stress maps as guides. The modeling results are presented in terms of global and local mechanical response for direct comparisons with the experimentally measured results.

6.1 Global Mechanical Response

Initially, the FSW was modeled as plane strain because it was believed that the heterogeneity associated with the weld might result in material constraint within this region. The local response, which will be shown later, indicates that the model provides an excellent description of the local material behavior; however, the predicted global response does not match the post yield behavior shown by the experimental data. The global response, in terms of engineering stress and strain, for the plane strain model is shown in Figure 6-1. Global stress levels for the model are determined by summing the reaction forces for all the nodes at the displaced end of the specimen and dividing by the original cross-sectional area. Although the model response exhibits the same shape as the experimental curve, it is clear that for a given stress level, the model significantly under-predicts the specimen strain. Based on these results, it was believed that the discrepancies between the experimental and model results were attributed to inaccurate material properties or to the constraint imposed by the plane strain condition.

To examine the possibility of inaccuracies in the material properties, associated with the iso-stress approximation, the plane strain model was re-run using the local constitutive data obtained from the *middle* reduced thickness specimen. The results from this model are also shown in Figure 6-1 as indicated by the Nominal (Plane Strain Iso) data. Again, the plain strain model does a poor job of predicting the global response even with improved material properties, which indicates that the problem is most likely associated with the plane strain condition. While the results from the two models do not match the experimental data, it is interesting to note that the differences between the two models are very slight. This provides solid evidence that the constitutive data obtained

from the full thickness specimen is very similar to the data obtained from the reduced thickness specimens, thus justifying the use of the iso-stress approximation.

The issue of constraint was then examined by modeling the FSW specimen as plane stress. In this case, the model accurately predicts the tensile response as shown in Figure 6-2. It is obvious from these results that the triaxial stress state developed in the plane strain model excessively constrains the material from deforming and is not an appropriate representation of the actual stress state within the FSW. Although the actual out of plane stress (σ_{33}) may not be identically zero, near plane stress conditions appear to exist and will therefore be used to model the *hot* and *cold* welds. However, three-dimensional models depicting specimens of varying width will be used to examine the triaxial stress state and justify the plane stress representation. The global responses for the hot and cold models are shown in Figure 6-3 and Figure 6-4, respectively. In both cases, the plane stress model does an excellent job of predicting the actual weld response.

One thing to note from the global results is that the strain range over which the model provides prediction is only a fraction of the total specimen strain. This is a consequence of the limited constitutive data obtained using the experimental technique. Information can only be gathered over the strain range determined by the weakest region in the weld. Reducing the intervals at which the images are recorded would provide more information but, in order to capture the maximum amount of data, an image would need to be recorded at a point in the loading history just prior to failure. However, this is not an easy task. At the same time, increasing the number of images recorded in a test greatly increases the time required for correlation and extraction of the local constitutive data. Strain hardening is included in the material definition through the addition of true stress-

true plastic strain values and the material behavior for the model is limited by the maximum true stress value included in the material definition. Once this value is exceeded, the material becomes perfectly plastic and the elements associated with this material become distorted, leading to solution problems. Therefore, the displacement applied to the model was chosen so that this situation did not occur.

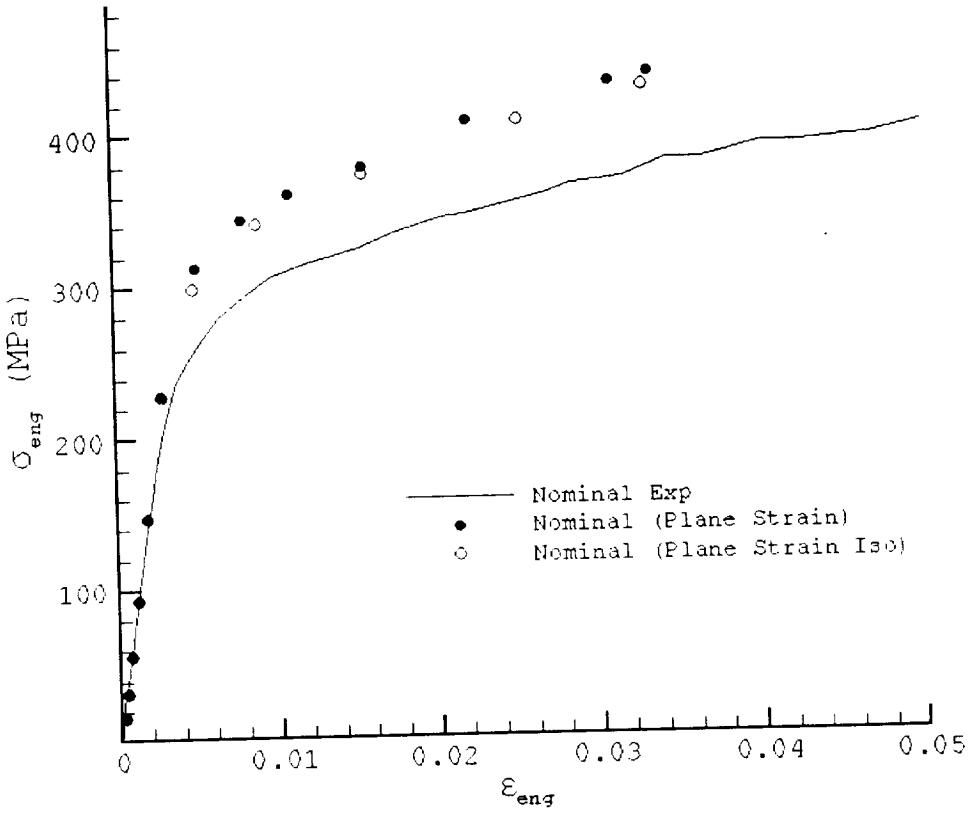

Figure 6-1 Nominal FSW Global Response Predictions (2-D Plane Strain). The Plane Strain Iso model used iso-stress materials.

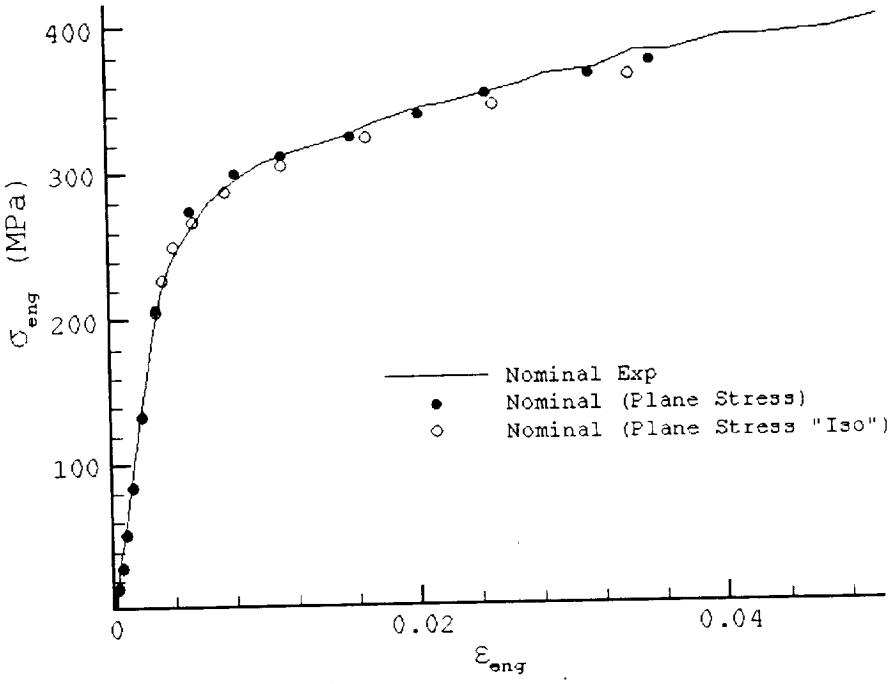

Figure 6-2 Nominal FSW Global Response Predictions (2-D Plane Stress). The Plane Stress Iso model used iso-stress materials.

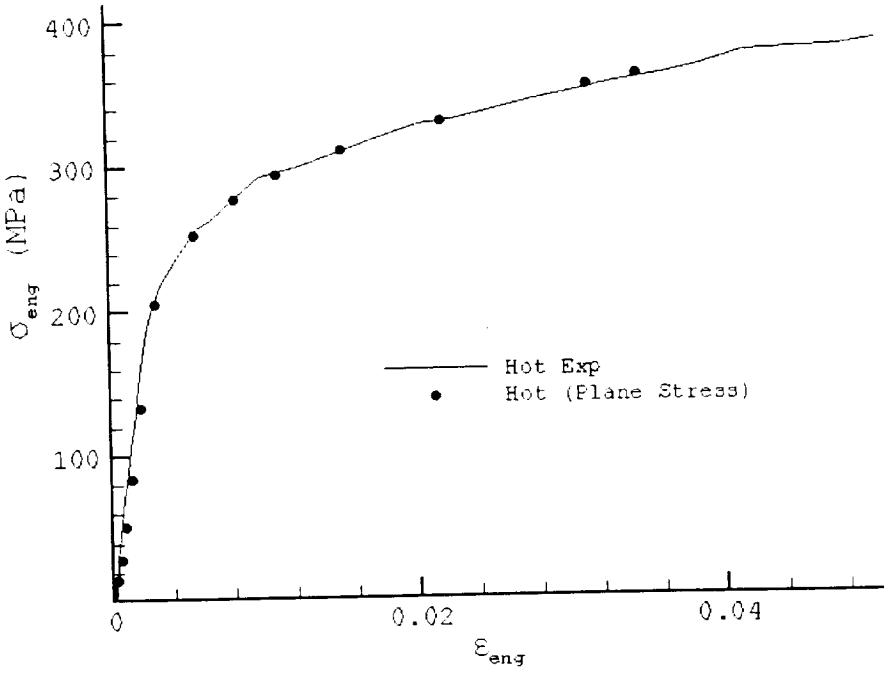

Figure 6-3 Hot FSW Global Response Prediction (2-D Plane Stress).

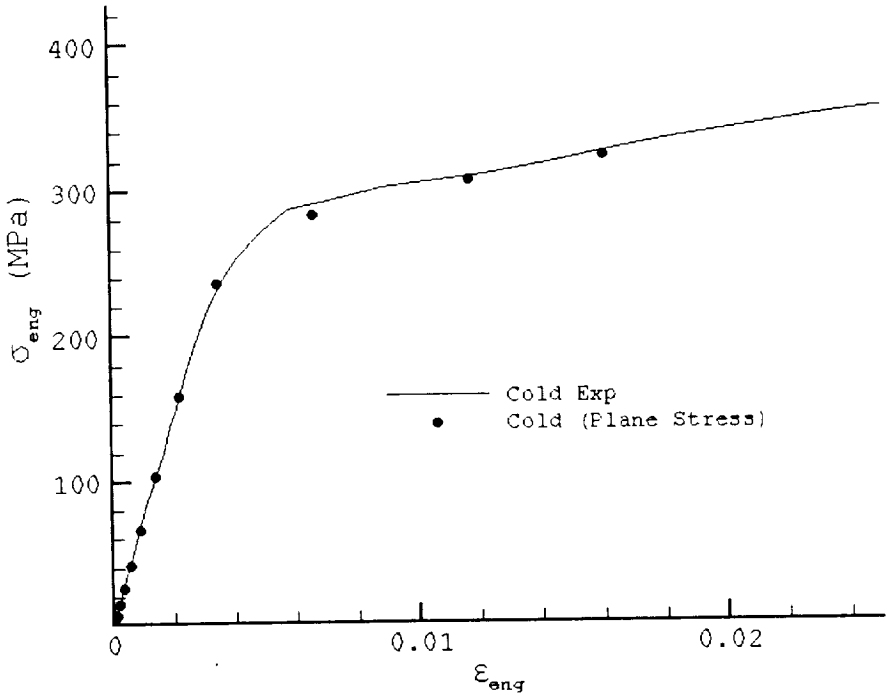

Figure 6-4 Cold FSW Global Response Prediction (2-D Plane Stress).

6.2 Local Mechanical Response

The ability to predict the global response of the FSW has been demonstrated by the 2-D plane stress model. Prediction of the global response, however, is only part of the requirement needed to show the accuracy of the model. The 2-D model must also be able to predict the local response that is observed in the full field experimental data. Results from the experimental data were presented as contour plots of the normal strain ($\varepsilon 11$) distribution at various global specimen strain levels. The results from the three weld models are presented in the same manner to provide visual comparison with the

experimental results. For each weld, the plots correspond to the maximum global strain level achieved in the model.

The plane strain and plane stress model results for the *nominal* weld are shown in Figure 6-5 and Figure 6-6, respectively. Qualitatively, the models show the same trends as the experimental data, with strain localizations occurring in the advancing and retreating side heat affected zones. Both models indicate maximum strain localizations in the retreating side HAZ, which is consistent with the experimental results for this weld. Overall, the differences between the two models do not appear to be that noticeable at approximately the same global elongation, however, it should be noted that the global stress level is 440 MPa for the plane strain model and 370 MPa for the plane stress model. This provides further evidence that the constraint imposed by the plane strain condition is unrealistic for the FSW.

The local responses for the *hot* and *cold* welds are shown in Figure 6-7 and Figure 6-8. From the *hot* weld experimental results, the retreating side HAZ localization was much more pronounced than the advancing side HAZ and the model demonstrates this result. The same was true for the *cold* weld, at least until the localization associated with the lack of penetration defect became dominant, and again the model shows this trend. These qualitative observations support the general viability of the model, however, a quantitative comparison of the model and experimental results is needed.

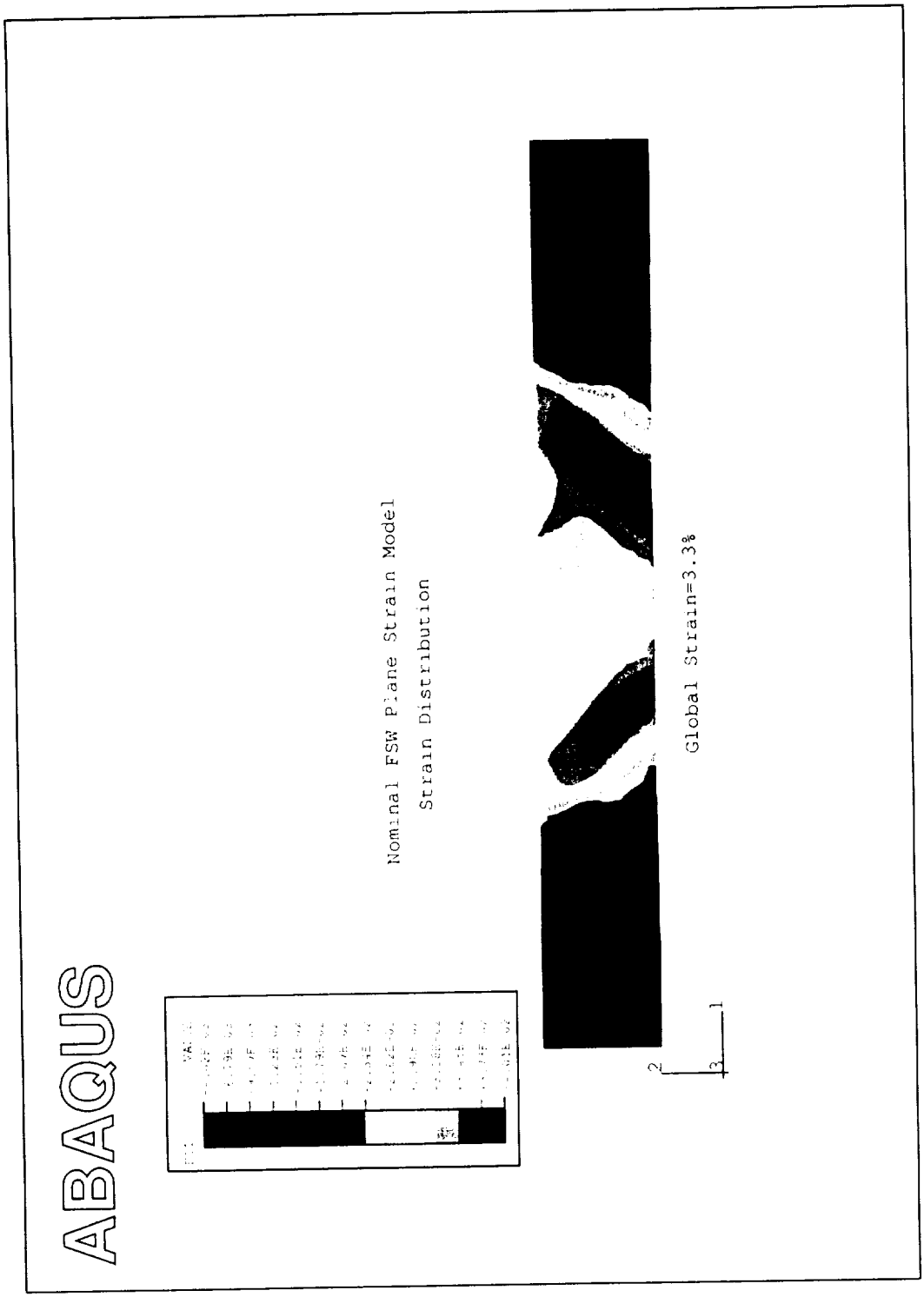

Figure 6-5 Nominal FSW Local Response Prediction. (2-D Plane Strain)

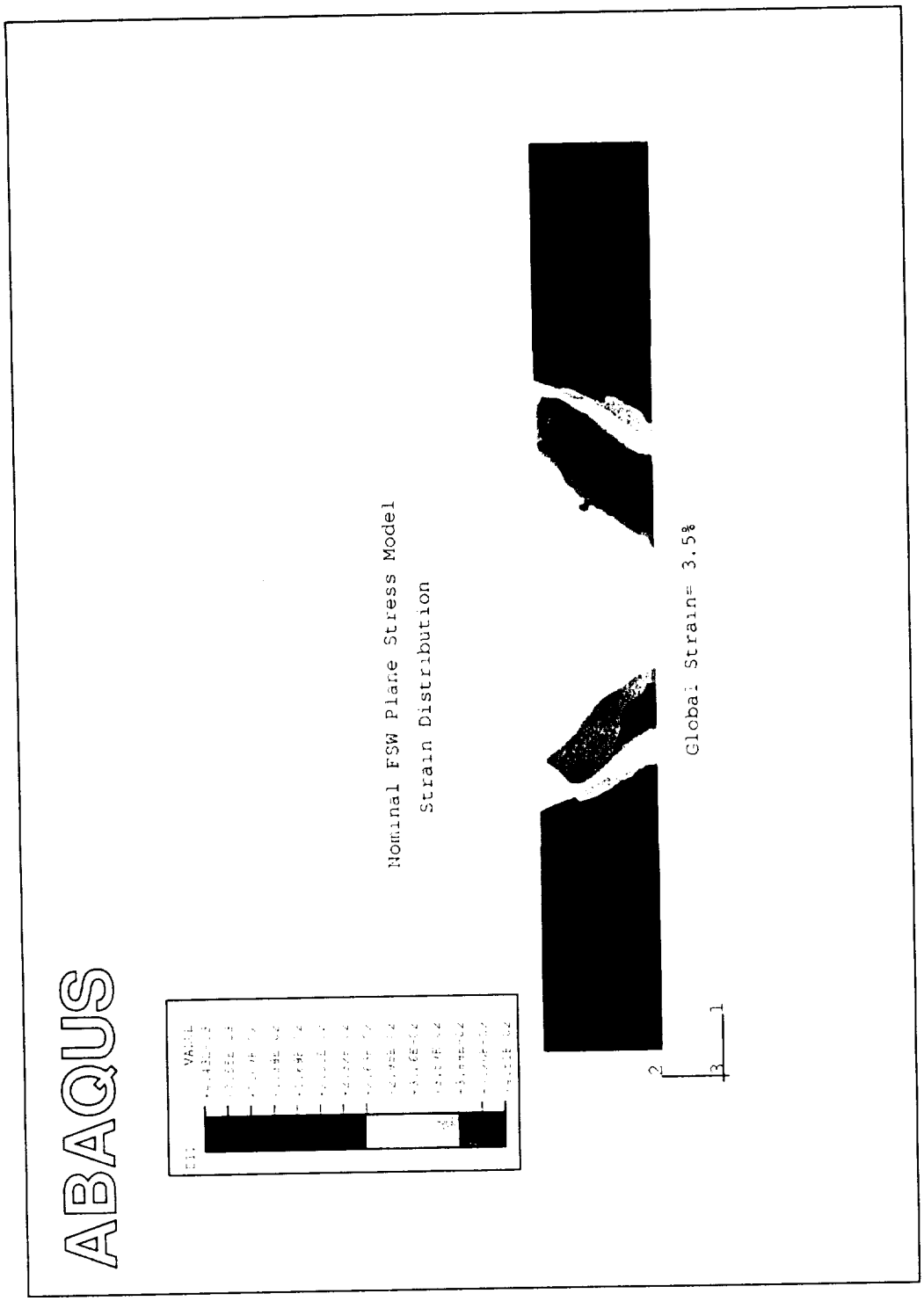

Figure 6-6 Nominal FSW Local Response Prediction (2-D Plane Stress).

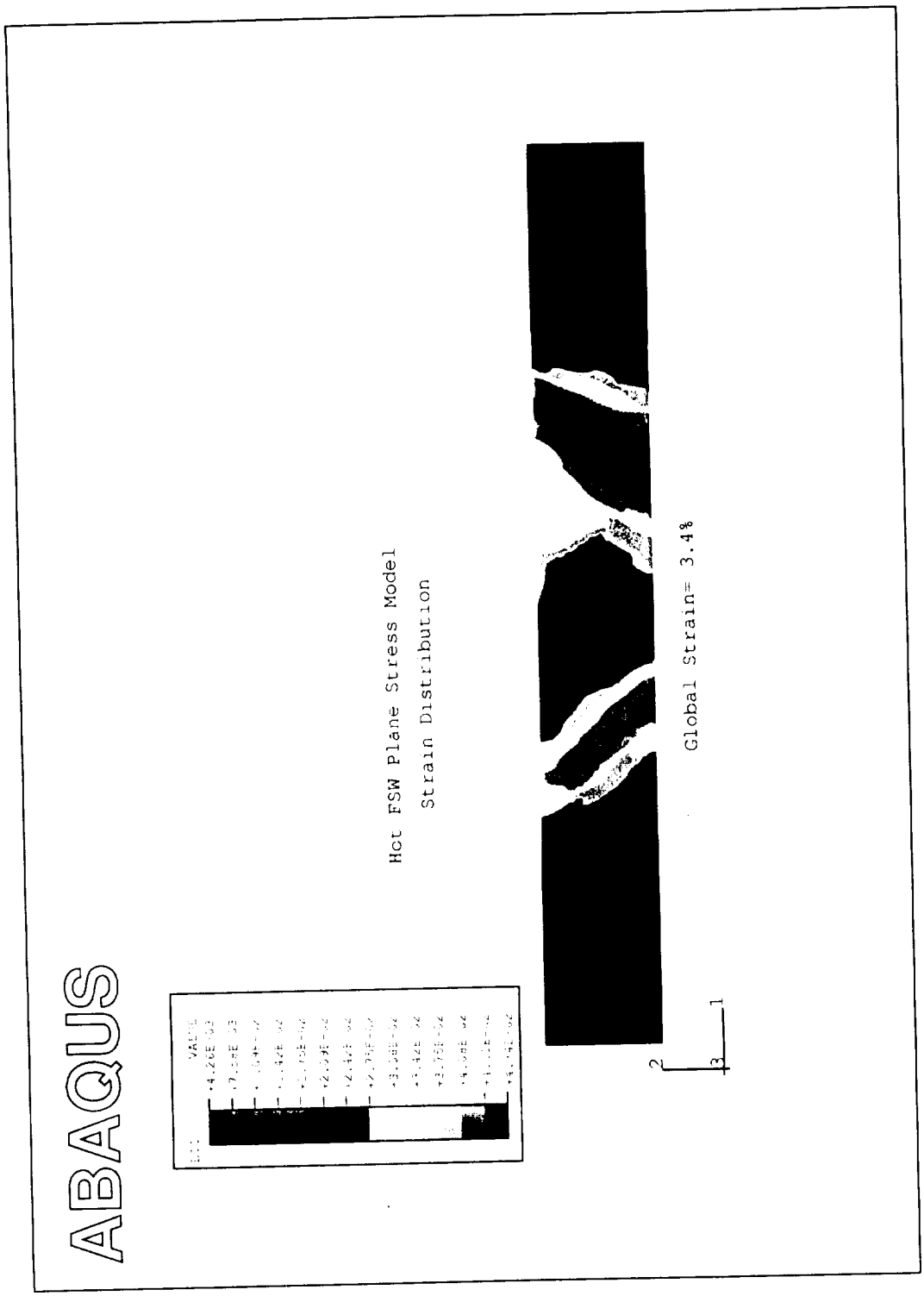

Figure 6-7 Hot FSW Local Response Prediction (2-D Plane Stress)

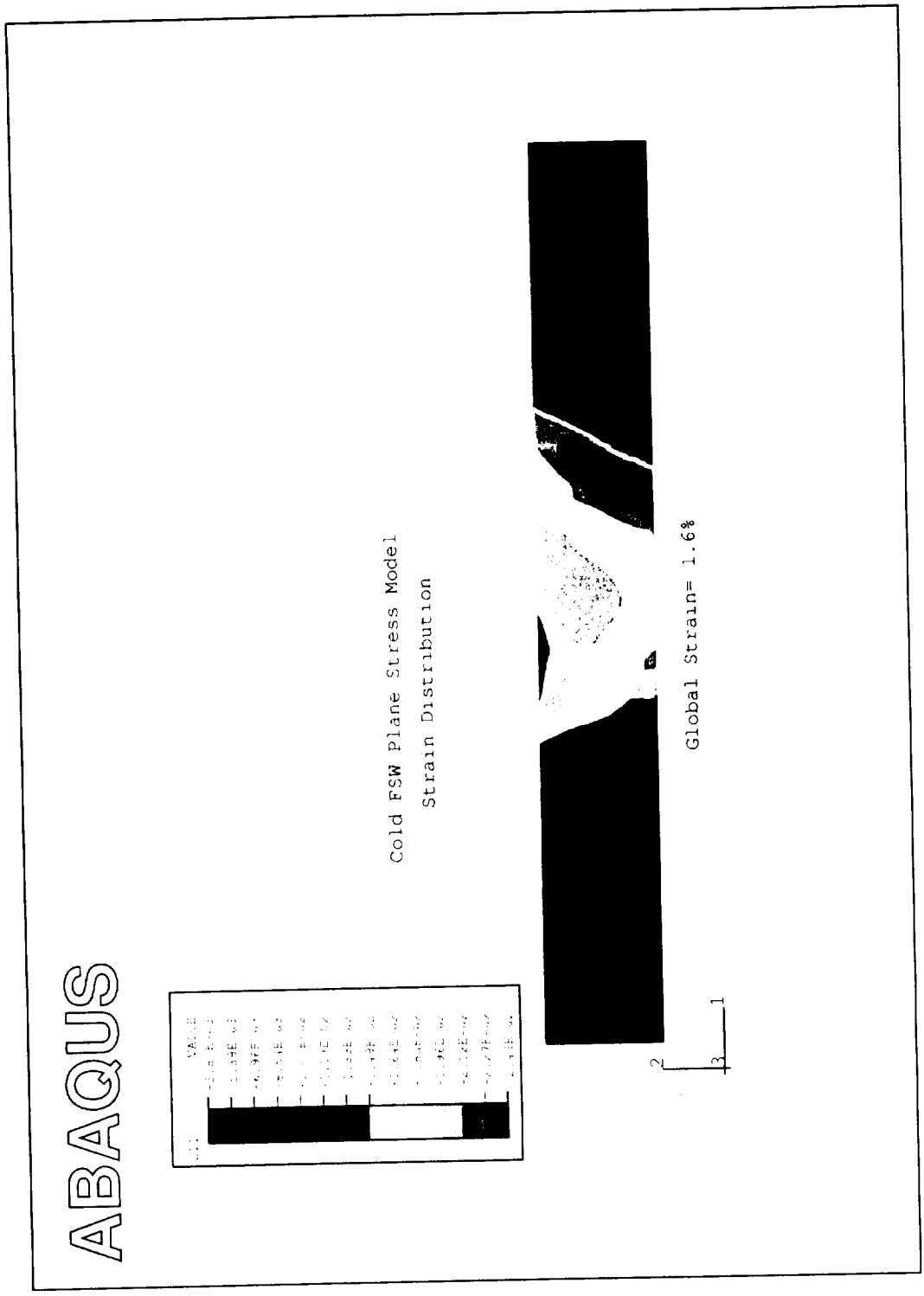

Figure 6-8 Cold FSW Local Response Prediction (2-D Plane Stress)

To provide a quantitative comparison of the experimental and model results, the local responses are evaluated at approximately equivalent global elongations. The normal strain (ε_{11}) is then plotted relative to the weld centerline at different locations within the weld to gauge the model performance. Locations near the top, middle and bottom of the weld are chosen for the comparisons.

The plane strain and plane stress model results for the *nominal* weld are shown in Figure 6-9 and Figure 6-10, respectively. For each case, the results are presented from two simulations. One corresponds to the model using the constitutive data from the full thickness specimen and the other to the model using the properties from the reduced thickness specimen (this model is labeled as "Iso"). The plane strain and plane stress models provide a good description of the variation in the normal strain across the entire width of the weld and from top to bottom; however, it is seen that the "Iso" models predict higher strain levels in the heat affected zones and lower strain levels in the nugget and are not as good overall. This does not imply that the material properties obtained from the reduced thickness specimen are less accurate than those from the full thickness specimen. In fact, these material properties are more accurate, but only for the general location, relative to the full thickness specimen, that the specimen represents. For example, the material properties from the *middle* specimen are accurate only for the regions at the mid-thickness of the full size specimen. Recall that each region in the model is defined by a single material behavior. Thus, using a material defined from the reduced thickness specimen in the model results in a poor prediction because it does not provide adequate representation of the region as a whole.

Effectively, the constitutive data defined from the full size specimen represent "average" properties for the respective regions because the effects of the material gradient, from the top of the weld to the bottom, are included in the experimental measurements. Consequently, the models using these materials provide better predictions. As shown by the results for these models, the locations of the strain localizations as well as the magnitudes are in good agreement with the experimental data. It should be noted that the actual global strain level from which the plane strain model results were obtained was approximately 3.3% while the experimental data correspond to a slightly lower strain level of 3.1%.

Model predictions for the *hot* and *cold* welds are shown in Figure 6-11 and Figure 6-12, respectively. These welds were modeled as plane stress and the results are in excellent agreement with the experimental data. For the *hot* weld, the model predicts almost identical distributions in the normal strain over the entire weld region. The predictions for the *cold* weld are also very close to the experimental data, particularly at the top and middle of the weld. At the bottom, however, the experimental data indicates the presence of the defect in the nugget region, which is not captured by the model. The material behavior defined for the nugget includes the effects of this localization, but its influence is averaged out in choosing a single point in the center of the specimen to construct the constitutive data. Overall, the model provides a very good representation of the local material behavior.

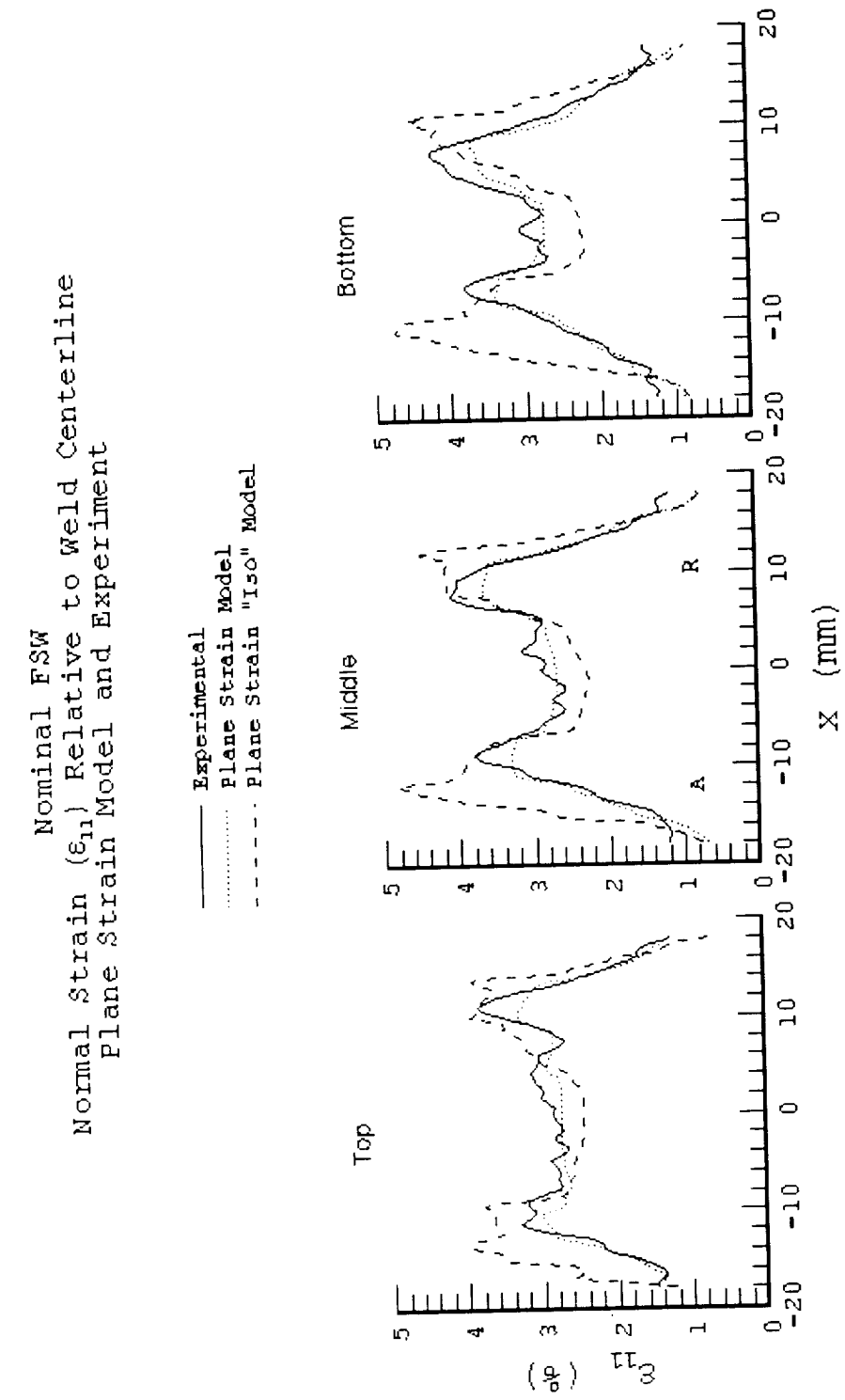

Figure 6-9 Nominal FSW Local Response Comparison (Plane Strain Model). Approximate global strain of 3.3%.

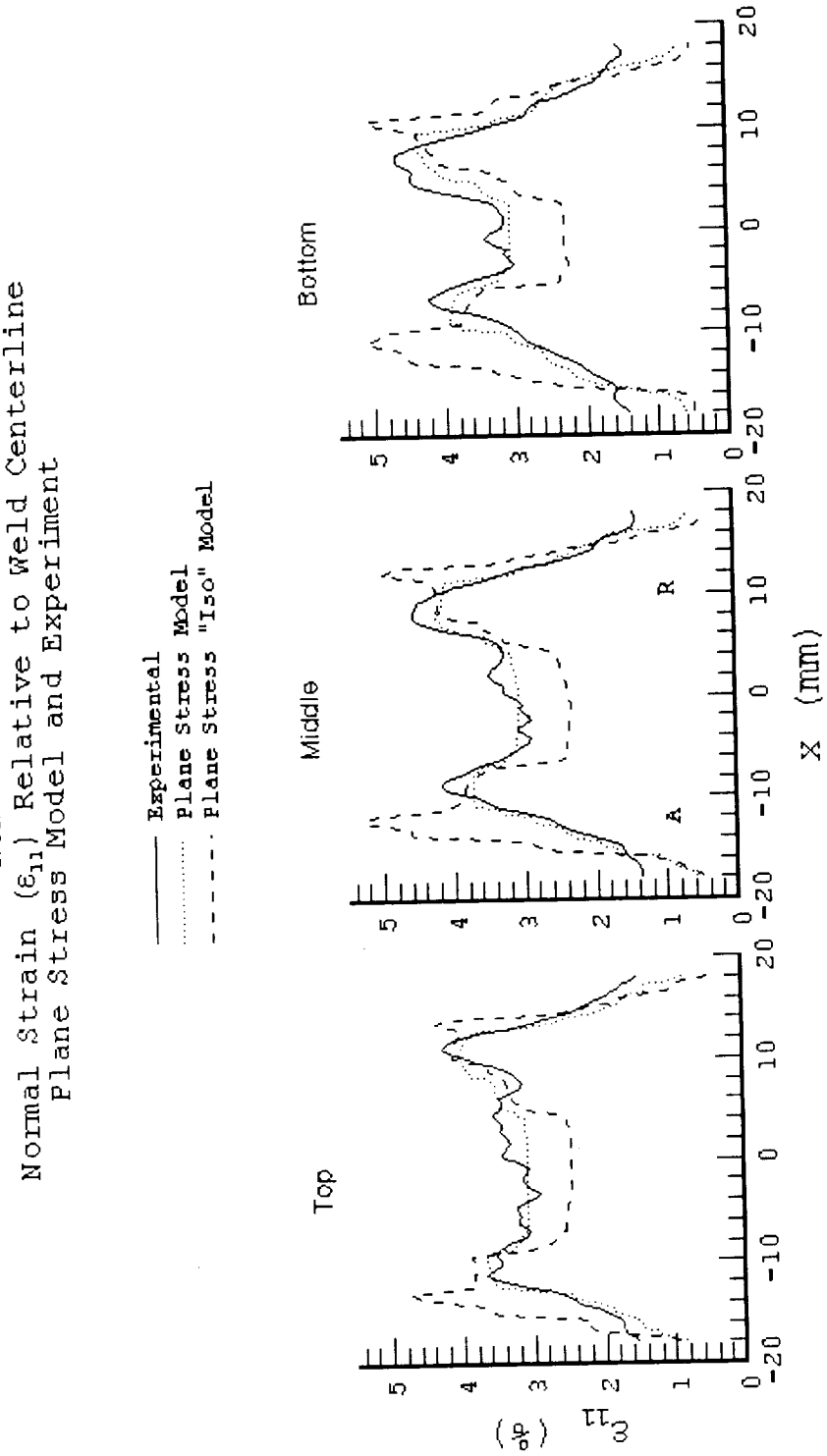

Figure 6-10 Nominal FSW Local Response Comparison (Plane Stress Model). Approximate global strain of 3.5%.

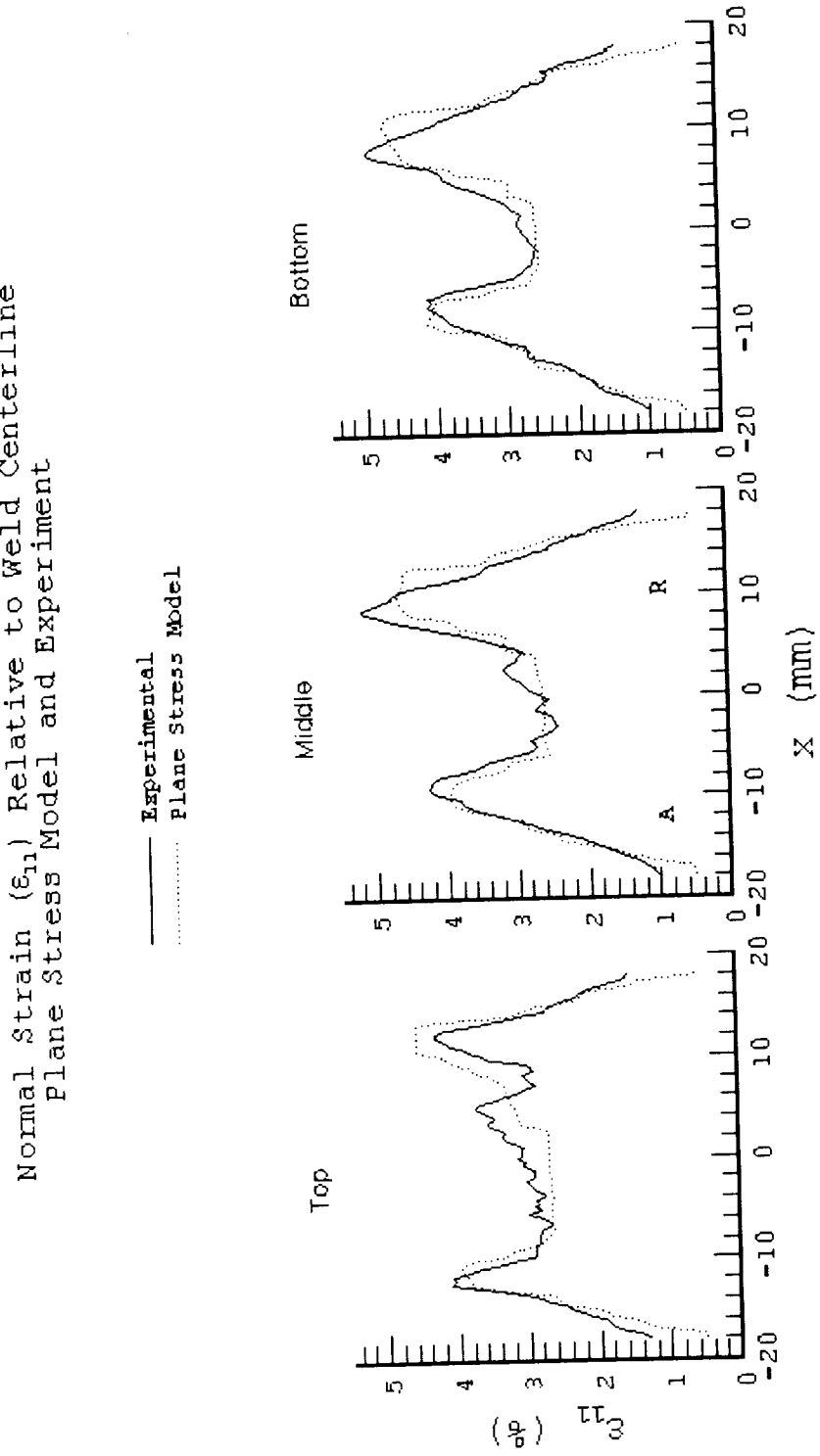

Figure 6-11 Hot FSW Local Response Comparison (Plane Stress Model). Approximate global strain of 3.4%.

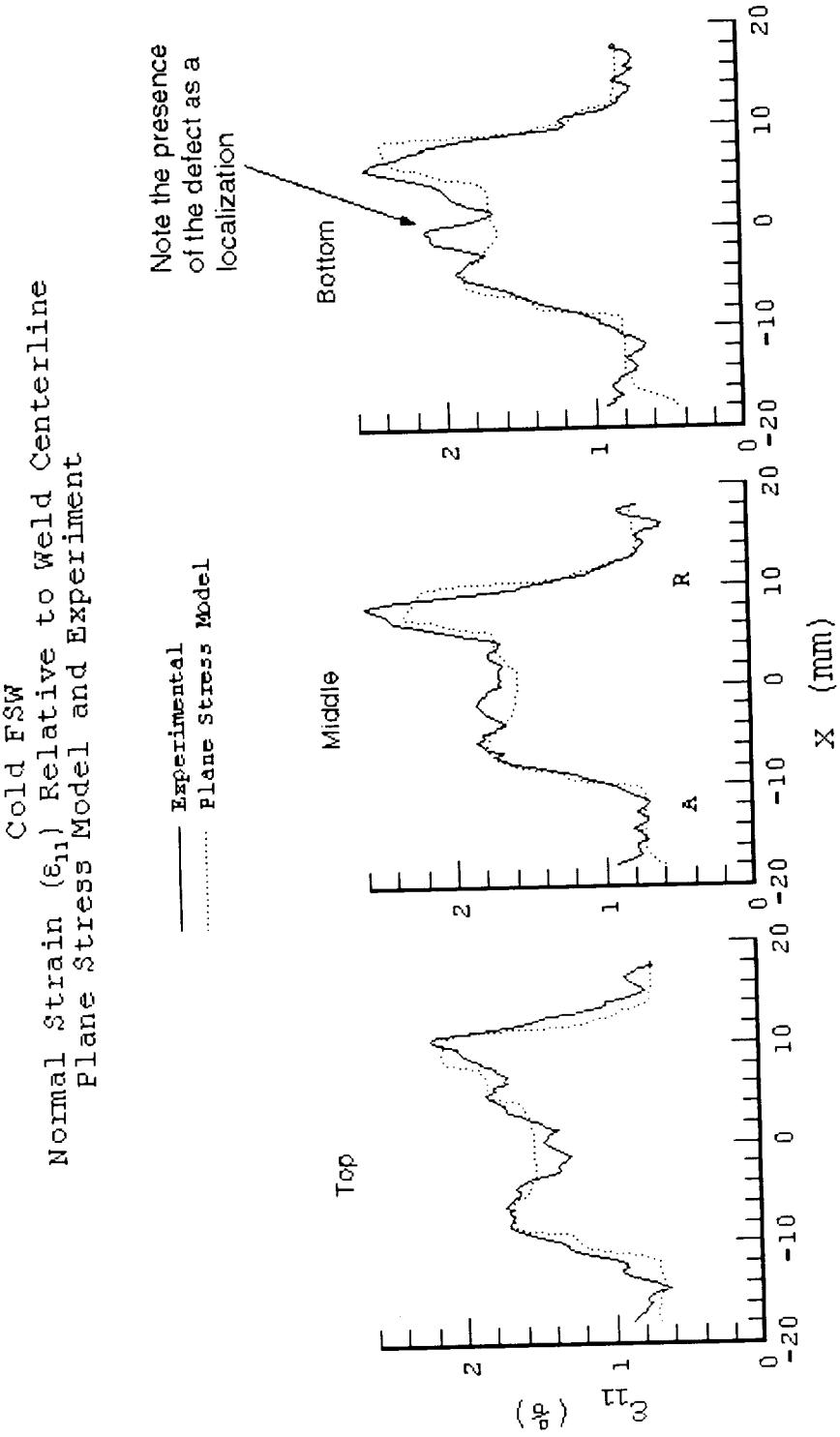

Figure 6-12 Cold FSW Local Response Comparison (Plane Stress Model). Approximate global strain of 1.6%.

Before discussing the justification for using the plane stress representation, it is appropriate to demonstrate the convergence of the 2-D model using an h-method mesh refinement. Due to the necessity to capture the gradients in the material distribution, a very fine, uniform mesh was required from the beginning. The element edge length for the original model was 0.25 *mm*, which resulted in 7680 elements and 7953 nodes. In the refined mesh, an element length of 0.125 mm was chosen so that each original element was divided in four. The new model consisted of 30720 elements and 31265 nodes.

Convergence through mesh refinement is used to demonstrate that the model has an adequate mesh density to capture the strain gradients that exist within the weld region. The *nominal* weld was chosen for this demonstration and the results are presented in Figure 6-13. It is clearly seen that the refined model predicts almost the identical response as the original model at each location in the specimen and across the width of the weld, indicating that the two models have converged to the same solution. Figure 6-14 shows the global response predictions for the original and refined models, which also demonstrate the convergence of the 2-D model.

The global and local response predictions that have been shown thus far have indicated that the plane stress model provides a much better representation of the friction stir weld response than does the plane strain model. However, these two limiting cases demonstrate the extremes in terms of material constraint. In order to examine intermediate levels of constraint and justify the plane stress representation, 3-D models of the *nominal* weld were analyzed. These results are presented next.

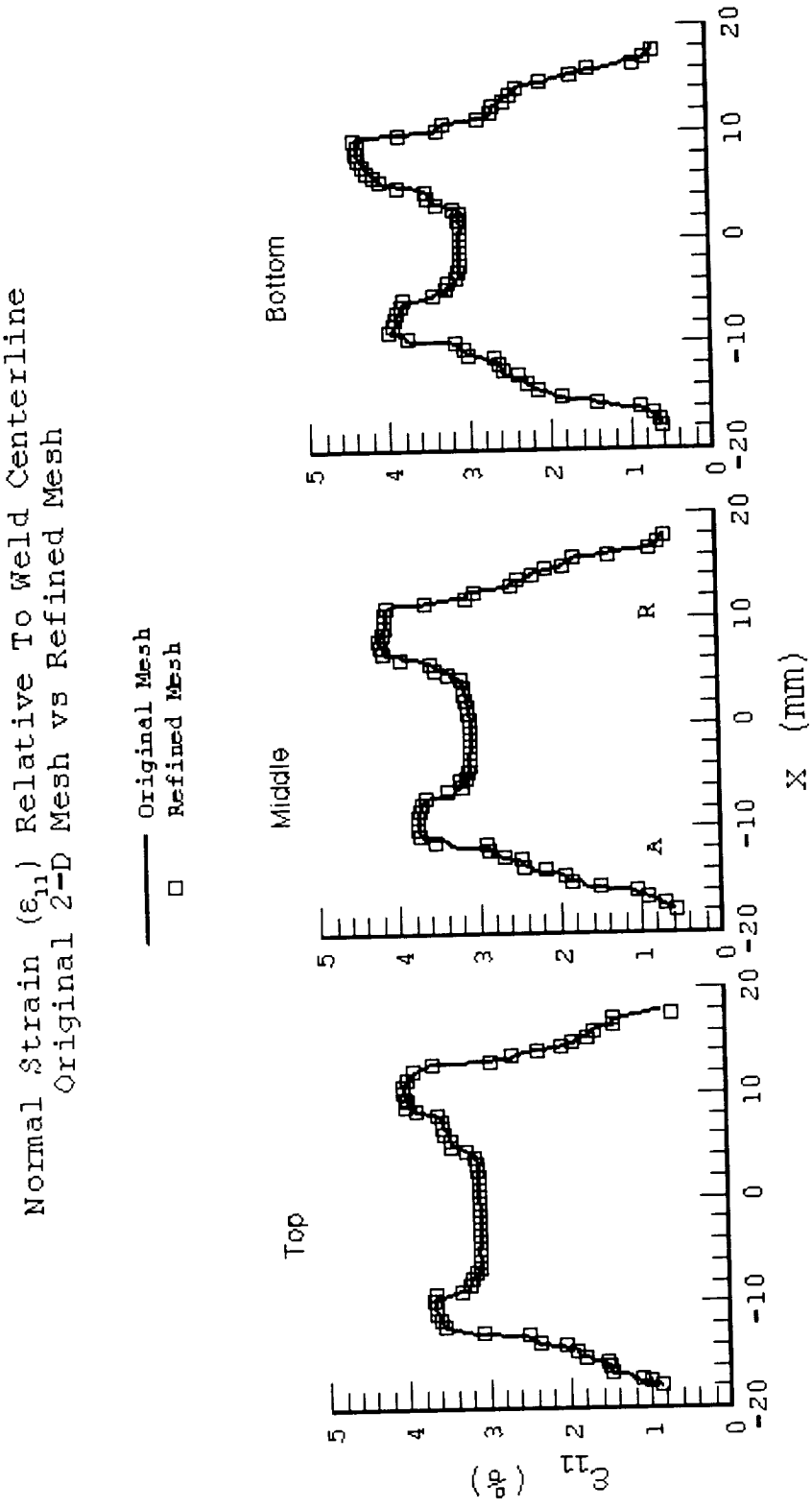

Figure 6-13 Results of the normal strain distribution in the nominal weld showing convergence of 2-D model using h-method mesh refinement.

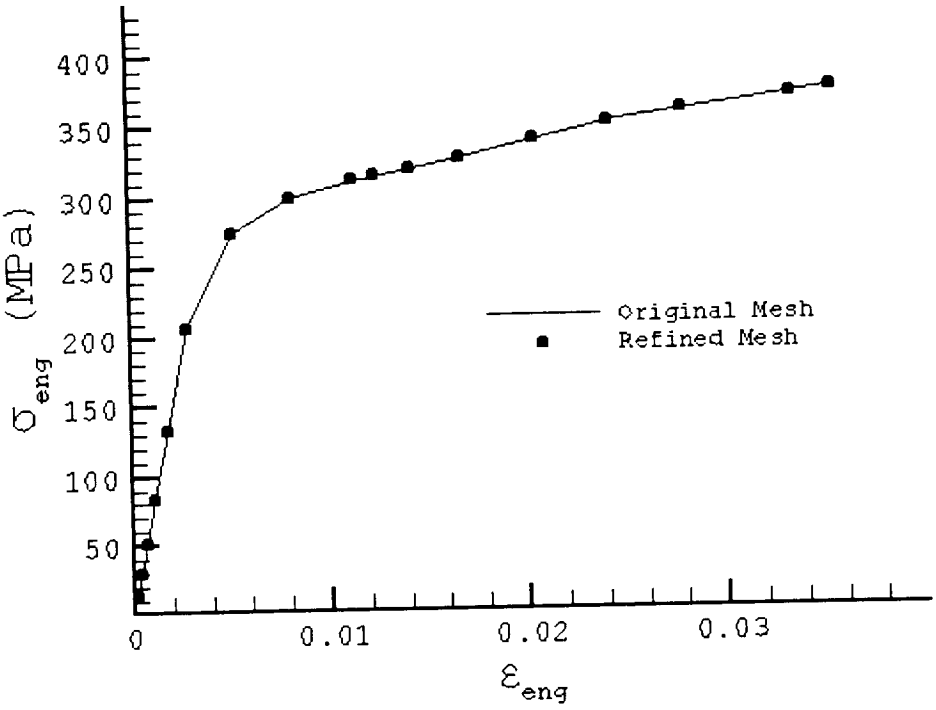

Figure 6-14 Global response prediction for the nominal weld showing convergence of the 2-D model using h-method mesh refinement.

6.3 3-D Model Results

The fact that the plane stress model provides a better representation of the friction stir weld in 2-D than plane strain suggests that the triaxial constraint is very nearly zero. Constraint is quantified by examining the levels of the 33 stress at various positions within the weld, which in reality will reach maximum values at some finite specimen width. Several models were constructed by incrementally increasing the specimen width until the observed stress levels approached constant values. The specimens considered were 6, 12, 24 and 30 *mm* in width.

Figure 6-15 shows the stress distributions (σ_{33}), relative to the weld centerline, at mid-thickness on the model mid-plane for each of the models examined. At

approximately equal levels of global specimen strain, the stress values (σ_{33}) appear to reach a maximum at a specimen width of 30 mm, which is two and a half times the width of the actual specimen used in the experimental testing. When this maximum constraint is compared to the theoretical limits obtained by the 2-D plane strain and plane stress models, as seen in Figure 6-16, it becomes evident that the constraint condition developed in the FSW specimen is very nearly plane stress. These results suggest that, although increasing the specimen width causes some increase in constraint, the amount of constraint developed is primarily limited by the specimen thickness.

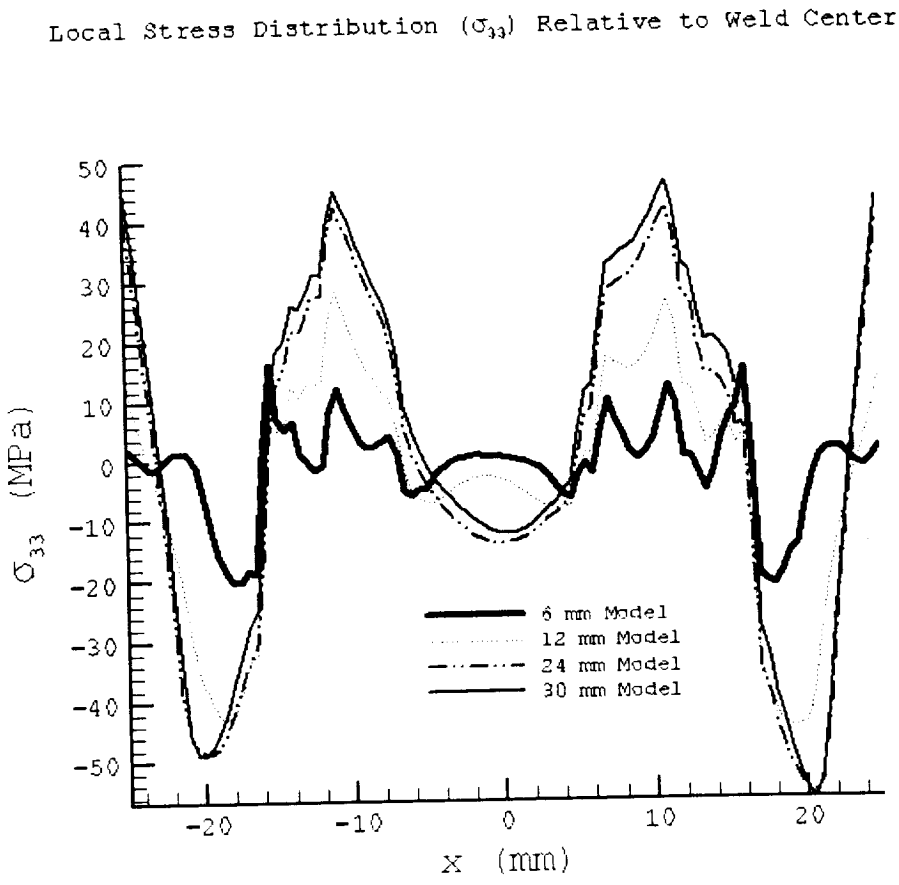

Figure 6-15 Stress distributions relative to weld centerline for all 3-D models. Data extracted from the mid-plane of each model at the mid-thickness

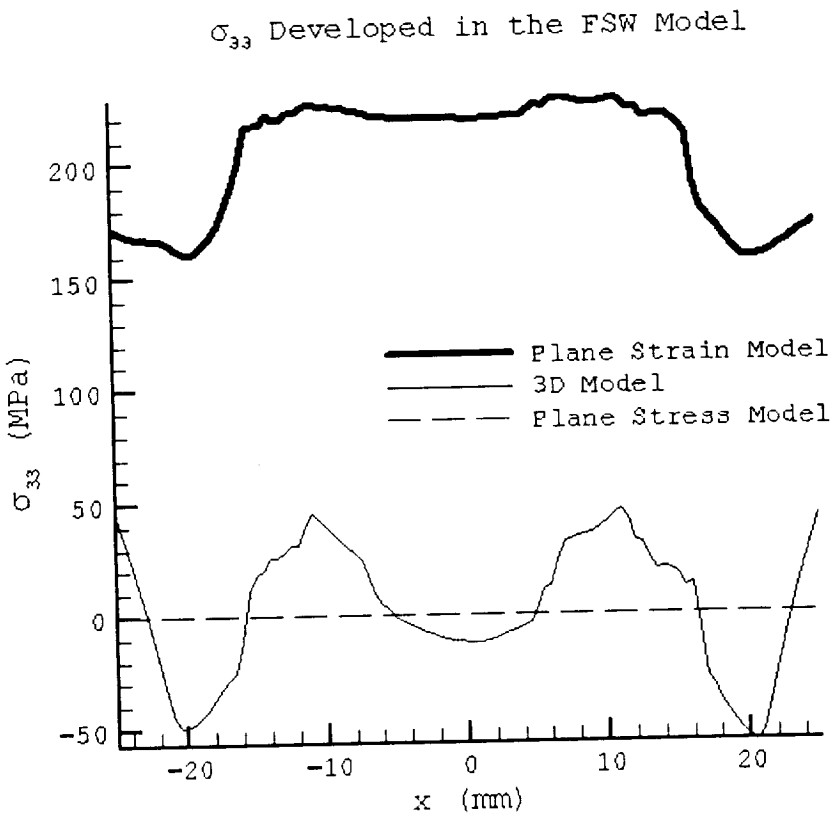

Figure 6-16 Constraint developed in the 3-D model compared to the plane strain and plane stress theoretical limits.

An interesting feature of the σ_{33} distribution that can be observed in Figure 6-15 and Figure 6-16 is the presence of regions of negative σ_{33} stress outside of the HAZ on both advancing and retreating sides of the weld. The negative values of σ_{33} will lower the apparent yield strength of material adjacent to but outside of the weld, thereby mitigating the strain localization resulting from the presence of low strength regions in the HAZ.

The triaxial stresses developed in the 3-D model will result in different responses than those predicted by the 2-D plane stress model. A comparison of the global and local

response predictions for the 2-D and 3-D models is presented here. Since the full size specimen used in the experiments was 12 mm wide, only the 12 mm wide 3-D model is considered. Figure 6-17 shows the global response predictions for the 2-D and 3-D models. The 3-D model does predict slightly higher post yield stress levels as a result of the additional constraint, but overall the two curves are nearly identical.

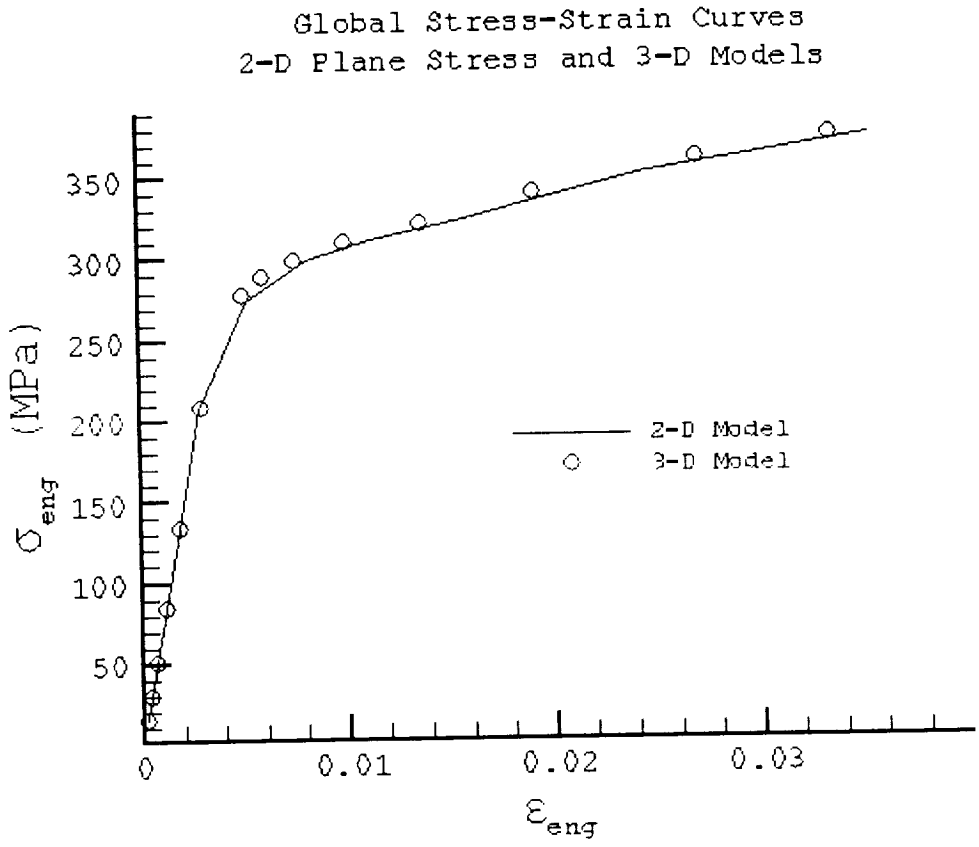

Figure 6-17 Comparison of 2-D and 3-D global response predictions.

The local response for the 3-D model is shown in Figure 6-18 as a contour plot of the normal strain (ε_{11}) distribution at a global strain level of approximately 3.3%. Qualitatively, the response is consistent with the trends predicted by the 2-D model (Figure 6-6). Strain localizations are present in the low strength heat affected zones and the nugget region exhibits a fairly uniform strain. A more detailed comparison is provided in Figure 6-19, which shows the normal strain distribution at the mid-thickness on the front surface of the 3-D model along with the mid-thickness distribution for the 2-D model. The effect of the triaxial stresses is evident in the slightly higher strains predicted by the 3-D model in the nugget and also in the transition region between the base metal and HAZ, but, overall, the two models are in very good agreement.

To summarize, the finite element model of a transversely loaded friction stir weld has been developed using experimentally measured local constitutive data and material distributions as input. Two-dimensional plane strain and plane stress simulations have indicated the state of constraint in the FSW specimen as that of nearly plane stress and the results of 3-D finite element models support these findings. The global and local response predictions for three different welds, modeled as plane stress, have been verified by the experimental results. In addition, 2-D simulations using material properties from the reduced thickness specimens confirm the use of full thickness material properties in characterizing the local constitutive behavior of the friction stir weld.

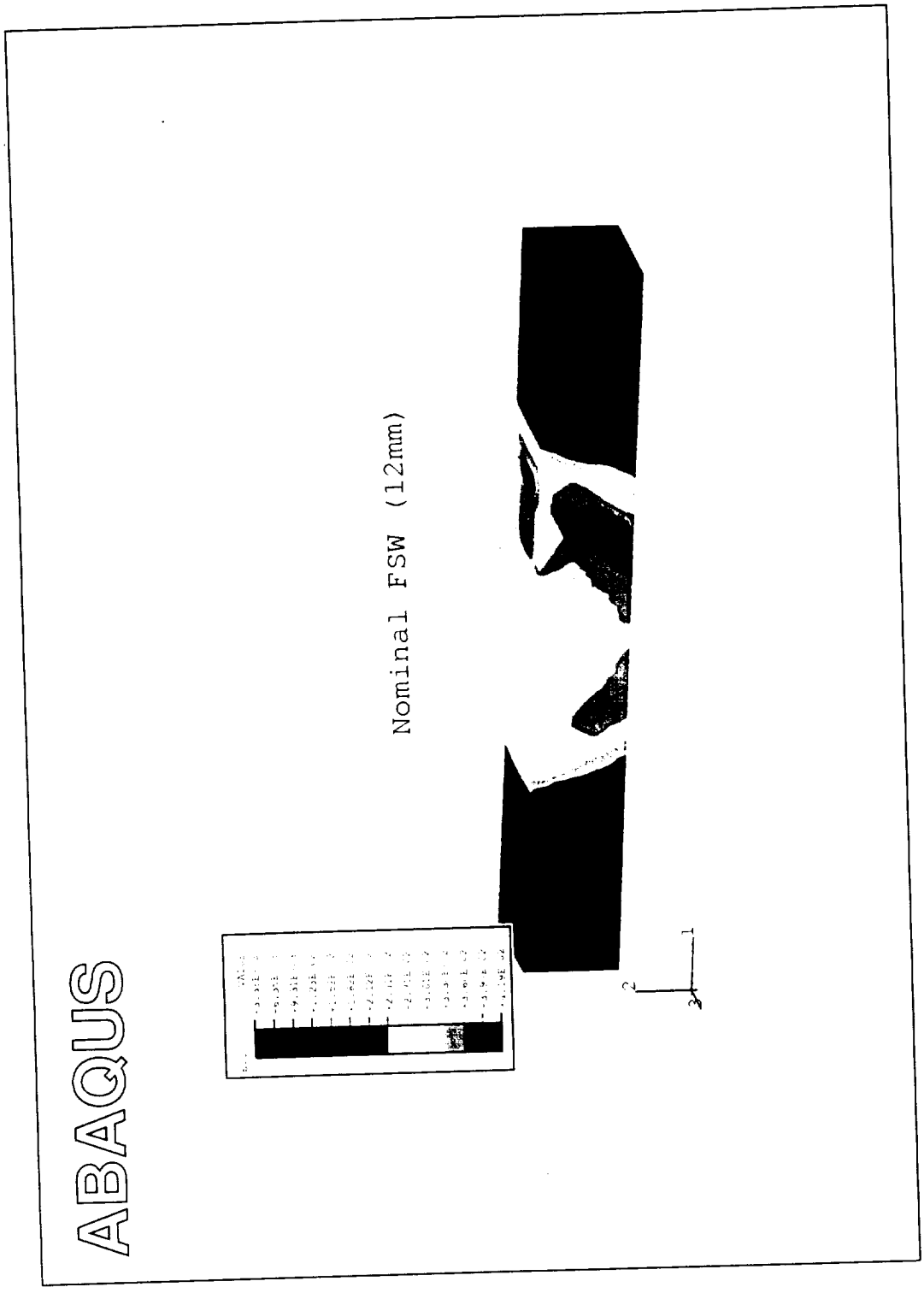

Figure 6-18 Contour plot of the normal strain distribution in the 12mm wide 3-D model. Global strain level is approximately 3.3%.

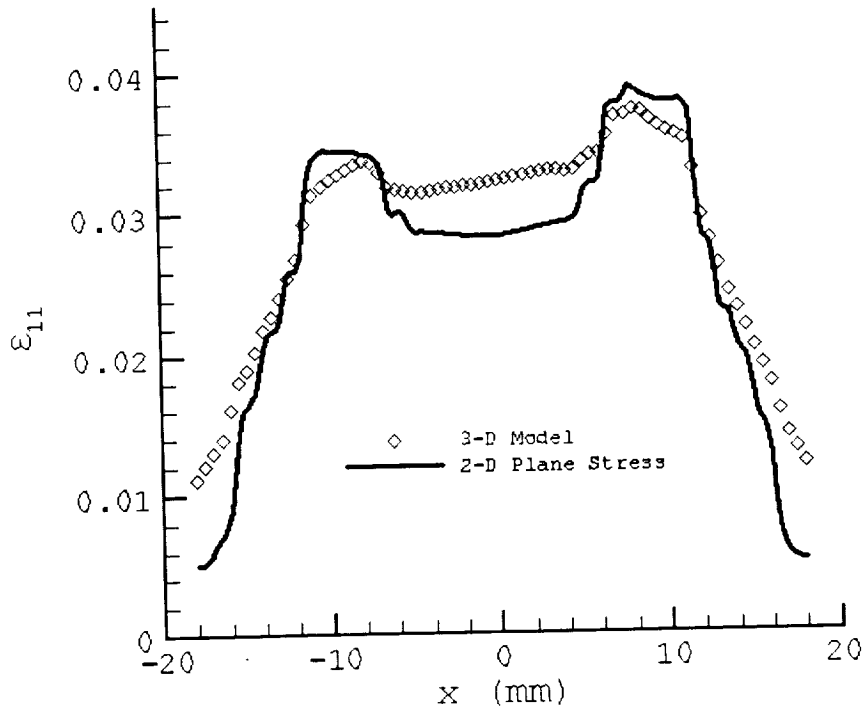

Figure 6-19 Comparison of normal strain distribution for 2-D and 3-D models at mid-plate thickness. 3-D model data is taken from the front surface.

Chapter 7 Model Applications

A working 2-D model of a friction stir weld has been developed and employed in the investigation of the mechanical response of the weld under transverse, uniaxial loading conditions and the ability of the model to accurately characterize the weld response has been verified by experimental observations. Based on the results of these investigations, the experimentally determined constitutive properties of the various weld materials have been verified and the condition of constraint has been established as that of near plane stress. To this point, the 2-D model has only been utilized to confirm the local constitutive data and demonstrate the viability of such a model in simulating the response of the heterogeneous structure. The advantage of a working model is its utility as a tool for supplementing the experimental process and investigating features that may not be available through experimental techniques. Ultimately, the goal of the model will be to provide input for analyses of three-dimensional structures containing weldments. The present chapter demonstrates the application of the 2-D model to a number of interesting situations.

First, a comparison of the original model with a model that incorporates a single "average" weld material is presented. This assessment is made for the *nominal* weld and used to justify the detail included in the original model. Next, the model is used to

demonstrate the potential for investigating the role of a weld defect. Finally, the model is used to simulate the response of the weld to 3 point bending.

7.1 "Average" Weld Material

The detail involved in developing the model, as far as the number of materials defining the weld and the material distribution are concerned, should be warranted by both the global and local predictive capabilities of the model. Since the heterogeneous structure of the weld varies with the process parameters, the model must be constructed for each type of weld considered. Ideally, the model should contain a sufficient amount of detail to provide accurate results, but not so much that it becomes impractical to use. Obviously, the most simplistic approach would be to use one material to represent the weld. In an attempt to justify the detailed description of the weld, the model is analyzed using an "average" weld material to define the entire weld region.

The original model of the *nominal* weld consisted of 14 individually defined materials, 13 weld materials and the base material, distributed throughout the weld in a pattern that mimicked the distribution provided by the experimentally determined yield stress map. This description was adopted in order to capture the non-symmetric nature of the weld response shown by the experimental data and the non-symmetric nature of the FSW process in general.

A new model is constructed using one material to define the weld, which represents an average constitutive behavior of three of the original 13 materials. Referring to the *nominal* weld yield stress map shown in Figure 4-11, the materials chosen to define the new weld material are selected from the nugget and the two low

strength regions in the advancing and retreating side heat affected zones. Average values of true stress are computed from the three materials at corresponding levels of true plastic strain and the new material is added to the model. The new material is assumed to occupy the same area of the model as the entire set of 13 materials in the original model and all boundary conditions were maintained.

Figure 7-1 shows the global response predictions for the original model and the model incorporating the average weld material together with the experimental data for the *nominal* weld. The average weld model does a fairly good job of predicting the actual response but overall provides less accurate results than the original model. In this respect, the average material description may be suitable for use in studies aimed at optimizing the welding process to achieve superior quality welds. This, however, would require knowledge of the effects of the welding parameters on the resulting local properties of the weld, which could possibly be provided with the aid of microstructural evolution models. If the model is to be used in studies where local effects are important, such as in three-dimensional structural models or crack propagation models, then it must be capable of predicting the local response as well as the global response.

The local response of the average weld model is shown in Figure 7-2. It is clear from this plot that the single material representation results in a much more uniform and symmetric strain distribution than was shown by the original model in Figure 6-6. The localizations present in the original model are somewhat visible in the average weld model but for the most part are indistinguishable. In addition, the strain gradients in the transition regions between the weld and the base material are very severe in comparison with the original model.

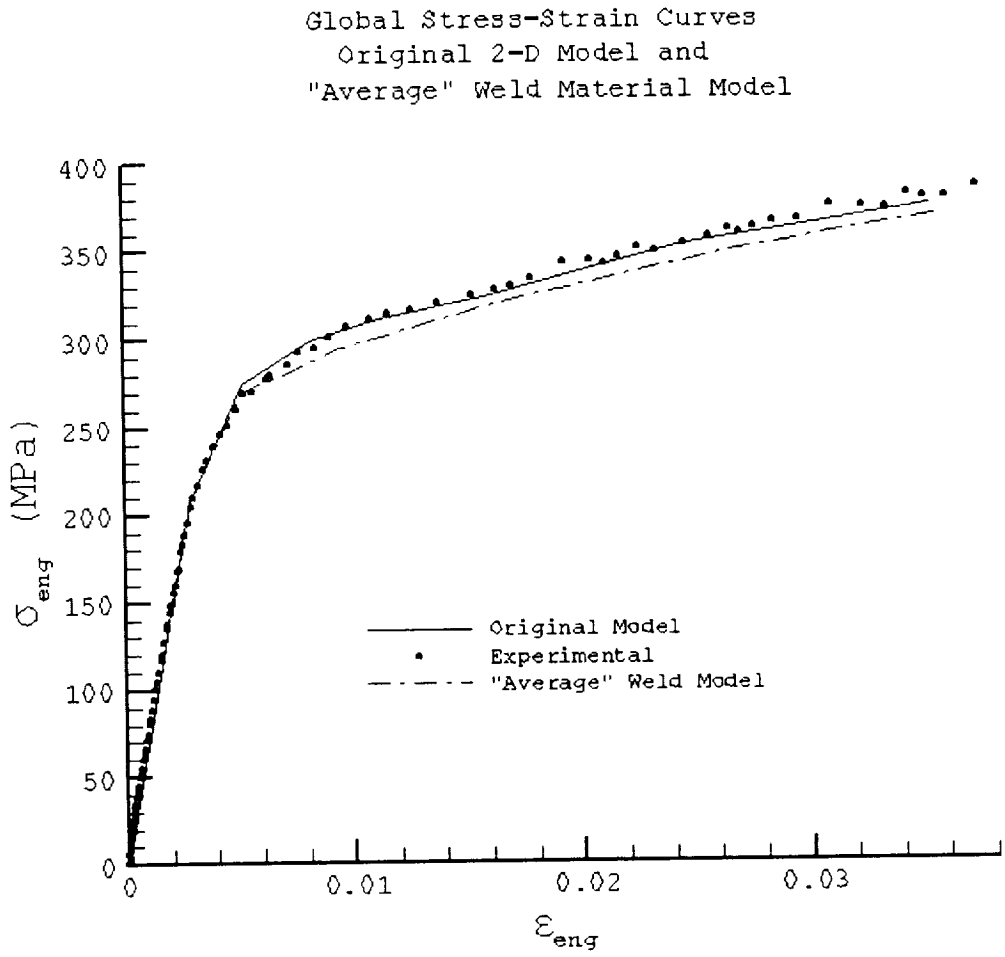

Figure 7-1 Nominal FSW global response predictions from the original 2-D model, which incorporates 13 different weld materials, and an "average" weld model that uses only one material to define the weld.

A more detailed comparison of the results for the two models is shown in Figure 7-3, where the normal strain distribution is plotted at locations near the top, middle, and bottom of the weld. At each location, the average weld model demonstrates severe strain gradients in the base metal-weld metal transition regions and relatively constant strain throughout the nugget. This is clearly inconsistent with the response predicted by the original model and is not an accurate representation of the actual weld response.

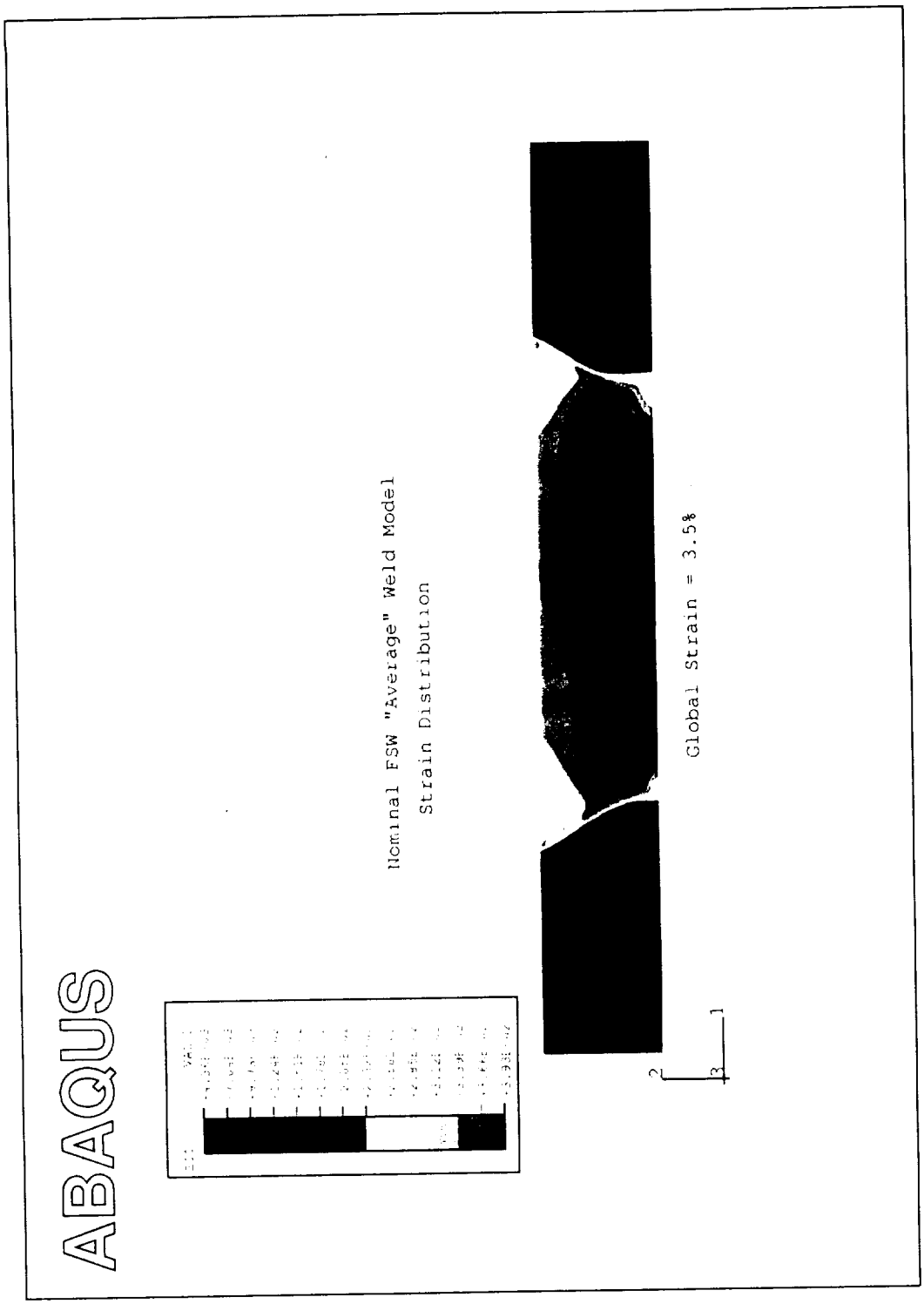

Figure 7-2 Normal strain distribution for the nominal FSW model using an "average" weld material to represent the weld.

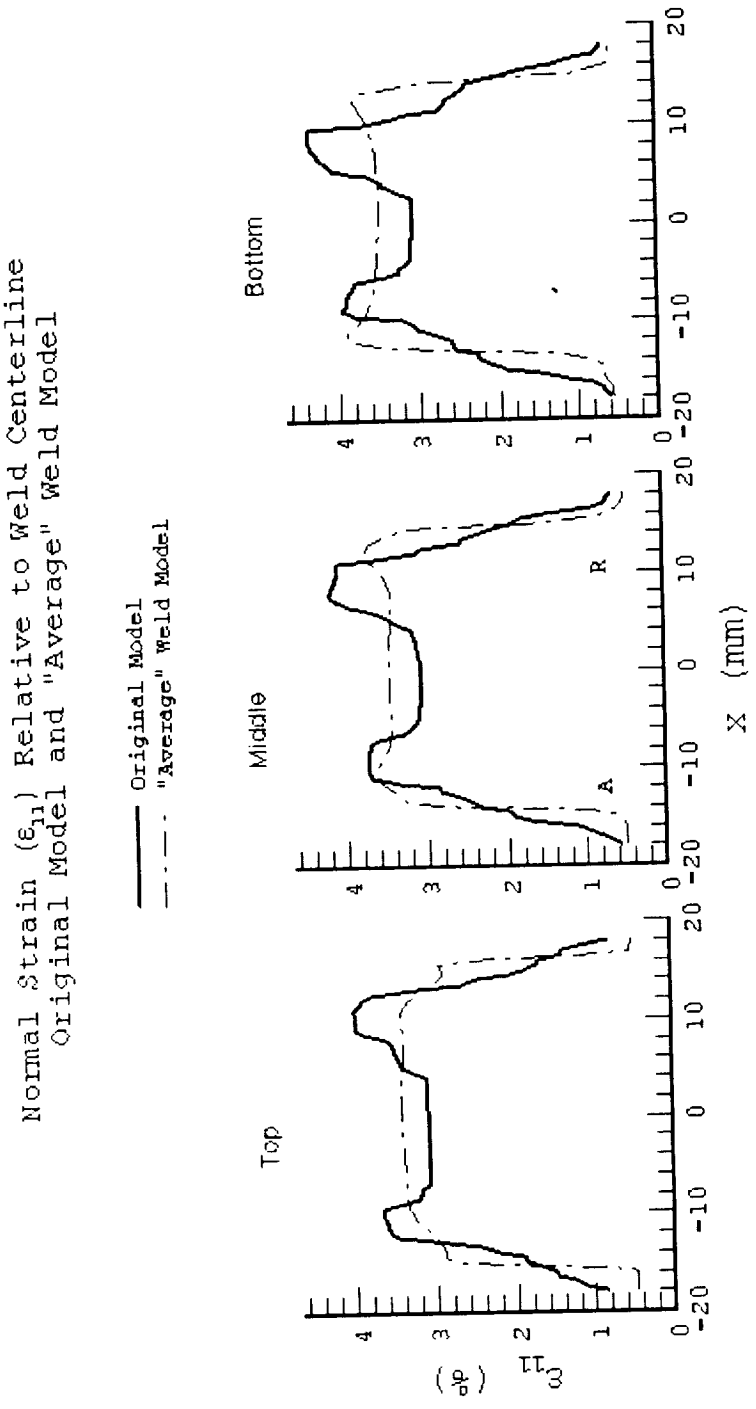

Figure 7-3 Comparison of the local response predictions for the original model and the average weld model.

Based on the results of the original model and the simplified "average" weld model, it is easily seen that a single material representation of the heterogeneous weld is insufficient to accurately model both the global and local responses. Although the global predictions are similar for both models, the simple model lacks the capability of capturing the local effects. For the model to provide accurate information in applications where the local effects are important, a more detailed description of the weld materials and their distributions is required. In regards to the original model, 13 different weld materials may be more than necessary but the added detail may be justified by the increased accuracy in the results, depending on the application.

7.2 Defect Model

Friction stir welds and welds in general are susceptible to defects. Careful control of process parameters can minimize the potential for defect formation, however, it is possible that defects will arise in a production environment. Friction stir welds are not prone to the types of defects characteristic of fusion welds but they are vulnerable to other types of defects. Two defects that have been associated with friction stir welding are the wormhole and the lack of penetration (LOP) defect.

Wormhole defects appear as tunnels, generally on the advancing side of the weld, and typically result from the improper selection of process parameters. By choosing the appropriate parameters for a particular material, these defects can normally be eliminated. A lack of penetration defect is indicated by the retained interface between the original plates at the bottom of the weld and is usually much harder to detect. While the LOP defect may be controlled by process parameters, it can also arise from tool wear even

when the optimum parameters are used. In a production environment, this type of defect may be more likely to occur and so the effect of such defects should be a subject of consideration. Specifically, it would be informative to know how large of a defect the weld can withstand before the defect becomes the dominant factor in failure.

A study to determine the critical defect size would require a model that included a detailed description of the weld in addition to a failure criterion. Although the friction stir weld model does not incorporate a failure criterion, it does contain the necessary detail to demonstrate its potential use in this type of application. To show this, a LOP defect is introduced into the model and the simulated tensile test results are compared to the results of a tensile test on an actual weld containing a LOP defect.

Since it would be a difficult task to manufacture a LOP defect of a specific size and at a specific location during the welding process, an artificially produced defect is introduced in a *nominal* FSW specimen using a slotting saw. A ¼ *mm* deep slot is cut along the weld centerline at the bottom of the weld to simulate the defect. Although there is normally some bonding at the interface of a LOP defect, the slot is realistic, in terms of the size, and provides an adequate representation of the defect for the present demonstration. The tensile test on the weld specimen included image acquisition for correlation and strain determination. To simulate the defect in the model, a single element (¼ *mm* edge length) is selected at the bottom of the weld along the weld centerline and assigned an elastic-perfectly plastic behavior with a low yield strength.

The local response for the model and experiment are shown in Figure 7-4 at a global strain level of approximately 1.3%. At this relatively early point in the loading, the experimental data show the presence of the strain localization around the defect in

addition to the characteristic localizations in the heat-affected zones. The model response also captures the HAZ localizations and indicates the LOP defect by the typical plastic zone shape associated with a crack-like defect. Although the plastic zone is not as noticeable in the contour plot of the experimental data, the strain distribution just above the defect is very similar to that predicted by the model, as shown in Figure 7-5.

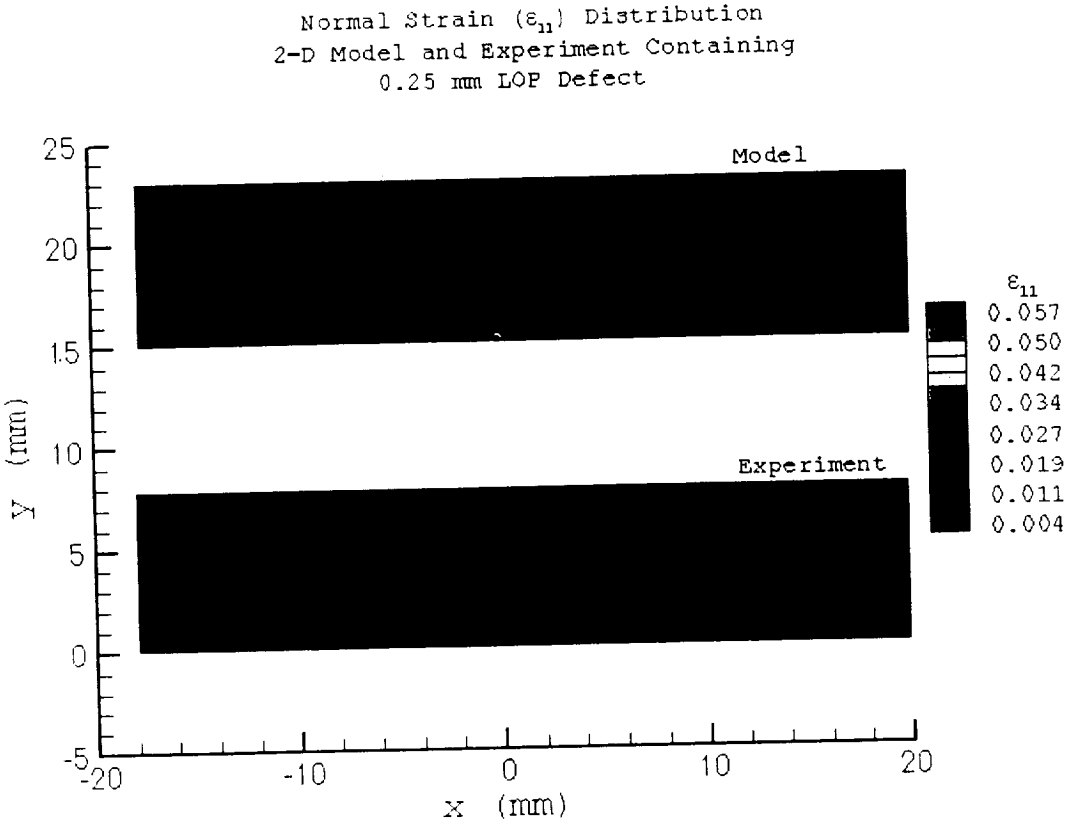

Figure 7-4 Local response from 2-D model and experiment on the nominal FSW specimen containing a 0.25 mm deep LOP defect. The global strain level is approximately 1.3%.

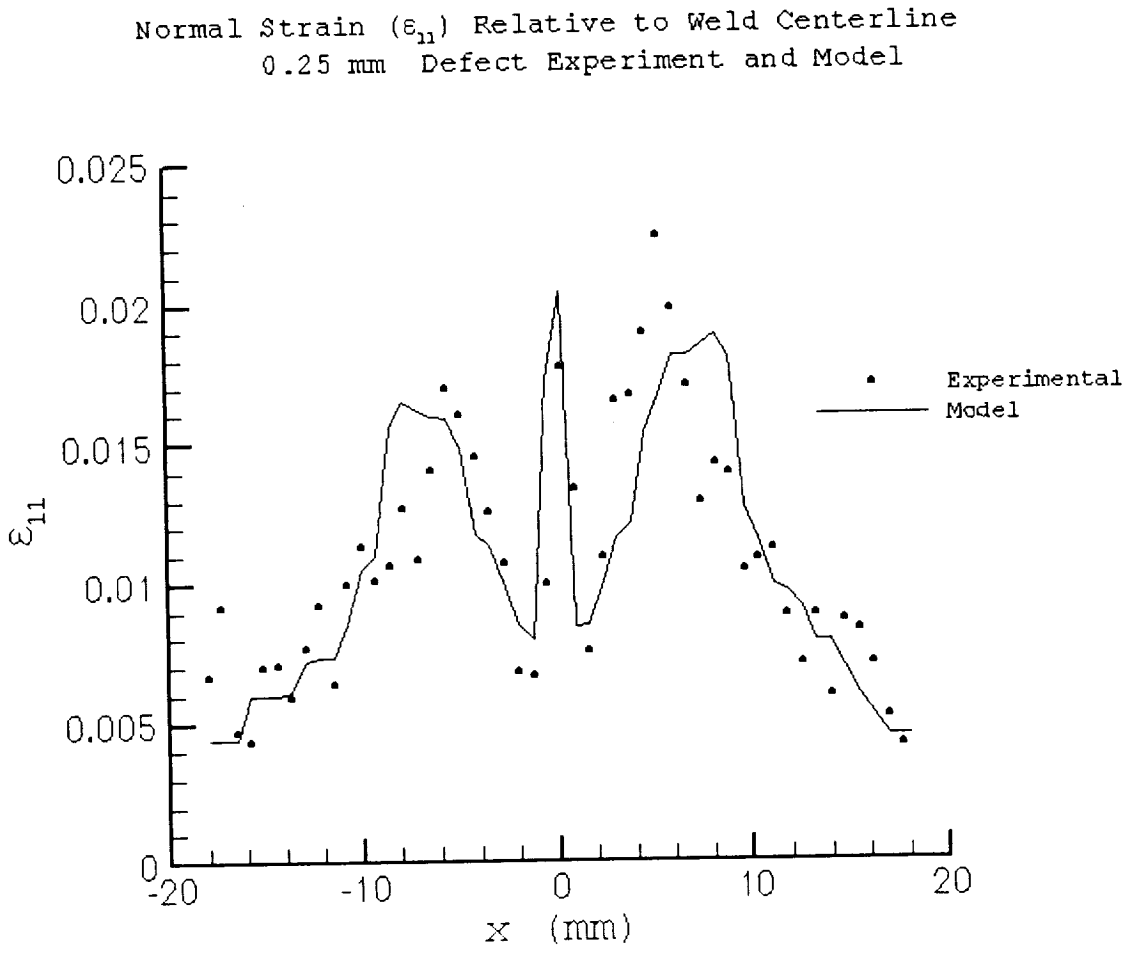

Figure 7-5 Model and experimental results of the normal strain distribution at the bottom of the weld, just above the LOP defect.

To provide further evidence that the response predicted by the model is a realistic representation of the behavior of a weld containing a defect, an additional experiment was conducted on a specimen with a 1 *mm* defect. Following the same procedures as for the first defect specimen, the tensile test was run and the full field information was obtained via DIC. Figure 7-6 shows a close-up view of the normal strain distribution in the vicinity of the 1 *mm* LOP defect. The local deformation around the defect shows the similar plastic zone shape that was predicted by the model with the ¼ *mm* defect,

indicating that the model is capable of providing realistic results in terms of the local response in the presence of a defect.

In order to use the model to determine a critical defect size, a failure criterion must be included in the model development, which is beyond the scope of the present work. A failure criterion would allow the model to predict when (i.e at what size defect) the localization due to the defect becomes dominant over the HAZ localizations. In the absence of this criterion, the model can only be used to show trends in the local behavior. Based on the results, the model demonstrates the potential for providing the foundation of a model to be used in this type of application.

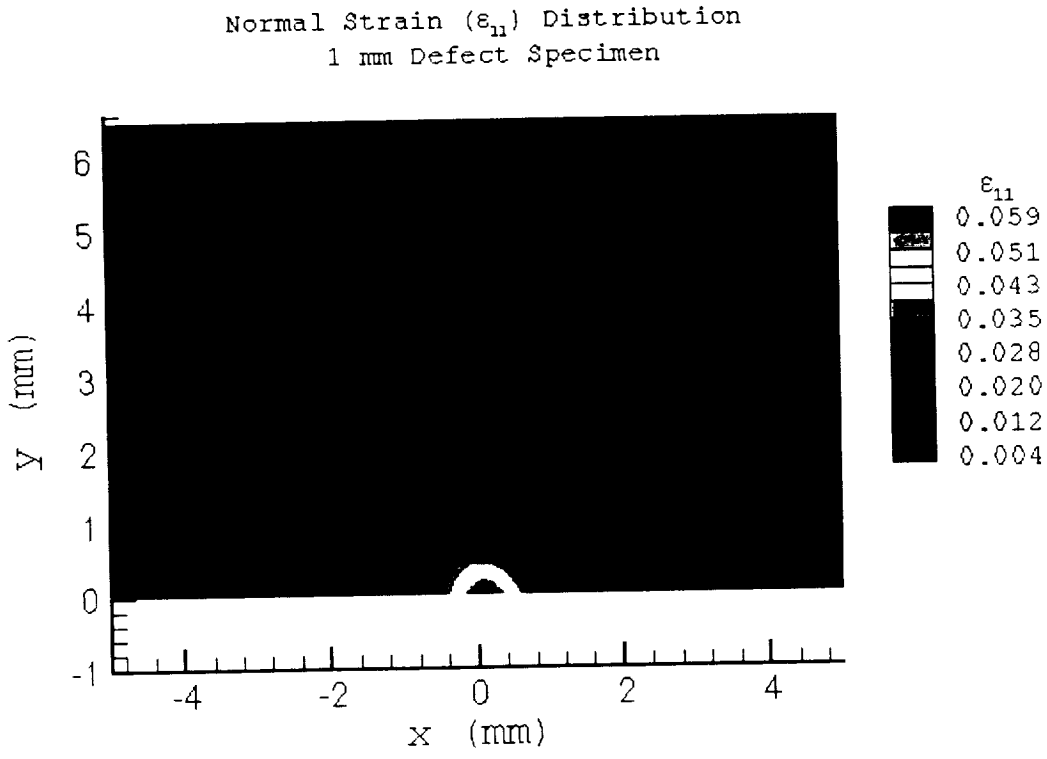

Figure 7-6 Close-up view of the nominal FSW local response in the vicinity of the 1 mm LOP defect.

7.3 3-Point Bend Test

The tensile response of a weld provides useful information regarding weld quality and general mechanical properties and in many structural applications welds will be subject to tensile loading. However, it is likely that other loading conditions will exist and a model should be able to handle such cases. To demonstrate the model capabilities in a situation other than transverse, uniaxial tension, the model is used to simulate three-point bend tests on an all base metal specimen and a *hot* FSW specimen. Results from these simulations are compared to the results from 3-point bend tests on actual base metal and *hot* FSW specimens.

The base metal and weld specimens used in the experiments were similar to the ones used in the tensile tests, with the exception that the top surface of the weld specimen was milled to remove the flash produced during welding and provide a smooth surface for contact with the test fixture. The 3-point bend fixture consisted of two cylindrical supports mounted on an aluminum block, with a center-to-center separation distance of 101.6 *mm* (4 in.), and a separate threaded support, which was attached to the load cell of the test machine. The block with the two supports rested on a flat plate fixture, attached to the moveable ram, and was positioned so that the load point acted midway between the two supports. Prior to testing, the specimens were centered on the supports and, for the weld test, the specimen was oriented with the load point acting on the crown side of the weld. All tests included image acquisition for correlation and strain determination.

To simulate the 3-point bend test, the problem was modeled as a contact problem between the deformable specimen and the rigid supports. Since a distance of approximately 100 mm separated the bottom supports on the fixture, the length of the

specimen was increased from 60 *mm* to 120 *mm*, resulting in 15360 elements and 15873 nodes. Reduced integration, plane stress elements (CPS4R) were used in the model due to the susceptibility of the fully integrated elements to shear locking in bending. The geometry of the model is shown in Figure 7-7. Contact between the supports and the specimen is identified by the definition of three contact pairs, which are surfaces that may come into contact with each other, and associated surface interactions. In the contact pair definition, one surface is identified as the master surface and the other is identified as the slave surface. When contact occurs between a rigid surface and a deformable surface, the rigid surface is set as the master surface. For each of the contact pairs, the normal and tangential surface interactions were defined using the available options in ABAQUS. Interaction normal to the surface was set using the default "hard" model, which prevents the slave surface from penetrating into the master surface, and a friction model was used for the tangential surface interaction such that sliding occurs when a user-defined shear stress limit is exceeded. The shear stress limit was chosen to be $0.577*\sigma_{ys}$, where σ_{ys} is the yield strength of the material involved in the contact.

Boundary conditions for the model included constraints on the supports and on the specimen. Each rigid support has an associated reference node that is used to define the motion of the surface and the boundary conditions are applied to these nodes. For the two bottom supports, the displacement and rotation degrees of freedom were set at zero. The vertical displacement (2 direction) of the upper support is used to apply the loading, so only the horizontal (1 direction) displacement and rotation degrees of freedom for this surface were set to zero. In addition, the horizontal displacement of a single node at the midpoint on the bottom of the specimen was set to zero to prevent translation

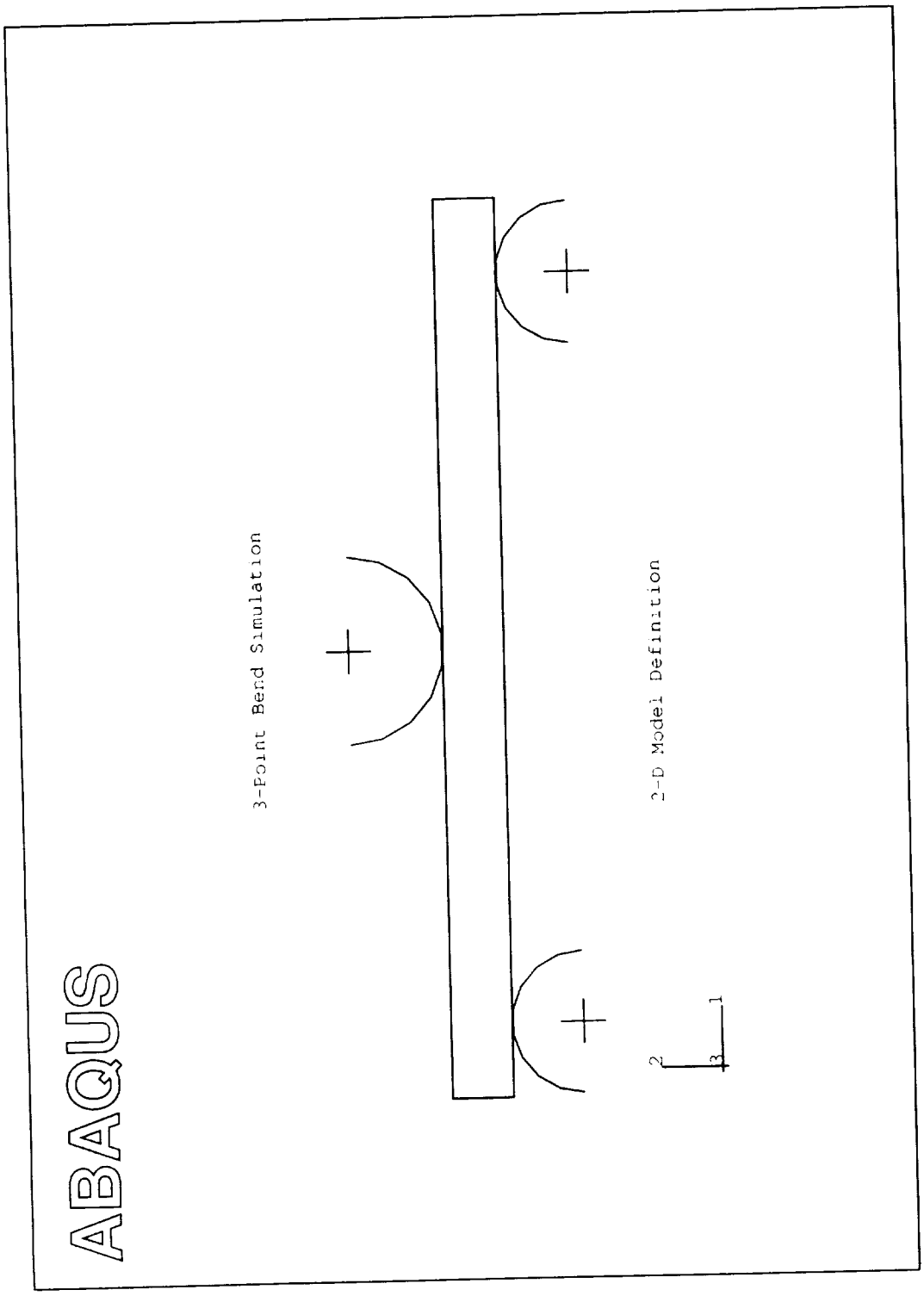

Figure 7-7 2-D model geometry for 3-point bend simulation.

Simulation results are compared to the experimental data to show that the model is capable of predicting both the global and the local response. The global response predictions, in terms of the reaction force versus the displacement of the upper support, for the base metal and FSW specimens are shown in Figure 7-8 along with the corresponding experimental data. For both the homogeneous base metal specimen, the model predicts slightly higher loads in the initial non-linear portion of the curve, but overall captures the response fairly well. The predicted response for the FSW specimen is in excellent agreement with the experimental data.

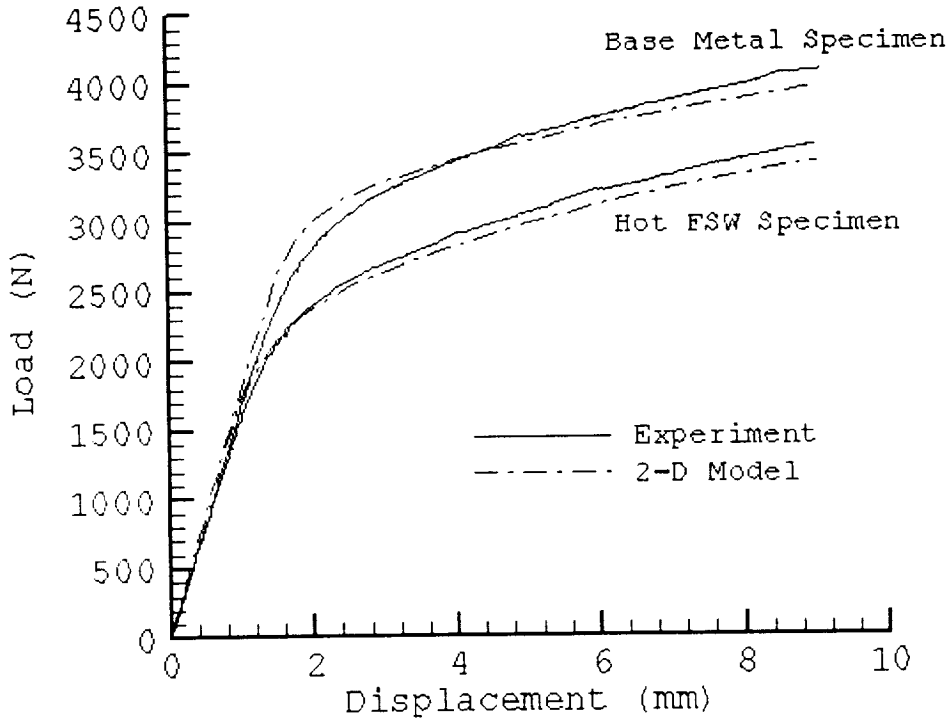

Figure 7-8 Global response data from 3-point bend tests. Results are shown for experimental tests and 2-D model simulations.

The local response for the two specimens, measured using the image correlation technique, is presented as contour plots of the normal strain (ε_{11}) distribution as seen in Figure 7-9. These contour plots correspond to a load-point displacement of approximately 9 *mm* and each demonstrate characteristics typical of bars subject to bending, with compressive strains on the surface where the loading was applied and tensile strains on the opposite surface. Differences in the response between the two specimens are observed in the extent of the deformed regions. The tensile and compressive regions of the base metal specimen are relatively localized, whereas, in the heterogeneous weld, the lowest strength material is not located at the highest stress region (i.e. centerline) so the deformation is spread over a greater region. The simulation results for the base metal and FSW specimens are shown in Figure 7-10 and Figure 7-11, respectively.

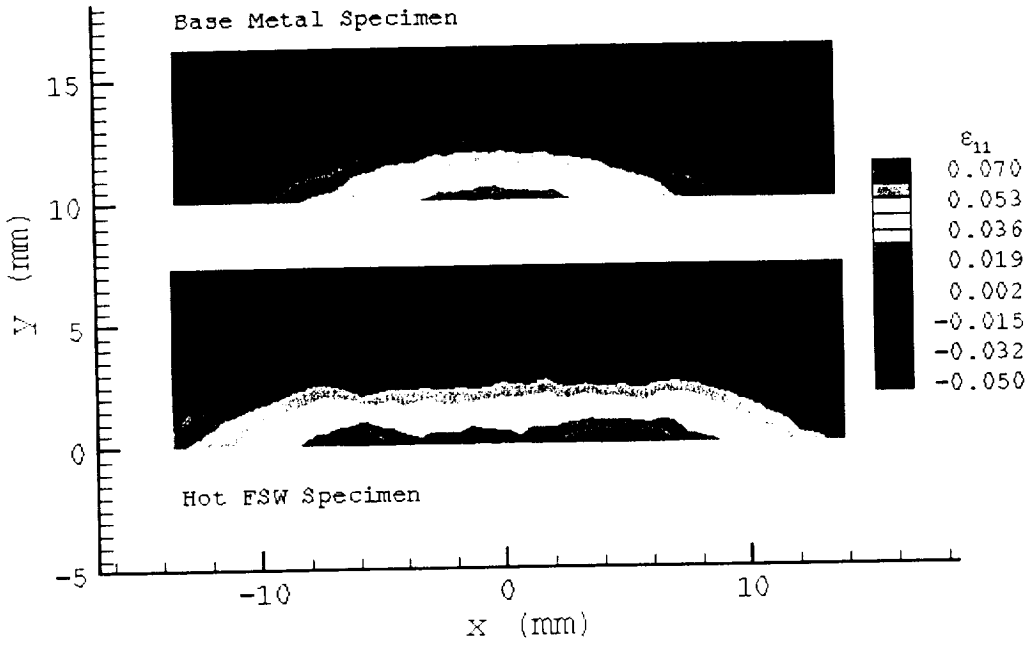

Figure 7-9 Local response of the base metal and weld 3-point bend specimens measured using the image correlation technique. Both contour plots correspond to a load-point displacement of approximately 9 mm.

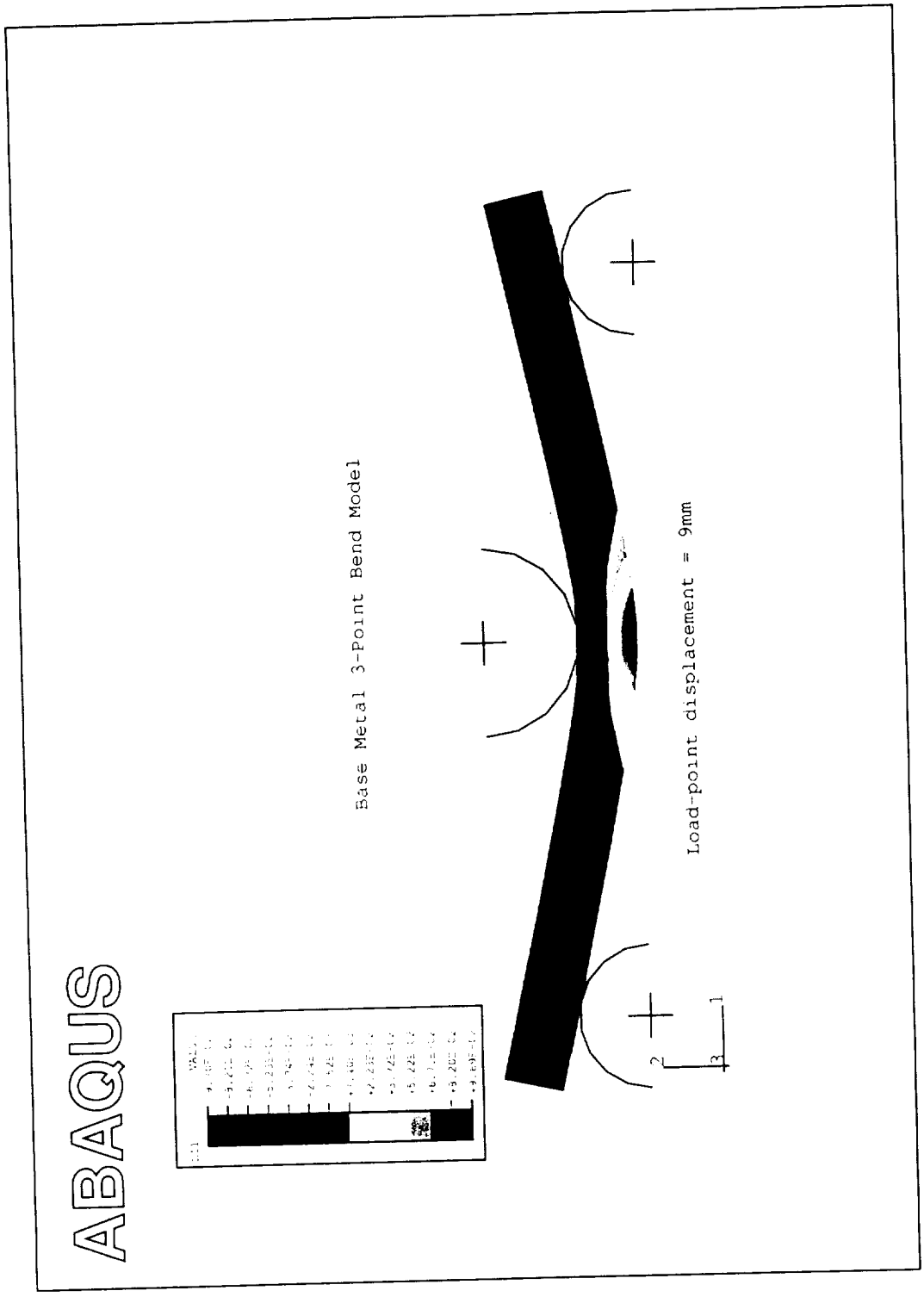

Figure 7-10 Local response prediction for the 2-D model of the base metal 3-point bend specimen.

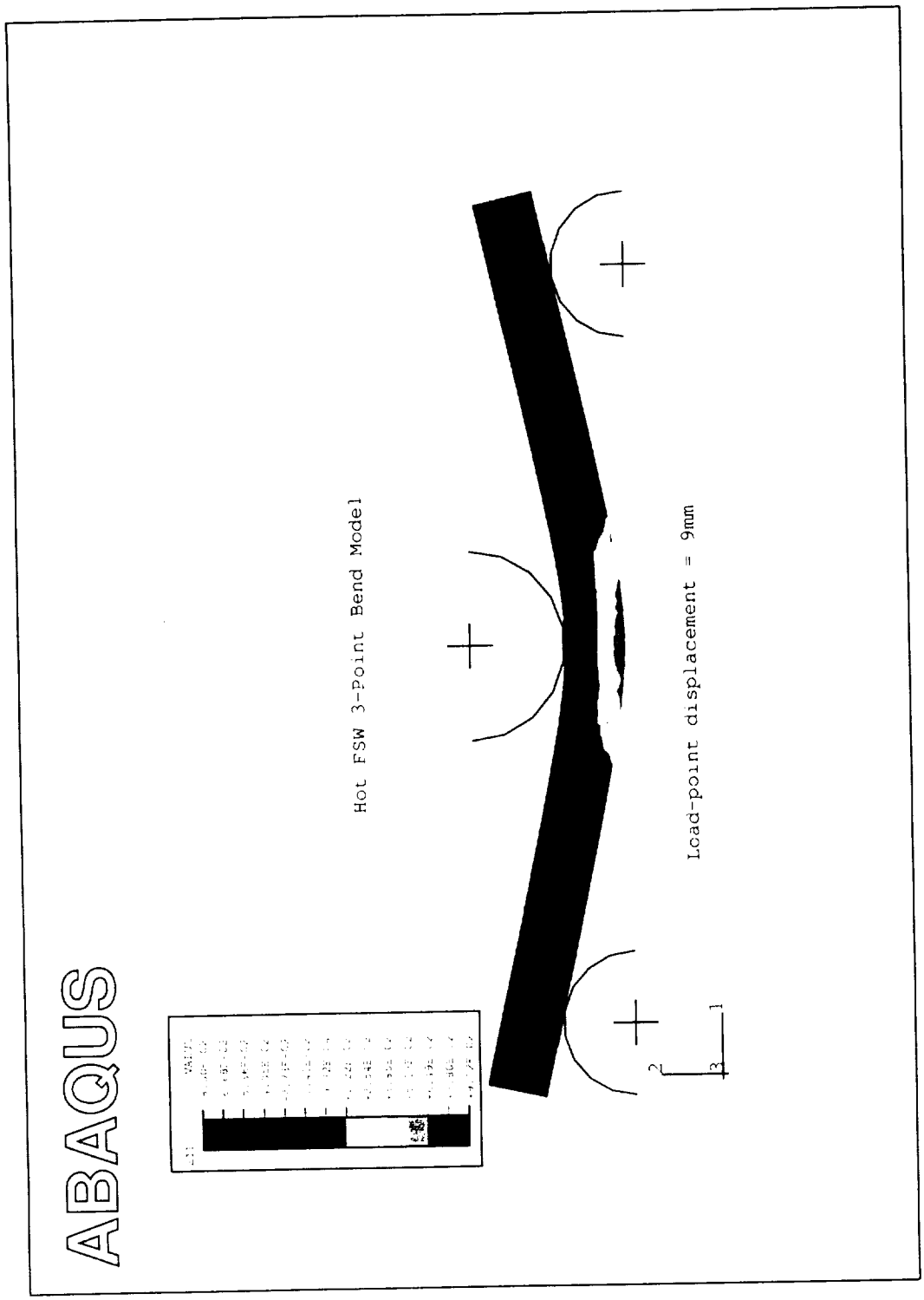

Figure 7-11 Local response prediction for the 2-D model of the Hot FSW 3-point bend specimen.

Qualitatively, the models demonstrate similar results in the normal strain distribution as were seen in the experimental data. Comparisons between the model and experiment are presented in Figure 7-12 and Figure 7-13. Normal strain distributions at locations near the top, middle, and bottom of the base metal specimen are shown in Figure 7-12. Overall, the model accurately predicts the shape of the distribution and the magnitude of the strain at each location, although there is a slight variation in the results on the top surface. Near the top surface the model predicts slight localizations on each side of the specimen centerline, however these are most likely due to the geometric approximation of the circular, rigid support surface.

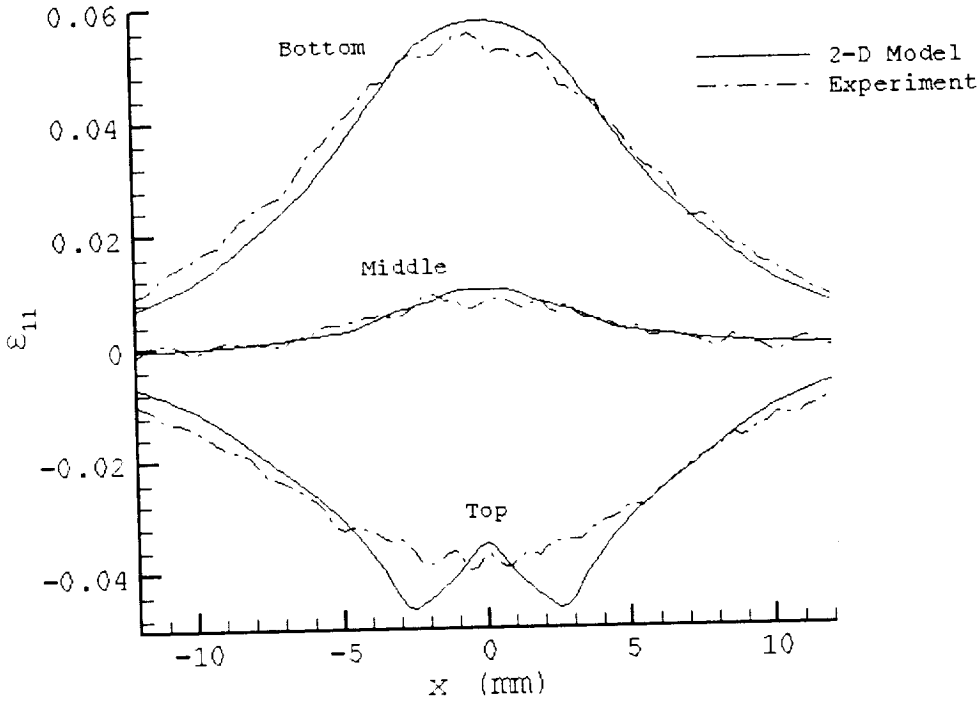

Figure 7-12 Local response predictions at the top, middle and bottom of the base metal 3-point bend specimen. Model results are compared to the experimental data at the same locations.

Figure 7-13 shows the normal strain distributions at the top, middle, and bottom of the *hot* FSW specimen. Compared to the experimental results for the base metal specimen, the weld experiences lower, maximum compressive and tensile strains and, for the most part, demonstrates fairly uniform strains at each location in the weld. The model predicts very similar trends throughout the weld; however, it does show higher tensile strains around the weld centerline on the bottom surface. This is most likely due to the limited data used to define the nugget material behavior. Recall that the material definition includes hardening up to the last pair of true stress-true plastic strain values and

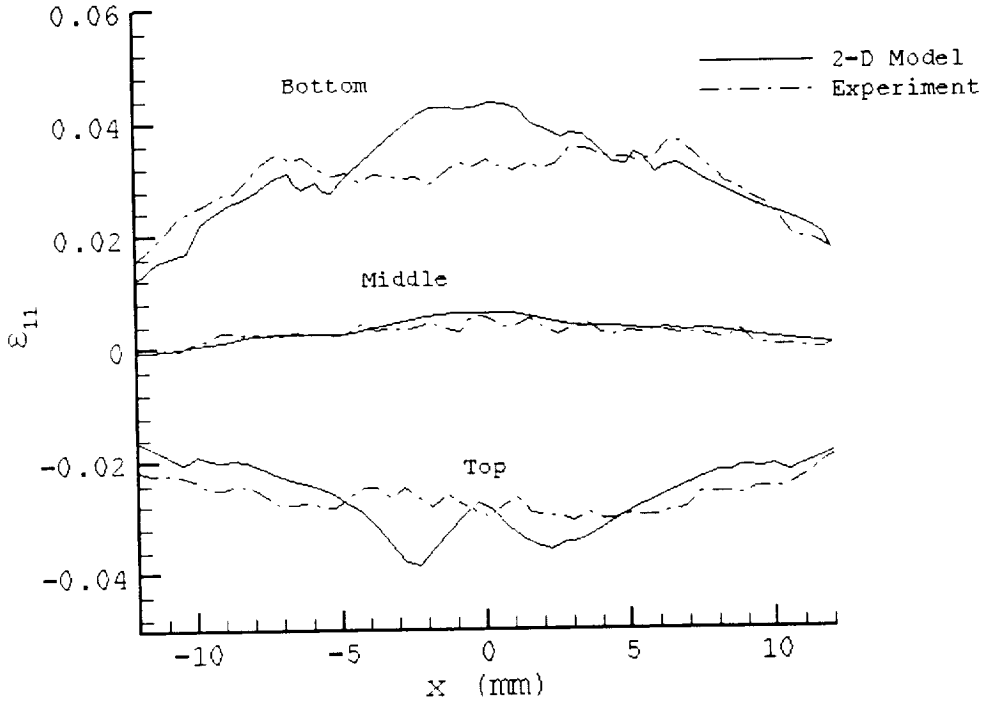

Figure 7-13 Local response predictions at the top, middle and bottom of the Hot FSW 3-point bend specimen. Model results are compared to experimental data at the same locations.

then becomes perfectly plastic. For the nugget material, this occurs once the strain has exceeded a value of approximately 3.6%. This limitation may be resolved by extrapolation of the local constitutive data. Near the top surface, the model does a good job of capturing the strain distribution, with the exception of the strain localizations resulting from the geometric approximation of the support surface. Overall, the model results agree well with the experimentally observed data for both the homogeneous and heterogeneous specimens.

The preceding demonstrations indicate that the 2-D model of the friction stir weld is capable of providing realistic information for a wide variety of applications. Besides presenting additional verification of the experimentally determined local material properties, these results appear to justify the detailed description of the weld composition and suggest that the model has the potential to be used as a valuable process development tool.

Chapter 8 Summary and Conclusions

A technique for determining local constitutive data in a heterogeneous material has been outlined and demonstrated in studying the mechanical behavior of friction stir welds in aluminum alloy 2024. The global and local mechanical response of several different welds was examined experimentally through transverse tensile tests. Full field measurements obtained via digital image correlation provided a detailed description of the local mechanical response in terms of the tensile stain distribution. Individual materials comprising each weld and the distribution of these materials within the weld were identified from yield stress maps constructed from local constitutive data. This information was then used to develop a finite element model of the FSW for verifying the assumptions inherent in the technique and validating the experimentally determined local constitutive data. Simulation results from the 2-D and 3-D models were compared with the experimental data and exhibited excellent agreement at both the global and local level.

The technique, presented as an alternative to some of the methods currently available, utilizes standard tensile testing procedures, digital image correlation and a simplifying assumption regarding the FSW. The use of digital image correlation in conjunction with the tensile test allows for full field measurements to be made during the loading of the specimen, resulting in a history of the deformation that can be used to

examine the local response of virtually any point in the weld. In order to construct the actual constitutive data for a particular position in the weld, the local stress must be known in addition to the local strain. Local strain data is determined from processing of the full field displacement data provided by the image correlation technique. The local stress is obtained from the global load using the assumption that the friction stir weld is a composite material undergoing nominally **iso-stress** loading conditions. The validity of this assumption is examined by comparing properties measured from full thickness and reduced thickness specimens and the results appear to justify the approximation.

One of the advantages of the proposed technique is the ability to determine the local material properties from a single transverse tensile test on the actual weld material. To demonstrate that the measured material properties are correct, the transverse tensile test of the FSW is simulated using 2-D and 3-D finite element models. The models are developed using the experimentally determined material properties and material distributions as input. Two dimensional plane strain and plane stress models of the FSW are analyzed and it is found that the plane stress representation provides the best results for both the global and local response. The actual constraint conditions are examined through 3-D simulations of specimens of varying widths and although some increase in constraint is developed, the 3-D results suggest that nearly plane stress conditions exist in the FSW. Two-dimensional simulations incorporating materials from the reduced thickness specimens are compared to models using the full thickness materials and the results indicate that the full thickness materials provide an accurate representation of the FSW, thereby validating the iso-stress approximation. In addition, comparisons of the 2-

D and 3-D model predictions demonstrate that the mechanical response of the FSW can be modeled as a two-dimensional problem.

Results provided by the finite element simulations show that the 2-D model is capable of accurately predicting the response of the FSW under transverse, uniaxial loading conditions. To demonstrate the potential of the model for providing useful predictions in other applications, several interesting situations are considered. To justify the detail included in the model, in terms of the number of materials used to define the weld and the distribution of these materials within the weld, a model incorporating a single, average weld material is constructed. The results indicate that this "simple" description of the weld does not accurately capture the local mechanical behavior thus supporting the detail used in the original model. The role of the model as a potential tool in examining the effect of a weld defect is also demonstrated. A lack of penetration defect is introduced in the model and its effect on the local mechanical response in tension is found to be consistent with the experimentally observed response of a FSW containing an artificially produced LOP defect. As a final example of the models predictive capabilities, the response of the FSW to 3-point bending is simulated. Global and local response predictions for all base metal and FSW specimens are compared with experimental data for the same specimens and the results are in excellent agreement.

Based on the findings in this work, the proposed technique presents a viable alternative to the current methods used in determining local material properties in heterogeneous materials. In utilizing standard tensile testing procedures and the digital image correlation technique, the method benefits from established property measurement practices and superior resolution. The principal assumption of iso-stress loading

conditions is requisite for local stress determination; therefore, the technique is applicable to materials that may be approximated by a series arrangement of constituent materials. A single transverse tensile test on a full size specimen is sufficient to accurately determine the local constitutive behavior as well as the distribution of the individual constituents. However, the technique is limited in the extent of the constitutive data that can be determined. By testing the heterogeneous material as a whole, the strain range over which the constitutive data can be measured is limited by the strength of the weakest region and once this region fails no further information on the remaining constituents is available. The finite element model of the heterogeneous material compliments the experimental portion of the technique and provides verification of the local constitutive behavior, material distribution and condition of constraint.

Although the results presented in this work demonstrate the excellent capabilities of the proposed technique, some recommendations are suggested for improvement of both the experimental and numerical components. Clearly, the amount of information available for constructing the local constitutive data is limited by the strength of the weakest region, however, this may be maximized by acquiring an image just prior to the point of failure. This is a difficult task with the current setup but one that may be achieved by using a video system capable of capturing frames at a very high rate. If such a system were to be used, it would be necessary to synchronize image and data acquisition systems so that the correct load is recorded for each image. This type of system would provide a marked improvement in accuracy and efficiency over the current setup.

Another area for improvement is in the construction of the yield stress map. The yield stress map, which is used to define material distribution, is created by manually determining the offset yield strength at many locations and, in order to achieve sufficient resolution, requires several hundred calculations and a great deal of time. A program that could be used to automatically provide this information would significantly improve the speed of the process and also eliminate some of the subjectivity regarding the calculations. In addition to the yield stress map, a more systematic approach to defining the material distribution may be provided by including other material property maps such as microhardness and microstructure maps.

The finite element model utilizes a very fine, uniform mesh to accommodate the definition of the material distribution and to capture the large gradients expected in the weld. This results in a relatively large model even in the 2-D case. Since a large portion of the model is base material and the gradients far from the weld are small, a coarser mesh could be used in these areas to reduce the size of the model and the computational time. Alternatively, automatic mesh generation could be used to speed up the process of generating the input file and minimize the model size by utilizing curve fits to the material boundaries and automatically generating the individual element sets. For the model to be used in failure prediction or damage assessment applications, a failure criterion must be incorporated and the material property definitions must be extrapolated to provide information over a wider strain range. The addition of these features would undoubtedly result in a valuable tool for the development and optimization of processes that produce globally heterogeneous materials.

References

1. Hashin, Z., "Analysis of Composite Materials - A Survey," Journal of Applied Mechanics, Vol. 50, 1983, pp. 481-505

2. Eshelby, J.D., "The Determination of the Elastic Field of an Ellipsoidal Inclusion, and Related Problems," Proceedings of the Royal Society of London. Series A, Mathematical and Physical Sciences, Vol. 241, No. 1226, 1957, pp 376-396

3. Hill, R., "Elastic Properties of Reinforced Solids: Some Theoretical Principles," Journal of Mechanics and Physics of Solids, Vol. 11, 1963, pp. 357-372

4. Hill, R., "Continuum Micro-Mechanics of Elastoplastic Polycrystals," Journal of Mechanics and Physics of Solids, Vol. 13, 1965, pp. 89-101

5. Mori, T., and Tanaka, K., "Average Stress in Matrix and Average Elastic Energy of Materials With Misfitting Inclusions," Acta Metallurgica, Vol. 21, 1973, pp. 571-574

6. Van der Sluis, O., Schreurs, P.J.G., Brekelmans, W.A.M., and Meijer, H.E.H., "Overall Behavior of Heterogeneous Elastoviscoplastic Materials: Effect of Microstructural Modeling," Mechanics of Materials, Vol. 32, No. 8, 2000, pp. 449-462

7. Garboczi, E.J., and Day, A.R., "An Algorithm For Computing The Effective Linear Elastic Properties of Heterogeneous Materials: Three Dimensional Results For Composites With Equal Phase Poisson Ratios," Journal of the Mechanics and Physics of Solids, Vol. 43, No.9, 1995, pp. 1349-1362

8. Reynolds, A.P., and Baxter, S.C., "Kinematic Hardening in a Dispersion Strengthened Aluminum Alloy: Experiment and Modeling," Materials Science and Engineering A, Vol. 285, 2000, pp. 265-279

9. Kanada, T. Lin, Z., and Li, V.C., "Tensile Stress-Strain Modeling of Pseudostrain Hardening Cementitious Composites," Journal of Materials in Civil Engineering, Vol. 12, No. 2, 2000, pp. 147-156

10. Davies, A.C., "The Science and Practice of Welding," New York: Cambridge University Press, 9th ed., 1989

11. West, E.G., "The Welding of Non-Ferrous Metals," New York: John Wiley and Sons Inc, 1951

12. Castro, R., and de Cadenet, J.J., "Welding Metallurgy of Stainless and Heat-Resistant Steels," New York: Cambridge University Press, 1975

13. Dawes, C.J., and Thomas, W.M., "Friction Stir Process Welds Aluminum Alloys," Welding Journal, Vol. 75, No. 3, 1996, pp. 41-45

14. Mahoney, M.W., Rhodes, C.G., Flintoff, J.G., Spurling, R.A., and Bingel, W.H., "Properties of Friction-Stir-Welded 7075 T651 Aluminum," Metallurgical and Materials Transactions A, Vol. 29, No. 7, 1998, pp. 1955-1964

15. Colligan, K., "Material Flow Behavior During Friction Stir Welding of Aluminum," Welding Journal, Vol. 78, No. 7, 1999, pp. S229-S237

16. Stewart, M.B., Adams, G.P., Nunes, A.C. Jr., and Romine, P., "A Combined Experimental and Analytical Modeling Approach to Understanding Friction Stir Welding," Journal of Material Processing and Manufacturing Science, in review

17. Reynolds, A.P., Seidel, T.U., and Simonsen, M., "Visualization of Material Flow in an Autogenous Friction Stir Weld," International Symposium on Friction Stir Welding, 1999

18. Bernstein, E.L., and Nunes, A.C. Jr., "The Plastic Flow Field in the Vicinity of the Pin-Tool During Friction Stir Welding," In review for publication in the Welding Journal

19. Li, Y. Murr, L.E., and McClure, J.C., "Solid-State Flow Visualization in the Friction-Stir Welding of 2024 Al to 6061 Al," Scripta Materialia, Vol. 40, No. 9, 1999, pp. 1041-1046

20. Li, Y. Murr, L.E., and McClure, J.C., "Flow Visualization and Residual Microstructures Associated With the Friction-Stir Welding of 2024 Aluminum to 6061 Aluminum," Materials Science and Engineering A, Vol. 271, No. 1-2, 1999, pp. 213-223

21. Chao, Y.J., and Qi, X., "Thermal and Thermo-Mechanical Modeling of Friction Stir Welding of Aluminum Alloy 6061-T6," Journal of Materials Processing and Manufacturing Science, Vol 7, Oct. 1998, pp. 215-233

22. Smith, C.B., Bendzsak, G.B., North, T.H., Hinrichs, J.F., Noruk, J.S., and Heideman, R.J.,"Heat and Material Flow Modeling of the Friction Stir Welding Process," International Symposium on Friction Stir Welding, 1999

23. Murr, L.E., Flores, R.D., Flores, O.V., McClure, J.C., Liu, G., and Brown, D., "Friction Stir Welding: Microstructural Characterization," Materials Research Innovations, Vol. 1, No.4, 1998, pp. 211-223

24. Sato, Y.S., Kokawa, H., Enomoto, M., Jogan, S., and Hashimoto, T., "Precipitation Sequence in Friction Stir Weld of 6063 Aluminum During Aging," Metallurgical and Materials Transactions A, Vol. 30, No. 12, 1998, pp. 3125-3130

25. Flores, O.V., Kennedy, C., Murr, L.E., Brown, D., Pappu, S., Nowak, B.M., and McClure, J.C., "Microstructural Issues in a Friction-Stir-Welded Aluminum Alloy," Scripta Materialia, Vol. 38, No. 5, 1998, pp. 703-708

26. Rhodes, C.G., Mahoney, M.W., Bingel, W.H., Spurling, R.A., and Bampton, C.C., "Effects of Friction Stir Welding on Microsructure of 7075 Aluminum," Scripta Materialia, Vol. 36, No. 1, 1997, pp. 69-75

27. Bussu, G., and Irving, P.E., "Fatigue Performance of Friction Stir Welded 2024-T351 Aluminum Joints," International Symposium on Friction Stir Welding, 1999

28. Biallas, G., Braun, R., Donne, C.D., Staniek, G., and Kaysser, W.A., "Mechanical Properties and Corrosion Behavior of Friction Stir Welded 2024-T3," International Symposium on Friction Stir Welding, 1999

29. Kinchen, D.G., Li, Z., and Adams, G.P., "Mechanical Properties of Friction Stir Welds in Al-Li-2195-T8," International Symposium on Friction Stir Welding, 1999

30. LaVan, D.A., "Microtensile Properties of Weld Metal," Experimental Techniques, Vol. 23, No. 3, 1999, pp. 31-34

31. Cam, G., Erim, S., Yeni, C., and Kocak, M., "Determination of Mechanical and Fracture Properties of Laser Beam Welded Steel Joints," Welding Journal, Vol. 78, No. 6, 1999, pp. 193s-201s

32. Rak, I., Treiber, A., "Fracture Behavior of Welded Joints Fabricated in HSLA Steels of Different Strength Level," Engineering Fracture Mechanics, Vol. 64, No. 4. 1999, pp. 401-415

33. Von Strombeck, A., Dos Santos, J.F., Torster, F., Laureano, P. and Kocak, M., "Fracture Toughness of FSW Joints on Aluminium Alloys," Proceedings of the 1st International Conference on Friction Stir Welding, 1999

34. Mathew, M.D., Murty, K.L., Rao, K.B.S., and Mannan, S.L., "Ball Indentation Studies on the Effect of Aging on Mechanical Behavior of Allot 625," Materials Science and Engineering A, Vol. 264, No. 1-2, 1999, pp. 159-166

35. Mathew, M.D., and Murty, K.L., "Non-destructive Studies on Tensile and Fracture Properties of Molybdenum at Low Temperatures (148 to 423 K)," Journal of Materials Science, Vol. 34, No. 7, 1999, pp. 1497-1503

36. Mathew, M.D., Lietzan, L.M., Murty, K.L., and Shah, V.N., "Low Temperature Aging Embrittlement of CF-8 Stainless Steel," Materials Science and Engineering A, Vol. 269, No. 1-2, 1999, pp. 186-196

37. Murty, K.L., Miraglia, P.Q., Mathew, M.D., Shah, V.N., and Haggag, F.M., "Characterization of Gradients in Mechanical Properties of SA-533B Steel Welds Using Ball Indentation," International Journal of Pressure Vessels and Piping, Vol. 76, No. 6, 1999, pp.361-369

38. Malow, T.R., and Koch, C.C., "Mechanical Properties, Ductility, and Grain Size of Nanocrystalline Iron Produced by Mechanical Attrition," Metallurgical and Materials Transactions A, Vol. 29, No. 9, 1998, pp. 2285-2295

39. Malow, T.R., Koch, C.C., Miraglia, P.Q., and Murty, K.L., "Compressive Mechanical Behavior of Nanocrystalline Fe Investigated with an Automated Ball Indentation Technique," Materials Science and Engineering A, Vol. 252, No. 1, 1998, pp. 36-43

40. Huber, N., and Tsakmakis, Ch., "Determination of Constitutive Properties from Spherical Indentation Data Using Neural Networks. Part I: The Case of Pure Kinematic Hardening in Plasticity Laws," Journal of the Mechanics and Physics of Solids, Vol. 47, No.7, 1999, pp. 1569-1588

41. Zuniga, S.M., and Sheppard, S.D., "Determining the Constitutive Properties of the Heat-Affected Zone In a Resistance Spot Weld," Modeling and Simulation in Materials Science and Engineering, Vol. 3, No. 3, 1995, pp. 391-416

42. Hval, M., Thaulow, C., Lange, J.H., Hoydal, S.H., and Zhang, Z.L., "Numerical Modeling of Ductile Fracture Behavior in Aluminum Weldments," Welding Journal, Vol. 77, No. 3, 1998, pp. 208s-217s

43. Wang, TJ., "Micro- and Macroscopic Damage and Fracture Behavior of Welding Coarse Grained Heat Affected Zone of a Low Alloy Steel: Mechanisms and Modelling," Engineering Fracture Mechanics, Vol. 45, No. 6, 1993, pp. 799-812

44. Rak, I., Gliha, V., and Kocak, M., "Weldability and Toughness Assessment of Ti-Microalloyed Offshore Steel," Metallurgical and Materials Transactions A, Vol. 28, No. 1, 1997, pp. 199-206

45. Reynolds, A.P., and Duvall, F., "Digital Image Correlation for Determination of Weld and Base Metal Constitutive Behavior," Welding Journal, Vol. 78, No. 10, 1999, pp. 355s – 360s

46. Wolters, W.J., Sutton, M.A., Peters, W.H., Ranson, W.F., and McNeill, S.R., "Determination of Displacements Using an Improved Digital Correlation Method," Computer Vision, Vol. 8, 1983, pp. 133-139

47. Bruck, H.A., McNeill, S.R., Sutton, M.A., and Peters, W.H., III, "Digital Image Correlation Using Newton-Raphson Method of Partial Differential Correction," Experimental Mechanics, Vol. 29, 1989, pp. 261-267

48. Babai, M., Jang, J., McNeill, S.R., and Sutton, M.A., "Effects of Subpixel Image Restoration on Digital Correlation Error Estimates," Optical Engineering, Vol. 27, No. 10, 1988, pp. 870-877

49. Helm, J, Vic_2D Manual, 1997

50. Sutton, M.A., Cheng, M., Peters, W.H., Chao, Y.J., and McNeill, S.R., "Application of an Optimized Digital Correlation Method to Planar Deformation Analysis," Image and Vision Computing, Vol. 4, No. 3, 1986, pp. 143-150

51. Reynolds, A.P., and Lockwood, W.D., "Digital Image Correlation for Determination of Weld and Base Metal Constitutive Behavior," International Symposium on Friction Stir Welding, 1999

52. Hao, S., Schwalbe, K.H., and Cornec, A., "The Effect of Yield Strength Mis-match on the Fracture Analysis of Welded Joints: Slip-line Field Solutions for Pure Bending," International Journal of Solids and Structures, Vol. 37, No. 39, 2000, pp. 5385-5411

53. Kim, Y.J., and Schwalbe, K.H., "Mis-match Effect on Plastic Yield Loads in Idealised Weldments I Weld Centre Cracks," Engineering Fracture Mechanics, Vol. 68, No. 2, 2001, pp. 163-182

54. Kim, Y.J., and Schwalbe, K.H., "Mis-match Effect on Plastic Yield Loads in Idealised Weldments II Heat Affected Zone Cracks," Engineering Fracture Mechanics, Vol. 68, No. 2, 2001, pp. 183-199

55. Matic, P., and Jolles, M.I., "The Influence of Weld Metal Properties, Weld Geometry and Applied Load on Weld System Performance," Naval Engineers Journal, March, 1988, pp 60-72

56. ASTM Standard E 8-90a, 1991 Annual Book of ASTM Standards, Vol. 3.01, Metals Test Methods and Analytical Procedures, ASTM, Philadelphia, Pa.

57. Murr, L.E., Liu, G., and McClure, J.C., "Dynamic Recrystallization in Friction Stir Welding of Aluminum Alloy 1100," Journal of Materials Science Letters, Vol. 16, No. 22, 1997, pp. 1801-1803

58. Murr, L.E., Liu, G., and McClure, J.C., "A TEM Study of Precipitation and Related Microstructures in Friction Stir Welded 6061 Aluminum," Journal of Materials Science, Vol. 33, No. 5, 1998, pp. 1243-1251

59. Liu, G., Murr, L.E., Niou, C-S., McClure, J.C., and Vega, F.R., "Microstructural Aspects of the Friction Stir Welding of 6061-T6 Aluminum," Scripta Materialia, Vol. 37, No. 3, 1997, pp. 355-361

60. Sato, Y.S., Kokawa, H., Enomoto, M., Jogan, S., "Microstructural Evolution of 6063 Aluminum During Friction Stir Welding," Metallurgical and Materials Transactions A, Vol. 30, No. 9, 1999, pp. 2429-2437

61. Mallick, P.K., "Fiber Reinforced Composites," New York: Marcel Dekker, Inc., 2nd ed., 1993

62. Reddy, J.N., "An Introduction to the Finite Element Method," New York: McGraw Hill, Inc., 2nd ed., 1993

63. Frederick, D., and Chang, T.S., "Continuum Mechanics," Boston: Scientific Publishers, Inc., 1965

64. Malvern, L.E., "Introduction to the Mechanics of a Continuous Medium," New Jersey: Prentice-Hall, Inc., 1969

65. Bathe, K-J., "Finite Element Procedures," New Jersey: Prentice-Hall, Inc., 1996

66. ABAQUS Theory Manual, Version 5.7, Hibbit, Karlsson & Sorensen, Inc., 1997